Statistical decision making for stochastic damage localization approaches

Luciano Heitor Gallegos Marin

ANNÉE 2013

THÈSE / UNIVERSITÉ DE RENNES 1
sous le sceau de l'Université Européenne de Bretagne

pour le grade de

DOCTEUR DE L'UNIVERSITÉ DE RENNES 1

Mention : Traitement du Signal et Télécommunications

École doctorale Matisse

présentée par

Luciano Heitor GALLEGOS MARIN

préparée à l'unité de recherche Inria
Institut National de Recherche en Informatique et Automatique

---

Statistical Decision Making for Stochastic Damage Localization Approaches

Thèse soutenue à Rennes
le 8 octobre 2013

devant le jury composé de :

Franck SCHOEFS
Professeur, Université de Nantes, France / rapporteur

Joseph MORLIER
Professeur, Institut Supérieur de l'Aéronautique et de l'Espace , France / rapporteur

Michael DÖHLER
Chercheur, Federal Institute for Materials Research and Testing, Allemagne / examinateur

Qinghua ZHANG
Directeur de Recherche, Inria Rennes, France / examinateur

Laurent MEVEL
Chargé de Recherche, Inria Rennes, France / directeur de thèse

Dionisio BERNAL
Professeur, Northeastern University, États-unis / co-directeur de thèse

To Regina.

It is with life as it is with a play: it matters not how long the action is spun out, but how good the acting is. It makes no difference at what point you stop. Stop whenever you choose; only see to it that the closing period is well turned.

Lúcio Anneo Sêneca [1]

[1] "Epistulae morales ad Lucilium"

Acknowledgments

First of all, I would like to express my gratitude to my advisor, Dr. Laurent Mevel. He had opened the doors for me to learn, to work and to share experiences in the Inria's I4S team. Thank you very much.

My gratitude is also extended to my co-advisor, Professor Dionisio Bernal. Thank you to drive me into the challenging field of structural engineering and to have me at Boston for an important internship period. I would like also to thank my second co-advisor, Dr. Michael Döhler, for been sharing his knowledge and for the incredible opportunity to work with him.

I would like to thank to the reviewers, Drs. Franck Schoefs and Joseph Morlier. They expended an important time reading and suggesting corrections about this thesis. I would extend my gratitude to Dr. Qinghua Zhang to accept the invitation to be in jury of this thesis.

It was a great pleasure to meet Ahmed Jhinaoui, Meriem Zghal, Alireza Esfahani and Philippe Mellinger, all them in the I4S team. Your experiences from different countries and the histories about your cultures were a real gift for me. Thank you for our always interesting lunch times, coffees and dinners.

I would like to thank my parents, Heitor, Berenice and Gustavo. Be writing this acknowledge just became possible because you had been supported me during important periods of my life. I would like to extend this acknowledgment to all the relatives that helped me in many different ways: advising, sharing their houses during the weekends, or by simply enjoying a nice time together. I will never forget it.

Finally, I would like to thank my wife, Regina. Your courage and optimism are my inspirations and your smile are the lights showing this world as a good place to live in. Thank you for believing and keep walking all these years side-by-side with me.

Luciano Heitor Gallegos Marin
Rennes, October 2013.

Contents

Resume in French

Introduction

Description générale

La sensibilité des structures aux vibrations est un problème de base en mécanique, particulièrement dans l'aérospatiale, l'automobile, le maritime, les chemins de fer, etc. C'est aussi d'importance croissante en génie civil, car non seulement la minceur des structures et des composants structurels augmentent continuellement, mais aussi leur chargement dynamique dû au traffic.

La vérification expérimentale des valeurs de design, utilisant les paramètres modaux, est essentielle pour le design et la validation de modèle pour garantir la sécurité et la sûreté de fonctionnement de la structure. Elle est aussi fréquemment employée pour le contrôle de qualité et la santé structurelle. L'amortissement et les conditions aux frontières dépendent de l'amplitude des vibrations et si la structure a des parties rotatives, les paramètres modaux dépendent de la vitesse de rotation de ces parties. Donc, il est important que la détermination expérimentale des paramètres modaux de la structure soit exécutée dans des conditions opérationnelles normales, c'est-à-dire, autour du point d'exploitation. Ceci appartient au domaine d'*Operational Modal Analysis* (OMA), où les paramètres modaux sont extraits de la réponse dynamique aux forces opérationnelles non mesurées.

En génie civil, OMA est devenue la méthode principale d'identification modale et le nombre d'études de cas rapportées est abondant. Ceci est particulièrement vrai pour la chaussée et des ponts de chemin de fer, mais les applications rapportées incluent aussi des passerelles [RDDRM10], silos [DDDRR06], toits suspendus [MCC08], tours de maçonnerie [GS07], plates-formes offshores [BAMT96], bâtiments [Bro05], parmi d'autres.

La recherche récente sur OMA s'est concentrée sur le fait de surmonter quelques défauts importants. Un premier est que les mesures *output-only* ne permettent pas de déterminer un modèle modal complet, puisque les formes de mode ne peuvent pas être mesurées dans un sens absolu, par exemple, à l'unité de la masse modale. Une des solutions possibles est d'executer une deuxième mesure après l'addition ou l'enlèvement d'une quantité significative de masse à ou de la structure [PVGVO02], mais ceci est souvent compliqué en pratique [PCB$^+$05]. Deuxièmement, l'excitation ambiante peut être limitée a une bande de fréquence étroite et en conséquence seulement un nombre limité de modes peut être extrait avec grande précision. Finalement, un défaut général de la plupart des algorithmes d'analyse modale

expérimentaux et opérationnels est qu'ils rapportent seulement des évaluations de point pour les paramètres modaux, c'est-à-dire, ils ne fournissent pas des informations sur leur incertitude quand l'estimation se fait à partir d'un test simple.

Essentiellement, l'OMA consiste en trois étapes: acquisition de données, analyse de données et évaluation des résultats. Cependant, dans le contexte OMA les caractéristiques inhabituelles suivantes doivent être prises en compte:

(a) Le nombre de capteurs peut être très grand (jusqu'à des centaines, ou des milliers dans l'avenir avec de nouvelles technologies). Les capteurs peuvent même être déplacés d'une campagne de mesure à une autre;

(b) Le nombre des modes d'intérêt peut être tout à fait grand (jusqu'à 100 ou au-delà), appelant ainsi à des méthodes qui peuvent traiter des grands ordres de modèle dans un temps de calcul raisonnable;

(c) L'excitation appliquée à la structure est d'habitude non mesurée, non contrôlée et naturelle, donc turbulente et non-stationnaire.

En raison de la nature inconnue des données acquises, l'identification de systèmes dans OMA est devenue un défi. L'identification du systèmes linéaires comme une discipline de recherche de l'ingénierie de contrôle est née à la fin des années 1960 et s'est développée au long de deux axes qui sont toujours dominants aujourd'hui. Le premièr axe est le cadre d'erreur de prédiction, où un modèle de système est identifié en minimisant la différence entre la réponse de système mesurée et la réponse prévue par le modèle, le plus souvent utilisant le principe du *Maximum Likelihood* (ML) [AB65, AE71]. Des développements importants dans cette direction incluent l'identification de systèmes comme un problème d'approximation qui a culminé dans le travail de référence par [Lju99], et le développement d'un cadre de ML pour données du domaine fréquentiel [SP91].

Le deuxième axe commencé en même temps avec le travail séminal de Ho et Kalman sur la réalisation de système [HK66], a été prolongé par Akaike vers l'identification *output-only* de systèmes excités par des processus stochastiques blancs [Aka74]. Plus tard, les méthodes plus générales que les méthodes dites *Instrumental Variable* (IV) ont été proposées, et sont basées sur des techniques de corrélation [SS83]. Dans les années 1990, les méthodes d'identification sous-espaces ont été développées [Vib95, VODM96]. Elles sont fortement reliées aux méthodes IV.

Les deux approches ont des avantages distincts: les méthodes ML ont des propriétés statistiques asymptotiques optimales conformément aux suppositions assez générales, tandis que des méthodes sous-espaces sont très robustes et beaucoup moins exigentes en termes de calcul. Les propriétés statistiques d'algorithmes sous-espaces ne sont pas faciles à dériver et pendant la décennie dernière, beaucoup d'efforts de recherche ont été consacrés là-dessus [Bau05].

Aujourd'hui, les systèmes *Linear Time-Invariant* (LTI) sont considérés comme un champ mûr [PS01, Gev06]. Du système LTI, la caractérisation de dommages peut être déduite. Puisque la caractérisation de dommages n'est pas directe, la même procédure peut être améliorée si la caractérisation est séparée en trois parties: la détection, l'isolement et la quantification de faute.

L'isolement de faute est un champ dans l'ingénierie de contrôle concernant l'isolation du sous-système d'un système dans des conditions anormales, indiquant où la faute arrive. Appliqué aux données de vibration de structures dynamiques, ceci correspond à la localisation de dommages et est fait en détectant des changements dans les caractéristiques de vibration ou dans les paramètres structurels d'une structure. La localisation de dommages appartient au *Structural Health Monitoring* (SHM) dans le contexte OMA et permet d'identifier des dommages dans un état précce.

L'identification de système et la probleématique de détection de faute sont actuellement mûrs. Pour la localisation de dommages, des techniques différentes comme notamment le recalage de modèle ont été développées. Malgré tous les efforts, la localisation de dommages reste un champ ouvert en raison des incertitudes inhérentes dans le système identifié et constitue un champ intéressant à être exploré. Cette thèse est développée en lien avec le problème de localisation de dommages dans les structures civiles et la prise en compte des incertitudes venant des données mesurées.

Motivations

L'identification de système LTI est faite après la mesure des données de structures où des capteurs, placés dans l'espace, rassemblent des données suffisantes au long d'une période de temps. Bien que les capteurs soient de plus en plus sophistiqués, ils ne peuvent pas éviter la perturbation inhérente dans les données rassemblées (c'est-à-dire le bruit ou d'autres influences externes). Lorsque des données réelles ne sont pas disponibles, la simulation est exécutée et une perturbation est ajoutée. La situation est pire quand l'identification est soumise aux scénarios stochastiques ou l'*input* est inconnu. Dans ce contexte, les incertitudes dans les données rassemblées exigent de l'analyse supplémentaire pour le SHM.

Quelques travaux récents ont abordé ces questions. Reynders and De Roeck [RDR10] et, plus récemment Pintelon, Guillaume and Schoukens [PGS07], fournissant des directives importantes pour surmonter les incertitudes inhérentes pour le SHM. Dans le contexte du SHM, la caractérisation de dommages est d'habitude partagée entre la détection de faute, l'isolement (la localisation) et la quantification. Récemment, Bernal a publié des articles dans le champ de localisation de dommages [Ber10, Ber13] où la décision est barre au seuil defini empiriquement pour définir l'élément ou la position endommagé. Donc, la nécessité est de fournir des méthodes de prise de décision statistique qui surpassent des approches empiriques pour trouver l'emplacement de dommages en environnement stochastique.

Contributions

Les méthodes d'identification de système sous-espace ont montré leur efficacité pour l'identification de systèmes LTI pour des données mesurées sous des suppositions d'excitation réalistes. Pour OMA, l'*eigenstructure* (*eigenvalues* et *eigenvectors*) du système linéaire sous-jacent devra être identifiée. Donc, les matrices du système et des nouvelles informations importantes peuvent être extraites pour la localisation de dommages dans des structures.

Les méthodes suivantes sont les contributions développées dans cette thèse :

(1) **Prise de décisions statistique pour localisation de dommages avec vecteurs**

de charge stochastiques : Des systèmes mécaniques sous l'excitation de vibration sont les candidats principaux à être modelisés par des systèmes LTI. La détection de dommages dans de tels systèmes touche au contrôle des changements de l'*eigenstructure* du système linéaire correspondant et reflète ainsi des changements de paramètres modaux et finalement dans le modèle aux eléments finis de la structure. La localisation de dommages utilisant tant les éléments finis que les données modales estimées de données de vibration ambiantes mesurées par des capteurs est possible par le *Stochastic Dynamic Damage Location Vector* SDDLV [Ber10]. Les dommages sont reliés à un certain résidu obtenu à partir de la différence entre les matrices de transfert tant en référence qu'en états de dommage ainsi qu'avec un modèle de l'état de référence. La décision que ce résidu est nul est jusqu'ici fait utilisant un seuil empiriquement défini. Dans cette première contribution, nous montrons comment l'incertitude dans les évaluations du système spatial d'état peut être utilisée pour tirer des limites d'incertitude sur les résidus de localisation de dommages pour décider de l'emplacement de dommages avec un test d'hypothèse.

(2) **Localisation de dommages statistique robuste avec vecteurs de charge stochastiques :** La première contribution (1) est consacrée au cas où le résultat d'emplacement de dommages est basé sur le choix d'une variable de Laplace. Les choix de différents variables de Laplace mènent aux résultats de localisation différents en raison d'un impact différent de la troncature modale. En prenant en compte que les incertitudes améliorent non seulement la robustesse statistique de l'approche, cela vise aussi à diminuer le nombre de fausse alertes potentielles. L'utilisation de différentes variables de Laplace devrait plus loin augmenter la robustesse de l'approche et aider la décision. Cette seconde contribution prolonge la contribution précédente (1) en se concentrant sur une approche statistique robuste, où des résultats de localisation de dommages multiples calculés aux variables de Laplace différentes seront agrégés en prenant en compte leur pertinence statistique. Aussi, l'étape d'identification des systèmes nécessaire ainsi que la construction des matrices du système paramétrique à partir des modes identifiés sera expliqué et la nouvelle méthode est appliquée sur des simulations numériques et des structures réelles.

(3) **Prise de décisions statistique robuste appliquée à la localisation de dommages avec des lignes de influence:** Le théorème de l'*Influence Lines Damage Location* (ILDL) [Ber13] démontre que l'utilisation de l'image des matrices de transfert tant en référence que dans les états endommagés plus un modèle de l'état de référence est utile pour les *influence lines* (IL) pour définir l'emplacement des dommages. Les dommages sont ainsi localisés aux points où l'angle sous-espace entre l'image et l'IL calculé du modèle d'éléments finis est près du zéro. Basé sur les contributions précédentes (1, 2), cette dernière contribution a pour but de remplacer les seuils empiriques qui sont utilisés dans l'approche d'ILDL pour décider où les dommages d'éléments sont localisés (c'est-à-dire où des angles sous-espaces sont près du zéro).

Ces contributions sont développées en détail et des propriétés importantes sont prouvées. Elles sont validées sur des données de vibration structurelles d'exemples numériques et réels,

le dernier cas quand les données étaient disponibles.

Chapitre 1 – L'état de L'art

Le processus de mettre en oeuvre la détection et la caractérisation de dommages, dans le domaine du contrôle et de l'ingénierie civil, est le SHM [Daw76]. Dans ce contexte, les dommages sont définis comme des changements dans les propriétés matérielles et-ou géométriques d'un système structurel, y compris des changements aux conditions de frontière et dans la connectivité du système, qui affecte défavorablement la performance du système.

Le problème de *fault detection and isolation* (FDI) consiste, dans la détection de changements, des paramètres d'un système dynamique (la détection) et la distinction entre les paramètres changés et les paramètres inchangés (l'isolement). En général, ces problèmes sont divisés dans deux étapes: la génération de résidus, qui sont idéalement près de zéro donc sans faute resultés aux bruits et des perturbations et au maximum sensibles aux fautes; et évaluation résiduelle, à savoir le design de règles de décision basées sur ces résidus [Bas98].

Dans beaucoup d'applications, le problèmes FDI est de détecter et diagnostiquer des changements de l'*eigenstructure* d'un système dynamique linéaire. Un exemple important est le SHM, où les dommages de structures civiles, mécaniques ou aéronautiques mènent à un changement de l'*eigenstructure* du système mécanique sous-jacent et donc dans les paramètres modaux. Rytter [Ryt93] a défini une classification de ces méthodes à quatre niveaux: détection de dommages, localisation de dommages, quantification de dommages, et prédiction de la durée d'utilisation restante de la structure examinée.

Les contributions de cette thèse sont concentrées sur la localisation de dommages, après l'étape où la détection de dommages est réalisée et quelques dommages sont détectés.

Chapitre 2 et 3 – Théorie de fond

La caractérisation de dommages dans quelques applications peut être réalisée de deux façons: vérification en ligne (a aussi appelé vérification de temps réel) ou interrogation *a posteriori*. Les algorithmes de vérification en ligne sont plus souvent basés sur l'analyse des résidus qui reflètent des contradictions entre les prédictions qu'un modèle prévoit et les prédictions mesurées. La localisation est abordée en concevant des observateurs où chaque résidu pour chaque faute possible ont des caractéristiques directionnelles particulières [Fra90]. Les stratégies *a posteriori* opèrent avec des données rassemblées à deux moments différents et offrent des informations sur les changements de la condition structurelle dans l'intervalle entre les mesures [DFP$^+$96, Fri05]. Dans la situation *a posteriori*, un modèle mis à jour est conceptuellement applicable mais le succès s'est avéré difficile dans des problèmes réalistes en taille en raison d'un conditionnement pauvre [MF93, Fri07]. Les difficultés dans la caractérisation de dommages peuvent être améliorées si le problème est séparé entre la détection, la localisation et la quantification [Ber13].

Plusieurs méthodes de localisation de dommages ont été décrites dans la littérature [Ber02, Ber06, Ber07, Ber10, Ber13]. Ces méthodes peuvent être classés comme les *input/output* (c'est-à-dire, quand on connaît l'excitation externe) ou comme les *output-only*. [Ber13]. Dans

le *output-only* cas, deux méthodes ont été utilisées avec succès: l'approche *Stochastic Dynamic Damage Location Vector* (SDDLV) [Ber10] et l'approche de l'*Influence Line Damage Location* (ILDL) [Ber13]. Le comportement d'une structure mécanique est décrite par un système LTI, oú le modèle d'état-spatial en temps continu correspondant est

$$\begin{cases} \frac{dx(t)}{dt} = A_c x + B_c e \\ y(t) = C_c x + D_c e \end{cases},$$

où les matrices de système A_c et C_c peuvent être obtenues par la méthode *covariance-driven subspace identification* et les matrices B_c et D_c sont seulement pertinentes pour des dérivations mathématiques. En fait, la méthode *covariance-driven subspace identification* est utilisée pour fournir les matrices de système puisqu'elles sont inconnues et soumises aux incertitudes. La localisation de dommages est ensuite exécute avec les approaches SDDLV et ILDL.

Chapitre 4 – Prise de décisions statistique pour localisation de dommages avec vecteurs de charge stochastiques

L'approche de SDDLV [Ber10] est une technique *output-only* de localisation de dommages qui utilise tant éléments finis qui paramètres modaux, supposant que quelques dommages sont arrivés. L'espace nul de la diférence entre les matrices de transfert respectives est obtenu des évaluations des matrices de système tant en référence que en états endommagés. Alors, les dommages sont reliés à un résidu tiré de cet espace nul et localisés où le résidu est près du zéro.

D'une part, ces SDDLV ne prennent pas en compte l'incertitude intrinsèque du problème en raison du bruit inconnu excitant le système. Le manque de considération d'incertitude s'avère être critique parce qu'aucune information n'est pas disponible sur le choix de seuil pour se décider si le résidu est le zéro ou pas dans des situations pratiques. Des seuils empiriques sont actuellement utilisés pour la décision. D'autre part, l'identification de matrices de système est affligée par l'incertitude, en raison du bruit et de la taille limitée de données. Des méthodes comme présentées en [PGS07] et en [RPDR08] fournissent quelques directives pour tirer des évaluations d'incertitude pour des paramètres modaux. Ce Chapitre a pour but de remplacer des règles empiriques selon des règles à base de sensibilité appliquées sur un certain critère de localisation de dommages.

La nouvelle méthode est validée dans beaucoup d'applications, y compris une treillis numériquement simulé (Figure 1). Dans la Figure 2 les résultats sont présentés avec 4 capteurs (le nombre 1,3,4,6 dans la Figure 1), où seulement 3 *mode pairs* sont utilisées de l'identification de système. L'utilisation de moins de capteurs et moins de modes mène évidemment à moins de contraste entre les valeurs χ^2 des éléments intacts et endommagés.

La théorie montre que comme le nombre de barres endommagées augmente, du même la dimension de l'espace nul, l'évaluation de vecteurs dans l'espace nul dans des conditions bruilée devient plus difficile. Dans ce cas, une évaluation plus précise est nécessaire. Dans la Figure 3, les résultats sont présentés pour deux dommages des barres 3 et 18, où maintenant 12 *mode pairs* et 12 capteurs ont été utilisés. Il devrait être noté que les tensions évaluées

dans les éléments endommagés sont petites, mais différentes du zéro en raison de la troncature modale et de bruit, qui devient plus important quand des dommages multiples sont présents.

Chapitre 5 – Localisation de dommages statistique robuste avec vecteurs de charge stochastiques

L'approche SDDLV [Ber10], décrite dans les Chapitres 2 et 4, garantie seulement que les éléments dont l'index de dommage n'est pas zéro ne sont pas affligés avec des dommages. En prenant en compte que les incertitudes améliorent non seulement la robustesse statistique de l'approche, cela vise aussi à diminuer le nombre de fausse alertes potentielles. Néanmoins, cela peut arriver qu'à cause de bruit, la réduction de modèle, l'instrumentation clairsemée ou d'autres limitations l'ensemble d'éléments près de l'index de dommages zéro est trop grand pour aider la prise de décision dans des applications réelles. Le Chapitre 4 a démontré que l'utilisation d'aides d'informations d'incertitude augmente le contraste entre les éléments. L'utilisation de différentes variables de Laplace devrait plus loin augmenter la robustesse de l'approche et aider la décision, qui est une extension importante du Chapitre 4 où juste une variable de Laplace est utilisée.

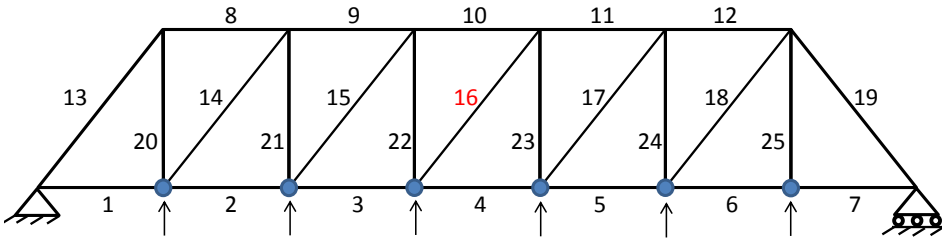

Figure 1 – Structure de une treillis avec six capteurs.

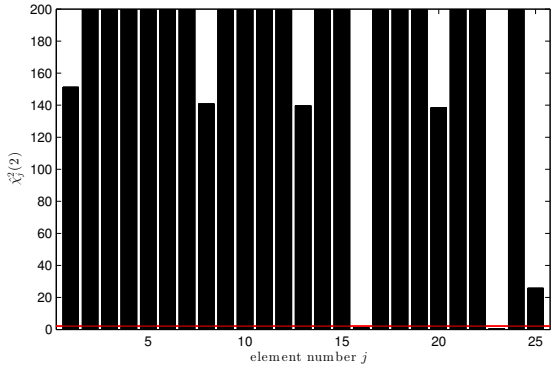

Figure 2 – Resultats χ^2 – 5% de bruit au output, 4 capteurs, 20% de déduction de rigidité de la barre 16.

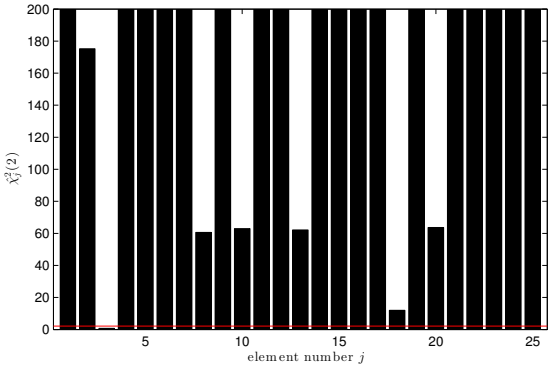

Figure 3 – Resultats χ^2 – 5% de bruit au output, 12 capteurs, 20% de déduction de rigidité de la barres 3 et 18.

Le Chapitre actuel prolonge le Chapitre 4 en se concentrant sur une approche statistique robuste, où des résultats de localisation de dommages multiples calculés aux différentes variables de Laplace seront agrégés en ce qui concerne leur pertinence statistique. Ceci enlèvera une partie des erreurs et de l'incertitude liée au choix de la variable de domaine Laplace. L'approche de SDDLV sous-jacente utilisant l'identification sous-espace et la méthodologie statistique sont expliqués, avant que l'approche statistique robuste sont derivée.

Entre plusieurs applications utilisées, la nouvelle méthode est validée dans une expérience de laboratoire où les tests de vibration ont été conduits sur une barre (Figure 4). Les expériences ont été conduites par Brüel & Kjær comme un banc d'essai pour la localisation de dommages. Ce barre est équipée avec 27 capteurs situés en haut et en bas.

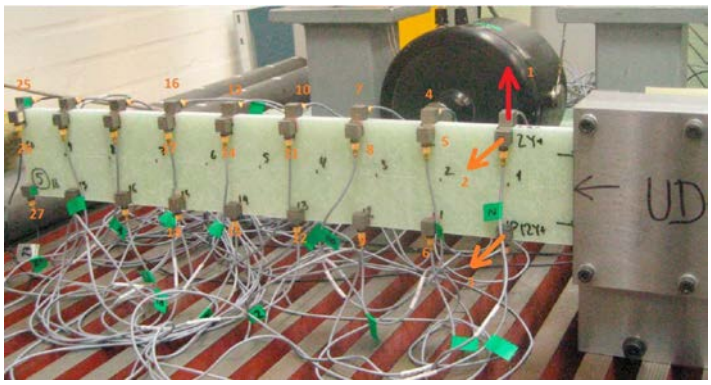

Figure 4 – Configuration exprimentale de la barre.

Les résultats (Figure 5) montrent que la procédure de localisation de dommages avec la nouvelle aggregation statistique (Figures (a), (c)) indique fortement des dommages et parfois dans les éléments directement adjacents, tandis que la localisation basée sur l'aggregation deterministe des résultats de stress (Figures (b), (d)) n'a pas du succès. Le changement de la position du "shaker" entre les états de référence et endommagés est clairement visible comme des dommages au milieu du bar, qui devraient être négligés.

Chapitre 6 – Prise de décisions statistique robuste appliquée a la localisation de endommage avec lignes de influence

Le théorème ILDL, récemment présenté en [Ber13], montre que l'image des diférences entre les matrices de transfert de système tant en référence que dans les états endommagés, est une base pour les *influence lines* (IL) pour les résultantes d'emplacement de dommages. Les dommages sont ainsi localisés aux points où l'angle sous-espace entre l'image et l'IL calculé du FEM est près du zéro. Actuellement, des seuils empiriques sont utilisés dans l'approche ILDL pour décider ou les dommages sont localisés et aucune approche stochastique n'est prise en compte.

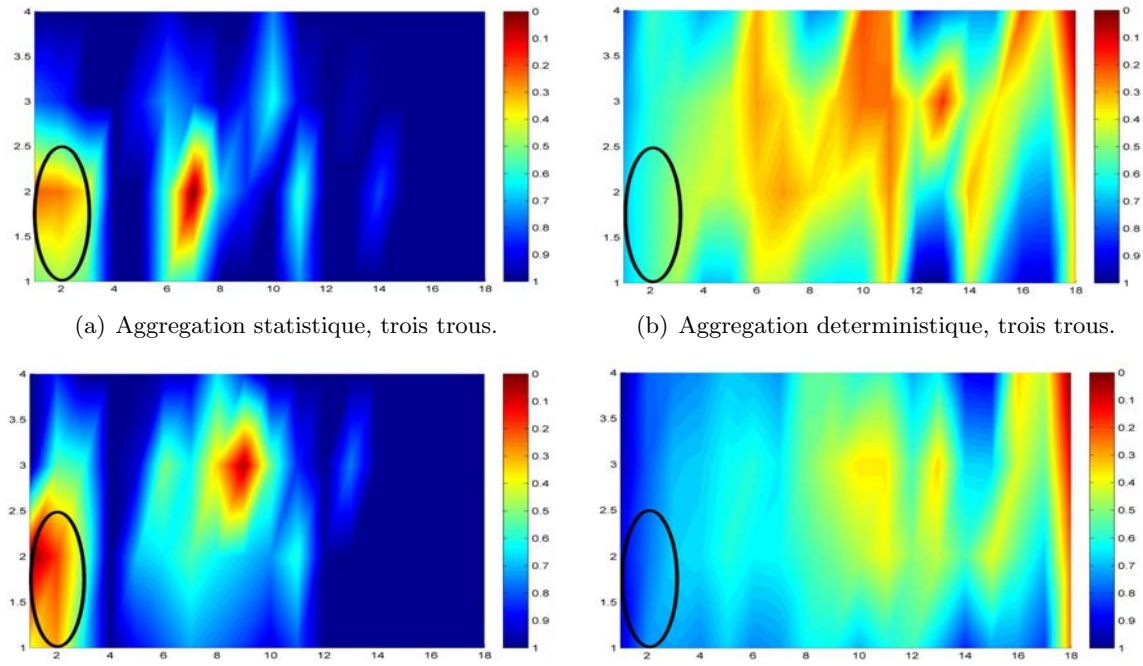

(a) Aggregation statistique, trois trous.

(b) Aggregation deterministique, trois trous.

(c) Aggregation statistique, cinq trous.

(d) Aggregation deterministique, cinq trous.

Figure 5 – Localisation de dommages utilisant dix valeurs de Laplace, avec la comparaison de la nouvelle aggregation statistique (gauche) et l'aggregation deterministique (droite) et des niveaux de dommages différents.

Dans ce Chapitre 6, le calcul de l'angle sous-espace est étendu au cas stochastique et aussi à l'évaluation d'incertitude produite par les données de mesure avec la méthode de base de la sensibilité [RPDR08]. Alors, la prise de décision statistique sur les emplacements de dommages remplace des seuils empiriques.

La même expérience avec le vrai barre conduit par Brüel & Kjær (Figure 4) comme un banc d'essai pour la localisation de dommages dans une expérience de laboratoire est utilisée dans ce Chapitre. Les deux résultats avec l'aggregation statistique présentent les dommages bien placés tandis que l'aggregation deterministe devrait être adandonée (Figure 6). En comparant seulement les résultats statistiques, l'ILDL présente une meilleure localisation de dommages que le SDDLV.

Conclusions

Les approches de localisation de dommages utilisées dans cette thèse, le SDDLV et l'ILDL, sont des méthodes complémentaires basées sur les changements dans la matrice de flexibilité d'un modèle structurel prédéfini. D'une part, le SDDLV utilise dans l'espace nul obtenu à partir de données *output-only* comme les charges appliquées un modèle aux éléments finis pour souligner des résultantes pour l'emplacement de dommages. D'autre part, l'ILDL utilise l'image obtenue à partir de données *output-only* et les dommages sont localisés aux points

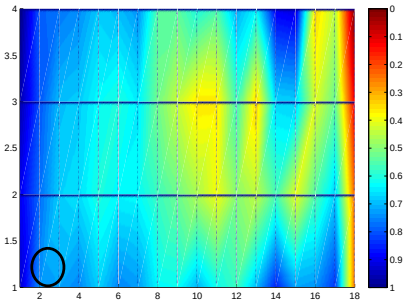

(a) Aggregation deterministique avec le SDDLV.

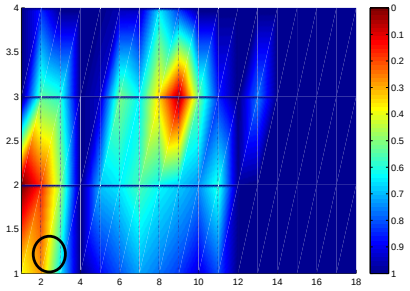

(b) Aggregation statistique avec le SDDLV.

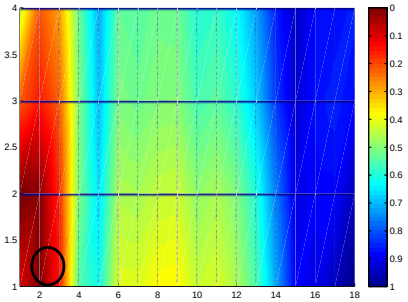

(c) Aggregation deterministique avec le ILDL.

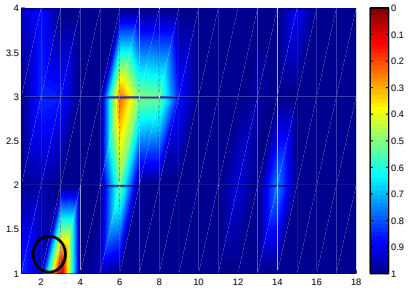

(d) Aggregation statistique avec le ILDL.

Figure 6 – Localisation de dommages dans la structure de la bar comparant les résultats statistique (droit) et deterministiques (gauches).

au l'angle entre l'image et l'IL calculé sur le modèle aux éléments finis sont près zero. De la dérivation des incertitudes intrinsèques tant dans SDDLV que par les méthodes ILDL cette thèse a fourni un cadre de prise de décision statistique complet, où les résultats d'application dans chaque contribution renforcent leur importance complémentaire.

Dans toutes les contributions, la méthode d'identification sous-espace a été utilisée et les matrices de système ont été construites des paramètres identifiés. Toutes les méthodes de localisation de dommages utilisées dans cette thèse sont dependentes du modèle, qui est cruciale pour le succès de la localisation de dommages. Ainsi, des modèles structurels bien cônçus mènent aux meilleurs résultats d'emplacement tandis que l'on ne recommande pas l'opposé. Toutes les contributions ont avec succès amélioré les approches de localisation de dommages liées en surmontant leurs incertitudes dans des nouvelles méthodes de prise de décisions statistiques.

Introduction

General framework

The susceptibility of structures to vibrations is a prime design issue in mechanics, especially in the aerospace, automotive, maritime, railway, and heavy equipment industries. It is also of growing importance in civil engineering, as not only the slenderness of structures and structural members is continuously increasing, but also their dynamic loading, e.g., when due to traffic.

The experimental verification of design values, in particular modal parameters (eigenfrequencies, damping ratios, mode shapes, and modal scaling factors), is essential for design and model validation, so for guaranteeing the safety and serviceability of the structure. It is also frequently employed for quality control and structural health monitoring purposes. Damping and boundary conditions depend on the vibration amplitude and, if the structure moves as a whole or contains rotating parts, the modal parameters depend on the (rotation) speed (of the parts). Therefore, it is important that the experimental determination of the modal parameters of the structure is performed in normal operational conditions, i.e., around the operating point. This belongs to the domain of *Operational Modal Analysis* (OMA), were modal parameters are extracted from the dynamic response to unmeasured operational forces.

One of the first successful applications of OMA in mechanics was for determining the modal parameters of wind turbines at different rotation rates [CI10]. Later applications include on-the-road modal analysis of cars and in-flight modal analysis of airplanes [HdAH99], modal testing of spacecraft during launch [Jam03], and modal testing of engines during startup and shutdown [CSC11], amongst others. In civil engineering, OMA has become the primary modal testing method, and the number of reported case studies is abundant. This is particularly true for roadway and railway bridges, but reported applications also include footbridges [RDDRM10], silos [DDDRR06], suspended roofs [MCC08], masonry towers [GS07], offshore platforms [BAMT96], highrise buildings [Bro05], grandstands [PVdAVG07], tall industrial chimneys [BEGG10] and dams [DdSCK00], amongst others.

Recent fundamental research on OMA has focused on overcoming some important shortcomings. A first one is that output-only measurements do not allow to determine a complete modal model, since the mode shapes can not be scaled in an absolute sense, e.g., to unit modal mass. One of the possible solutions is performing a second measurement after adding or removing a significant amount of mass to or from the structure [PVGVO02], but this is often cumbersome in practice [PCB$^+$05]. Secondly, the ambient excitation may be confined

to a narrow frequency band, and as a result only a limited number of modes may be extracted with high quality. Finally, a general shortcoming of most experimental and operational modal analysis algorithms is that they only yield point estimates for the modal parameters, i.e., they do not provide information on their uncertainty when estimated from a single test.

Basically, OMA consists of three steps: data acquisition, data analysis and evaluation of the results. However, in the OMA context the following unusual features must be taken into account:

(a) The number of sensors can be very large (up to hundreds, or thousands in the future with new technologies). Sensors can even be moved from one measurement campaign to another;

(b) The number of modes of interest can be quite large (up to 100 or beyond), thus calling for methods that can deal with large model orders at a reasonable computation time;

(c) The excitation applied to the structure is usually unmeasured, uncontrolled and natural, thus turbulent and non-stationary.

Due to the unknown nature of the acquired data, system identification in OMA became a challenge. *Linear system identification* as a research discipline of control engineering originated in the late 1960s, and developed along two lines that are still dominant today. The first line is the prediction error framework, where a system model is identified by minimizing the difference between the measured system response and the response predicted by the model, most often using the Maximum Likelihood (ML) principle [AB65, AE71]. Important developments in this direction include the view of system identification as an approximation problem which culminated in the reference work by [Lju99], and the development of a ML framework for frequency-domain data [SP91].

The second line started around the same time with the seminal work of Ho and Kalman on system realization [HK66], which was extended by Akaike towards output-only identification of systems driven by white stochastic processes [Aka74]. Later, more general Instrumental Variable (IV) methods, which are based on correlation techniques, were proposed [SS83]. In the 1990s, subspace identification methods were developed [Vib95, VODM96]. They are strongly related to both the realization and the more general IV methods.

Both approaches have distinct advantages: maximum likelihood methods have optimal asymptotic statistical properties under fairly general assumptions, while subspace methods are very robust and computationally much less demanding. The statistical properties of subspace algorithms are not easy to derive, and during the last decade, a lot of research effort has been spent hereon [Bau05].

Identification of Linear Time-Invariant (LTI) systems can by now be considered as a mature field [PS01, Gev06]. Important recent developments include the identification of nonlinear system models, such as Hammerstein and Wiener models and their combinations [GPSDM05, SPE08], as well as the estimation of nonlinear distortions in the measurement data and their impact on the estimates of linear system models [SPDR05]. From LTI system, damage characterization can be inferred. Since damage characterization is not straightforward, the same procedure can be ameliorated if the characterization can be decoupled into fault detection, isolation, and quantification.

Fault isolation is a field in control engineering concerning to isolate the subsystem from a system with abnormal conditions, pointing to where the fault occurs. Applied to vibration data of dynamic structures, this corresponds to *damage localization* and is done by detecting changes in the vibration characteristics or in structural parameters of a structure. Damage localization belongs to the Structural Health Monitoring (SHM) field in the OMA context and holes an important paper since it allows to identify damage in an early state.

SHM has become an important emerging field, in which non-intrusive damage detection techniques are used to monitor structures. As such, SHM technologies have a large commercial and economic potential. They can help to identify damages at an early stage, where relatively minor corrective actions can be taken at the structure before the deterioration or damage grows to a state where major actions are required. Another example for SHM applications is post-earthquake damage assessment. There, they could ensure prompt reoccupation of safe civil infrastructure and transport networks, which would mitigate the huge economic losses associated with major seismic events. Also, and equally important, monitoring the infrastructure that is approaching or exceeding their initial design life would assure their reliability and support economically sensible condition-based maintenance. In general, it is desirable to detect damage in an automated way without the need of visual inspections, which would require manpower and is difficult to realize in hazardous or remote environments. SHM systems also allow engineers to learn from previous designs to improve the performance of future structures.

System identification and fault detection fields are currently mature fields. For the damage localization, developments with different techniques such as model updating (i.e. structural aspects are changed and verified) and changes in the modal parameters have been produced. Despite all efforts, damage localization remains an open field due to the inherent uncertainties in the identified system and constitutes and interesting field to be explored. This thesis is related to the field of damage localization of civil structures and the uncertainties from the measured data, where the above features (a)–(c) are taken into account.

Motivations

The identification of LTI system is done after gathering data from structures where sensors, spatially positioned, collect sufficient data along a period of time. Although sensors are more and more sophisticated, they cannot avoid the inherent disturbance in the collected data (i.e. noise or other external influences). When real data is not available, some simulation can be performed and some disturbance is added. The situation is even worst when the identification is subject to stochastic scenarios and the input is unknown. In this context, the uncertainties in the collected data demand additional analysis for the SHM.

Some recent works have been tackling these issues. Reynders and De Roeck [PGS07] and, more recently Pintelon, Guillaume and Schoukens [RDR10], provided important guidelines to overcome the inherent uncertainties for the SHM. In the SHM context, damage characterization is usually decoupled in fault detection, isolation (localization) and quantification. Recently, Bernal has published works in the damage localization field [Ber10, Ber13] where empirical decision is made to define the damaged place or position. Then, the necessity

to provide robust statistical decision making methods that overcome empirical decisions on damage location that are subject to stochastic environments becomes evident.

Contributions

Subspace-based system identification methods have been shown efficient for the identification of LTI systems from measured data under realistic excitation assumptions. There are methods that deal with input/output data as well as output-only data, where the unmeasured excitation is assumed as a stochastic process. For Operational Modal Analysis of vibrating structures, the eigenstructure (eigenvalues and eigenvectors) of the underlying linear system needs to be identified. Then, system matrices and further important information can be extracted for the damage localization in structures.

The following methods are the contributions developed in this thesis:

(1) **Statistical decision making for damage localization with stochastic load vectors:** Mechanical systems under vibration excitation are prime candidate for being modeled by LTI systems. Damage detection in such systems relates to the monitoring of the changes in the eigenstructure of the corresponding linear system, and thus reflects changes in modal parameters (frequencies, damping, mode shapes) and finally in the finite element model of the structure. Damage localization using both finite element information and modal parameters estimated from ambient vibration data collected from sensors is possible by the Stochastic Dynamic Damage Location Vector (SDDLV) approach [Ber10]. Damage is related to some residual derived from the kernel of the difference between transfer matrices in both reference and damage states and a model of the reference state. Deciding that this residual is zero is up to now done using an empirically defined threshold. In this first contribution, we show how the uncertainty in the estimates of the state space system can be used to derive uncertainty bounds on the damage localization residuals to decide about the damage location with a hypothesis test.

(2) **Robust statistical damage localization with stochastic load vectors:** The first contribution in item (1) is dedicated to case where the damage location result is based on the choice of just one chosen Laplace variable. Different choices of Laplace variables lead to different localization results due to a different impact of the modal truncation. Taking into account that uncertainties not only improves the statistical robustness of the approach, it also aims at decreasing the number of potential false alarms. Using different Laplace variables should further increase the robustness of the approach and help the decision. This second contribution extends the previous contribution in item (1) by focusing on a robust statistical approach, where multiple damage localization results computed at different Laplace variables will be aggregated with respect to their statistical relevance. Also, the necessary system identification step with the construction of parametric system matrices from identified modes is explained and the new method is applied on numerical simulations and real structures.

(3) **Robust statistical decision making applied to influence lines damage localization:** The Influence Lines Damage Location (ILDL) theorem [Ber13] shows that the image from the transfer matrices in both reference and damage states and a model of the reference state is a basis for the influence lines (IL) for the damage location resultants. Damage is thus located at points where the subspace angle between the image and the IL computed from the finite element model is near zero. Although the kernel and the image contain the same complementary information in theory, in practice only an estimate of this matrix is available. Based on the previous contributions (item (2)), this last contribution aims to replace empirical thresholds that are used in the ILDL approach for deciding at which elements damage is located (i.e. where subspace angles are close to zero).

These contributions are derived in depth and important properties are proven. They are validated on structural vibration data from numerical and real examples, the last case when data was available.

Outline

This thesis is organized in four parts and contains seven chapters.

Part I comprises the state of the art, which is described in Chapter 1. There, baselines on structural health monitoring, damage assessment as well as fault detection and isolation (localization) are described. Also, some of the current fault localization approaches are introduced.

Part II comprises the background theory that was necessary for the development of this thesis and is organized in two Chapters. Chapter 2 provides the theoretical background on dynamic models of structures as well as the baselines of the damage localization approaches used in this thesis. Then, in Chapter 3, the background of subspace-based system identification and uncertainty quantification is explained in detail from the literature.

Part III comprises the contributions of this thesis in three Chapters. Chapter 4 introduces in details the development and the replacement of empirical rules that are currently used in a specific fault localization approach by sensitivity-based rules. Then, in Chapter 5, the previous contribution (Chapter 4) is extended into a robust statistical decision making method where multiple damage localization results are aggregated with respect to their statistical relevance. Finally, Chapter 6 describes a damage localization approach based in subspace angles that is extended to the stochastic case and sensitivity-based rules are applied to the uncertainty estimation originated from the measurement data for statistical decision making.

The thesis concludes with an assessment of the developed methods and perspectives for future research.

Notation

Symbols

A^T	Transposed matrix of A
A^*	Transposed conjugated complex matrix of A
A^{-1}	Inverse of A
A^{-T}	Transposed inverse of A
$A^\dagger$	Pseudoinverse of A
$\stackrel{\text{def}}{=}$	Definition
i	Imaginary unit, $\mathrm{i}^2 = -1$
$\mathrm{Re}(a)$	Real part of variable a
$\mathrm{Im}(a)$	Imaginary part of variable a
$\overline{A}$, $\overline{a}$	Complex conjugate
$\ker A$	Kernel, right null space of A
$\mathrm{vec}\, A$	Column-wise vectorization of matrix A
$A \otimes B$	Kronecker product of matrices or vectors A and B
$\widehat{X}$	Estimate of variable X
$\mathbf{E}(X)$	Expected value of variable X
$\mathbf{E}_\theta(X(\mathcal{Y}))$	Expected value of variable X, where data $\mathcal{Y}$ corresponds to parameter θ
$\mathcal{N}(M, V)$	Normal distribution with mean M and (co-)variance V
$\mathbb{N}$, $\mathbb{R}$, $\mathbb{C}$	Set of natural, real, complex numbers
I_m	Identity matrix of size $m \times m$
$0_{m,n}$	Matrix of size $m \times n$ containing zeros

Variables

n	System order
r	Number of sensors
$r^{(\text{ref})}$, r_0	Number of reference sensors
x_k	System state at index k
y_k	System output at index k
A	State transition matrix
C	Output mapping matrix
$\mathcal{H}$	Subspace matrix
$\mathcal{J}$	Jacobian matrix
$\mathcal{O}$	Observability matrix

$\mathcal{O}^{\uparrow}$, $\mathcal{O}^{\downarrow}$	Matrices, where the last resp. first block row (usually containing r rows) of $\mathcal{O}$ are deleted
Σ	Covariance matrix
$\mathcal{Y}$	Data matrix or vector
N	Number of samples
N_s	Number of setups

Abbreviations

DOF	Degree of freedom
FEM	Finite element model
ILDL	Influence lines damage localization
OMA	Operational modal analysis
OMAX	Operational modal analysis with exogenous inputs
SHM	Structural health monitoring
SDDLV	Stochastic dynamic damage locating vector
SSI	Stochastic subspace identification
SVD	Singular value decomposition
UPC	Unweighted principal component algorithm (for data-driven SSI)

Part I

State of the Art

Chapter 1

State of the art

1.1 Introduction

Structure health monitoring techniques have been widely used in the damage assessment of beams, plates, bridges, buildings, etc, and is usually performed in two kinds of evaluation: destructive and nondestructive. Destructive evaluation of structures have usually high costs and is hard to be tacked. However, nondestructive evaluation of structures have been significantly increasing since it overcomes the problems of cost and due to its easy-of-use procedure. In this sense, nondestructive evaluation of structure is basically performed in four step [DFP$^+$96, Ryt93]: fault detection and isolation, damage quantification and time-life prediction of the structure.

This chapter is dedicated to the field of structural health monitoring and to the state of the art of some of the most used fault isolation (damage localization) approaches in the nondestructive evaluation paradigm.

1.2 Structural health monitoring and damage assessment

The process of implementing a damage detection and characterization strategy, in the field of control and civil engineering, is referred as Structural Health Monitoring (SHM) [Daw76]. In this context, damage is defined as changes to the material and/or geometric properties of a structural system, including changes to the boundary conditions and system connectivity, which adversely affect the systems performance. After extreme events, such as earthquakes or blast loading, SHM is used for rapid condition screening and aims to provide reliable information regarding the integrity of the structure.

The field of damage assessment for structures has a particularly extensive body of literature. As a critical component of the SHM process, damage detection methodologies have been subject of research for several decades both for mechanical and structural systems. In

the case of civil engineering, the process initially involves the observation of a structure over time using periodically spaced measurements. Subsequently, it requires the extraction of damage sensitive features from these measurements, and finally, the statistical analysis of these features to determine the current state of the structural system [FW07]. During this process, global and local structural properties are assessed on the basis of measured variables. Then, the structures are periodically supervised with the aim of minimizing the safety risk and of keeping the maintenance cost as low as possible. Farrar and Worden [FW07] presented a general discussion on the challenges related to damage identification and provided a historical overview for the SHM technology development including a variety of disciplines. The authors referred to SHM as the "big challenge" for the engineering community since significant developments implies multi disciplinary research efforts amongst fields such as structural dynamics, signal processing, computational hardware and statistical pattern recognition.

Another important reference in the SHM literature was presented in a series of reports by Los Alamos National Laboratory [DFP$^+$96, SFH$^+$04]. The first report includes an exhaustive survey of technical literature until the late 1990's, classifying the methods according to required measured data and analysis technique. It also categorizes the applications according to the type of structure analyzed (beams, trusses, plates, bridges etc.). The second report was presented as an update of the previous version and reviews the publications appearing in the technical literature between 1996 and 2001. It is organized following the definition of the statistical pattern recognition paradigm, namely as a four part process, which includes: Operational evaluation, data acquisition, feature extraction and statistical model development. The latest report contains a comparison of SHM algorithms applied to standard data sets obtained for an aluminum frame structure. It focuses mostly in the feature extraction/system identification techniques, namely the process of finding or identifying the modal parameters from vibration data.

1.3 Fault detection and isolation

The problem of fault detection and isolation (FDI) consists in detecting changes in the parameters of a dynamical system (detection) and distinguishing the changed parameters from the unchanged parameters (isolation). There are many FDI techniques originating from control. An overview can be found, for example, in the survey papers [Wil76, Fra90] or in the books [PFC89, BN93]. In general, these FDI problems are split in two steps: generation of residuals, which are ideally close to zero under no-fault conditions, minimally sensitive to noises and disturbances, and maximally sensitive to faults; and residual evaluation, namely design of decision rules based on these residuals [Bas98].

In many applications, the FDI problem is to detect and diagnose changes in the eigenstructure of a linear dynamical system. An important example is in SHM, where damages of civil, mechanical or aeronautical structures lead to a change in the eigenstructure of the underlying mechanical system and thus in the modal parameters. For example, Kirmser [Kir44] demonstrated that a crack in a beam has an influence on its natural frequencies. Rytter [Ryt93] defined a classification of these methods into four levels:

1. Damage detection,

2. Damage localization,

3. Damage quantification,

4. Prediction of the remaining service life of the investigated structure.

An overview of damage identification methods can be found in [DFP98, CF04]. Amongst them are the necessity of a comparison between two system states for the assessment of damage, or the necessity of feature extraction through signal processing and statistical classification to convert sensor data into damage information.

Since the aim of this thesis is focused in the damage localization field, which necessarily demands the damage detection, in the following section some of the most popular and current damage detection and localization approaches are introduced.

1.4 Damage localization approaches

1.4.1 Flexibility methods

In structural engineering, the flexibility method is the traditional procedure for computing member forces and displacements in structural systems. Its modern version formulated in terms of the members' flexibility matrices also has the name the matrix force method due to its use of member forces as the primary unknowns [Hib09].

A class of methods exploits changes in the flexibility matrix, which is the inverse of the stiffness matrix, for damage detection, localization and quantification. Pandey and Biswas [PB94] have shown that changes in the flexibility matrix can indicate the presence and location of damage, where the flexibility matrix is estimated from modal parameters of only a few lower frequency modes. Yan and Golinval [YG05] consider both changes in the flexibility and the stiffness for damage localization, where mass-normalized mode shapes are needed. Output-only localization methods based on the null space of the subspace-based data matrices have been investigated in [BMG04, BBM$^+$08].

Assuming that damage occurs, Bernal [Ber10] presents a damage localization technique using both finite element information and modal parameters, namely the Stochastic Dynamic Damage Location Vector (SDDLV) approach. This approach has evolved over the years from being restricted to input/output deterministic systems to handle output-only stochastic systems [Ber02, Ber06, Ber07, Ber10]. From estimates of the system matrices in both reference and damaged states, the null space of the difference between the respective transfer matrices is obtained. Then, damage is related to a residual derived from this null space and located where the residual is close to zero. A similar approach is also considered in [RDR10].

A complementary approach to the SDDLV is the Influence Lines Damage Localization (ILDL) [Ber13]. There, damage location is determined from the subspace angle of each position in the structure by computing the column space of the change in flexibility and a known FEM.

This thesis is focused in the works of Bernal [Ber10, Ber13], described above, as the basis for the damage localization development.

1.4.2 Genetic algorithms

In the field of Artificial Intelligence (AI), a Genetic Algorithm (GA) is a search heuristic that mimics the process of natural evolution. This heuristic (also called a metaheuristic) is routinely used to generate useful solutions to optimization and search problems [BNKF97]. In fact, GA belong to the larger class of evolutionary algorithms (EA), which generate solutions to optimization problems using techniques inspired by natural evolution, such as inheritance, mutation, selection, and crossover [RN09]. Among many application fields, GA find application in bioinformatics, computational science and engineering.

GA was first introduced in the 1960s by John Holland [Hol92] and developed in the engineering are by Goldberg's work [Gol89] for diverse optimization problems in civil engineering and structural identification [CPH03, KCL03]. Friswell and Penny [FP97] stated that GA have been seen as a promising choice for the solution of hard problems in damage identification. The great advantage in using GA is the ability in finding global minimum on a difficult optimization problem where there are many local minima as happens in damage location.

Sazonov et al. [CA79] used the GA to produce a sufficiently optimized amplitude characteristic filter to extract damage information from the strain energy mode shapes. There, a FEM was used to generate training data set with the known location. More recently, Gomes and Silva [GS08] developed a method using GA and a modal sensitivity to identify and evaluate damage cases in a parametric numerical finite element model, where GA is used as an optimization tool. Perera et al. [PRM07] developed a model updating method based on GA to locate damage and estimate its severity.

1.4.3 Modal strain energy

Strain is a description of deformation in terms of relative displacement of particles in the body [Bow09] and strain energy is released when the constituent atoms are allowed to rearrange themselves in a chemical reaction or a change of chemical conformation [TN04]. There, the deformation (also known as torsion strain) is the transformation of a body from a reference configuration (set containing the positions of all particles of the body) to a current configuration [TN04]. A deformation may be caused by external loads, body forces (such as gravity or electromagnetic forces), or temperature changes within the body [Wu04].

Modal strain energy has been widely used to quantify the participation of each element in particular vibrating mode and in the selection of a candidate set of elements for damage localization [LK94]. Hearn and Testa [Lin90] have illustrated that the ratio of the elemental strain energy to the total kinetic energy of the whole system is a fraction of the eigenvalue, and the ratio of this fraction for two different modes is dependent only on the location of the damage.

The change of modal strain energy in each structural element before and after the occurrence of damage can also be used for damage localization. In [SL98], the ratio of change in the modal strain energy is proposed for detecting the damage location. This parameter is based on the estimation of the change of modal strain energy in each element after the occurrence of damage. Information required in the identification are the measured mode shapes and elemental stiffness matrix only without knowledge of the complete stiffness and mass

matrices of the structure. *A priori*, no other information about the structure is required.

1.4.4 Neural networks

The research on Artificial Neural Networks (ANN) is considered to have started in 1943 with the paper written by Warren McCulloch and Walter Pitts [MP43]. They created a computational model for neural networks based on mathematics and algorithms. Since then, a rich literature in the field has risen with a strong concentration in the 80s and 90s. Several books, journals, articles and applied works have been dedicated to the development of the NN in different fields such as engineering, biology, pattern recognition, theoretical physics, applied mathematics, statistics, etc. Basically, an ANN is an interconnected group of natural or artificial neurons that uses a mathematical or computational model for information processing based on a connectionistic approach to computation [Hay98].

ANN offers capabilities such as self-adaptiveness, generalization, abstraction and suitability for applications in cases where algorithmic solutions are too complicated to be found and handled [BJ90, Meh97]. Sahin and Shenoi [SS03] developed an ANN combining global (changes in natural frequencies) and local (curvature mode shapes) vibration-based analysis data as inputs for an ANN for location and severity prediction of damage in a beam-like structures. There, artificial random noise has been generated numerically and added to noise-free data during the training of a trained feed-forward backpropagation ANN. Another damage localization approach was developed by González and Zapico [GZ08] where the inputs of the ANN are the first flexural modes (frequencies and mode shapes) at each principal direction of the structure and the outputs are the spatial variables (mass and stiffness).

1.4.5 Shape curvature

Mode shapes describe the configurations into which a structure will naturally displace. Typically, displacement patterns are of primary concern. Mode shapes of low-order mathematical expression tend to provide the greatest contribution to structural response. A normal mode of an oscillating (vibrating) system is a pattern of motion in which all parts of the system move sinusoidally with the same frequency and with a fixed phase relation. The frequencies of the normal modes of a system are known as its natural frequencies or resonant frequencies. Physical object, such as a building, bridge or molecule, has a set of normal modes that depend on its structure, materials and boundary conditions.

According to the process to treat the measured modal parameters, the vibration-based damage identification methods can be classified as model based and non-model based. The model-based methods identify damage by correlating an analytical model, which is usually based on the FEM, with test modal data of the damaged structure [HF95, ZK94, Doe96]. To detect the damage other than the artificial errors from the model construction, a good quality finite element model that could accurately depict the intact structure is required but is often difficult to achieve.

Non-model-based damage detection methods, also named as damage index methods, are relatively straightforward. The changes of modal parameters between the intact and damaged states of the structure are directly used, or correlated with other relevant information, to

develop the damage indicators for localizing damage in the structure [WL04]. Pandey et al. [PBS91] further demonstrated that changes in mode shape curvature could be a good indicator of damage for beam structures.

Some researchers found that the modal flexibility can be a more sensitive parameter than natural frequencies or mode shapes alone for structural damage on detection. Zhao and Dewolf [ZD99] presented a theoretical sensitivity study comparing the use of natural frequencies, mode shapes, and model flexibility for structural damage detection. Pandey and Biswas [PB94] proposed a damage localization method based on directly examining the changes in the measured modal flexibility of a beam structure. Lu et al. [LRZ02] pointed out that Pandeys method is difficult to locate multiple damages, and they recommended the modal flexibility curvature for multiple damage localization due to its high sensitivity to closely distributed structural damages.

Zhang and Aktan [ZA98] comparatively studied the modal flexibility and its derivative, called uniform load surface (ULS), for their truncation effect and sensitivity to experimental errors. They suggested that the ULS has much less truncation effect and is least sensitive to experimental errors. Wu and Law [WL04] describe a damage localization method based on changes in ULS curvature was developed. The proposed method requires only the frequencies and mode shapes of the first few modes of the plate before and after damage. When integrated with other techniques, such as the gapped-smoothing technique [Rat00], the proposed method does not require any prior information of the intact structure.

1.4.6 Wavelets

The development of wavelets can be linked to several separate trains of thought [Dau92, Add02, Kai10]. Historically, wavelets have started with Haar's work in the early 20th century. Later work by Dennis Gabor yielded Gabor atoms in 1946, which are constructed similarly to wavelets, and applied to similar purposes. Notable contributions to wavelet theory can be attributed to Zweigs discovery of the continuous wavelet transform in 1975, Pierre Goupillaud, Grossmann and Morlet's formulation of what is now known as the continuous wavelet transform (CWT) in 1982, Jan-Olov Strömberg's early work on discrete wavelets in 1983, Daubechies' orthogonal wavelets with compact support in 1988, Mallat's multiresolution framework in 1989, Akansu's binomial quadrature mirror filter (QMF) in 1990, Nathalie Delprat's time-frequency interpretation of the CWT in 1991, Newland's harmonic wavelet transform in 1993 and many others since.

The applicability of various wavelets for the detection and localization of damage in structures has been studied by Douka et al. [DLT03], Quek et al. [QWZA01] as well as Gentile and Messina [GM03] and Ovanesova and Suarez [OS04]. Hong et al. [HKLL02] and Douka et al. [DLT03] showed that the effectiveness of wavelets for damage localization is limited by the measurements precision and the sampling distances. They used the dynamic mode shapes extracted from the acceleration measurements.

In Rucka and Wilde [RW06] the estimated mode shapes of the beam structure are analysed by one-dimensional and two-dimensional continuous wavelet transform, where the location of the damage is indicated by a peak in the spatial variation of the transformed response. There, the proposed wavelet analysis can effectively identify the damage position without

knowledge of neither the structure characteristics nor its mathematical model.

Part II

Background Theory

Chapter 2

Dynamic models of structures and damage localization approaches

2.1 Introduction

The susceptibility of structures to vibrations is a prime design issue in mechanics, especially in the aerospace, automotive, maritime, railway, and heavy equipment industries. It is also of growing importance in civil engineering, as not only the slenderness of structures and structural members is continuously increasing, but also their dynamic loading, e.g., when due to traffic. The experimental verification of design values, in particular modal parameters (eigenfrequencies, damping ratios, mode shapes, and modal scaling factors), is essential for design and model validation, so for guaranteeing the safety and serviceability of the structure. It is also frequently employed for quality control and structural health monitoring (SHM) purposes. Damping and boundary conditions depend on the vibration amplitude and, if the structure moves as a whole or contains rotating parts, the modal parameters depend on the (rotation) speed (of the parts). Therefore, it is important that the experimental determination of the modal parameters of the structure is performed in normal operational conditions, i.e., around the operating point. This belongs to the domain of *Operational Modal Analysis* (OMA), were modal parameters are extracted from the dynamic response to (partly) unmeasured operational forces.

The damage characterization in some applications can be realized in two ways: either as an online verification (also called real time verification) or as an offline interrogation. Online verification algorithms are most often based on the analysis of residuals that reflect discrepancies between the outputs that a model predicts and the measured outputs. Localization is addressed by designing observers where the gain is selected to make the residual for each possible fault have particular directional characteristics [Fra90]. Offline strategies operate with data collected at two different times and offer information about changes in the structural

condition in the interval between the measurements [DFP$^+$96, Fri05]. In the offline situation, a model updating solution is conceptually straightforward but success has proven difficult in realistically sized problems due to poor conditioning [MF93, Fri07]. The difficulties in damage characterization can be ameliorated if the problem can be decoupled into detection, localization, and quantification [Ber13].

Several damage localization methods have been described in the literature [Ber02, Ber06, Ber07, Ber10, Ber13]. These methods can be applied in both input/output (i.e., when external excitation is known) or output-only cases. In the output-only case, two methods have been sucessfully used: the Stochastic Dynamic Damage Location Vector (SDDLV) approach [Ber10] and the Influence Line Damage Location (ILDL) approach [Ber13].

This chapter provides the theoretical background on dynamic models of structures in section 2.2 as well as the baselines of the SDDLV and ILDL approaches in sections 2.3 and 2.4.

2.2 Dynamic models of structures

Constructing a model of a dynamic system can be viewed as defining its behavior, i.e., restricting its time trajectories to a subset of a set of a priori possible trajectories by mathematical equations. The models that are studied in this section all define a Linear and Time-Invariant (LTI) behavior of the described vibrating structure. In reality, however, all structures are to some extent nonlinear and non-stationary. It should therefore be kept in mind that the LTI assumption, as well as any other modeling assumption, creates a misfit between the system and the model.

Excitation and response signals are almost never stored as continuous-time signals, but rather as sequences of sampled values. Sampling a continuous function $f(t)$ with time step T at $t = kT$, $k \in (0, 1, ..., N-1)$, boils down to selecting the image of kT under f. Mathematically, this process can be described by multiplying $f(t)$ by a series of Dirac impulses $\delta(t - kT)$

$$\sum_{k=0}^{N-1} f(t)\ \delta(t - kT) = \sum_{k=0}^{N-1} f(kT)\ \delta(t - kT).$$

The discretization is defined by a function that maps each term $f(kT)\ \delta(t-kT)$ of the sampled function onto an element of the sequence of sampled values (f_k) : $f(kT)\ \delta(t - kT) \mapsto f_k = f(kT)$. Conversely, if a sequence of discrete-time samples f_k is available, the inverse function may be used to construct an equivalent continuous-time sampled function

$$\sum_{k=0}^{N-1} f(t)\ \delta(t - kT) = \sum_{k=0}^{N-1} f_k\ \delta(t - kT). \tag{2.1}$$

Suppose the signal $f(t)$ is integrable. Its double-sided Laplace transform $f(s)$ is then defined as the image under

$$\mathbb{R} \ \rightarrow\ \mathcal{C}\ :\ f(t) \mapsto f(s) \stackrel{\text{def}}{=} \int_{\mathbb{R}} f(t)e^{-st}dt, \tag{2.2}$$

where $\int_{\mathbb{R}}$ denote the Lebesgue integral over $\mathbb{R}$. The Fourier transform $f(\omega)$ [Fou22] of the integrable function $f(t)$ is defined as the image under

$$\mathbb{R} \ \rightarrow \ \mathcal{C} \ : \ f(t) \mapsto f(\omega) \stackrel{\text{def}}{=} \int_{\mathbb{R}} f(t) e^{-i\omega t} dt,$$

It follows immediately that the Fourier transform equals the Laplace transform restricted to the imaginary axis: $f(\omega) = f(s)|_{s=i\omega}$. To construct the Laplace transform $f_d(s)$ of a discrete-time sequence (f_k), the equivalent continuous-time sampled function (2.1) is used:

$$f_d(s) \stackrel{\text{def}}{=} \int_{\mathbb{R}} \sum_{k=0}^{N-1} f_k \ \delta(t - kT) e^{-st} dt = \sum_{k=0}^{N-1} f_k e^{-kTs} dt.$$

The substitution $z = e^{Ts}$ yields the z-transform [Jur64] of the sequence (f_k):

$$f(z) \stackrel{\text{def}}{=} \sum_{k=0}^{N-1} f_k \ z^{-k}.$$

As a result, the Laplace transform of a sampled continuous-time function equals the z-transform of the equivalent discrete-time sequence (f_k). The Fourier transform $f_d(\omega)$ of (f_k) or its equivalent sampled function $\sum_{k=0}^{N-1} f_k \ \delta(t - kT)$ is obtained by restricting z to the unit circle or s to the imaginary axis, respectively:

$$f_d(\omega) \stackrel{\text{def}}{=} \sum_{k=0}^{N-1} f_k e^{-i\omega kT}, \tag{2.3}$$

where $f_d(\omega)$ is a continuous periodic function in ω with period $2\pi/T$.

Since $f_d(\omega)$ is periodic, its discrete counterpart can be obtained by sampling one period only. If again N samples are used, one has

$$\sum_{k=0}^{N-1} f_d(l\Omega) \ \delta(\omega - l\Omega) = \sum_{k=0}^{N-1} \sum_{l=0}^{N-1} f_k e^{-il\Omega kT} \ \delta(\omega - l\Omega),$$

where $\Omega = 2\pi/(NT)$. Discretization yields f_l^D, the Discrete Fourier Transform (DFT) [BH95] of (f_k):

$$f_l^D \stackrel{\text{def}}{=} \sum_{k=0}^{N-1} f_k e^{-il\Omega kT} = \sum_{k=0}^{N-1} f_k e^{-i\frac{2\pi kl}{N}}. \tag{2.4}$$

The Fast Fourier Transform (FFT) algorithm [CT65] offers a numerically efficient computation of the DFT.

The relation between the Fourier transform $f(\omega)$ of a continuous, integrable function $f(t)$ that is nonzero only for $t \in [0, (N-1)T]$ and the Fourier transform $f_d(\omega)$ of its sampled version is given by $f(\omega) = f_d(\omega)T$, $T \mapsto 0$. So for small T , one has $f(l\Omega) \approx f_l^D T$.

If both a function $f(t)$ and its Fourier transform $f(\omega)$ are integrable, their inverse relationship is given by

$$f(t) = \frac{1}{2\pi} \int_{\mathbb{R}} f(\omega) e^{i\omega t} d\omega.$$

For the time sequence (f_k) and its DFT f_l^D, the inverse relationship is

$$f_k = \frac{1}{N} \sum_{l=0}^{N-1} f_l^D e^{i\frac{2\pi kl}{N}}.$$

Very often, expressions in the Laplace domain for continuous-time system descriptions will be found to be very similar to expressions in the z-domain for the corresponding discrete-time system descriptions, with the only formal difference being the variable s or z. The symbol ζ will be used to denote either s or z.

Impulse response: Consider a structure with r output Degrees of Freedom (DOFs) and m input DOFs of interest. The element $h_{lb}(t)$ of its *Impulse Response Function* (IRF) $H(t) \in \mathbb{R}^{r\times m}$ is defined as the response at DOF l due to an impulsive input along DOF b, applied at $t = 0$ under zero initial conditions on the outputs. Once $H(t)$ is determined, the response $y(t)$ at the outputs due to any input vector $u(t) \in \mathbb{R}^m$ can be computed by convolution, since any $u(t)$ can be written as

$$u(t) = \int_{\mathbb{R}} \delta(t-\tau) u(\tau) d\tau,$$

so that, using the LTI assumption,

$$y(t) = \int_{\mathbb{R}} H(t-\tau) u(\tau) d\tau = \int_{\mathbb{R}} H(\tau) u(t-\tau) d\tau = H(t) \star u(t). \tag{2.5}$$

Because sampling an impulse is both physically and mathematically is undefined and thus impossible [Rey12], the impulse response $H_k \in \mathbb{R}^{r\times m}$ of a discrete system is defined as its response to the following input:

$$u_k = \begin{cases} 1, & k = 0, \\ 0, & k \neq 0. \end{cases}$$

Using the LTI assumption, it follows immediately that the response to an arbitrary input obeys

$$y_k = \sum_{l=-\infty}^{\infty} H_{k-l} u_l = \sum_{l=0}^{k} H_{k-l} u_l.$$

Transfer Function: Consider a damped harmonic input at DOF b, $u_b = e^{st}$ with $s \in \mathcal{C}$. Using (2.5), the response at DOF l can be computed as

$$y_l(t) = \int_{\mathbb{R}} H_{lb}(t-\tau) e^{s\tau} d\tau = \int_{\mathbb{R}} H_{lb}(t-\tau) e^{-s(t-\tau)} d\tau e^{st} = H_{lb}(s) e^{st},$$

where, using (2.2), $H(s) \in \mathcal{C}^{r\times m}$ is the Laplace transform of $H(t)$. The Laplace transform of the impulse response is called the transfer function. From the above analysis, it is clear that

$H(s)$ equals the systems response due to e^{st}, divided by e^{st}. Since the Laplace transform of a convolution equals the product of the Laplace transforms, it follows from (2.5) that

$$y(s) = H(s)u(s).$$

Similarly, the transfer function of a discrete system is defined as the z-transform $H(z)$ of its discrete impulse response (H_k), and the relationship $y(z) = H(z)u(z)$ holds. The zeros and poles of a continuous-time (discrete-time) system are defined as the values of ζ for which $det(H(\zeta))$ equals zero or goes to infinity, respectively [Kai80].

Linear equations of motion:

When a linear time-invariant (LTI) vibrating structure with general viscous damping can be described or approximated by a finite number of DOFs, its behavior is governed by the following system of second-order ordinary differential equations:

$$M\frac{d^2v(t)}{dt^2} + C^v\frac{dv(t)}{dt} + Kv(t) = B_3u(t), \tag{2.6}$$

where $v(t) \in \mathbb{R}^{n/2}$ is the vector with nodal displacements, $M \in \mathbb{R}^{n/2\times n/2}$, $C^v \in \mathbb{R}^{n/2\times n/2}$ and $K \in \mathbb{R}^{n/2\times n/2}$ are the mass, viscous damping, and stiffness matrices, respectively, and $B_3 \in \mathbb{R}^{n/2\times n_f}$ is a selection matrix such that the vector with externally applied forces, $u(t) \in \mathbb{R}^m$, has only elements that are not identically zero. Equation (2.6) is obtained when the structure consists of localized masses, springs and dampers, when the behavior of a continuum is approximated with a finite number of displacements and rotations as in the finite element method [Bat96, ZTZ05], or when the behavior of a continuum is approximated with a finite number of eigenmodes [Mei75]. Damping models other than viscous, such as hysteretic (structural) damping, or Coulomb (friction) damping, could also be considered. They fall outside the scope of this work, however.

Continuous-time state-space model: By rearranging (2.6) and assuming that M has full rank, a continuous-time state-space model

$$\frac{dx(t)}{dt} = A_cx(t) + B_cu(t), \tag{2.7}$$

where

$$x(t) = \begin{bmatrix} v(t) \\ \frac{dv(t)}{dt} \end{bmatrix}, \quad A_c = \begin{bmatrix} 0 & I \\ -M^{-1}K & -M^{-1}C^v \end{bmatrix}, \quad B_c = \begin{bmatrix} 0 \\ M^{-1}B_3 \end{bmatrix}$$

are obtained with the state vector of the structure $x(t) \in \mathbb{R}^n$, the state transition matrix $A_c \in \mathbb{R}^{n\times n}$ and the input influence matrix $B_c \in \mathbb{R}^{n\times m}$, where n is the system order and m is the number of inputs. The number of elements "n" of $x(t)$ is called the *model order*. When the state at $t = 0$ is known, the system of ordinary differential equations (2.7) can be solved for $x(t)$:

$$x(t) = e^{A_ct}x(0) + \int_{[0,t]} e^{A_c(t-\tau)}B_cu(\tau)d\tau. \tag{2.8}$$

If the output quantities of interest are linear combinations of displacement, velocity, or acceleration DOFs, one has

$$y(t) = C_{\ddot{v}}\frac{d^2v(t)}{dt^2} + C_{\dot{v}}\frac{dv(t)}{dt} + C_vv(t)$$

which can be expressed as

$$y(t) = [C_v - C_{\ddot{v}} M^{-1} K \vdots C_{\dot{v}} - C_{\ddot{v}} M^{-1} C^v] x(t) + C_{\ddot{v}} M^{-1} B_3 u(t)$$

and finally

$$y(t) = C_c x(t) + D_c u(t), \tag{2.9}$$

where $C_{\ddot{v}} \in \mathbb{R}^{r \times n}$, $C_{\dot{v}} \in \mathbb{R}^{r \times n}$ and $C_v \in \mathbb{R}^{r \times n}$ are selection matrices, $y(t) \in \mathbb{R}^r$ is the output vector, $C_c \in \mathbb{R}^{r \times n}$ is the output mapping matrix and $D_c \in \mathbb{R}^{r \times r}$ is the direct transmission matrix. Finite strains can be included in $y(t)$, since they can be obtained by dividing the difference between two displacement DOFs by the initial distance between their nodes [RDRBS07].

Using (2.7)–(2.9), a state-space parametrization of the impulse response is obtained:

$$H(t) = C_c e^{A_c t} B_c + D_c \delta(t).$$

A Laplace transform of both sides of (2.7) and (2.9) leads to a parametrization of a transfer function:

$$y(s) = (C_c (sI - A_c)^{-1} B_c + D_c) u(s) = H(s) u(s)$$

and following the Cramer's rule

$$(sI - A_c)^{-1} = \frac{adj(sI - A_c)}{det(sI - A_c)},$$

where $det(\bullet)$ denotes the determinant and $adj(\bullet)$ the adjoint matrix of a square matrix. Since $det(sI - A_c)$ is the characteristic polynomial of A_c, one has that, if all modes are observed in the output, $det(H(s)) \to \infty$ when s approaches an eigenvalue of A_c. Hence, the poles are the eigenvalues of A_c.

When the state is transformed to a new basis, $x \mapsto T^{-1} x$ with $T \in \mathcal{C}^{n \times n}$ nonsingular, the input-output map provided by the state-space description is preserved when $(A_c, B_c, C_c, D_c) \mapsto (T^{-1} A_c T, T^{-1} B_c, C_c T, D_c)$, as follows from (2.7), (2.9). In particular, when A_c has a similarity transform,

$$A_c = \Psi_c \Lambda_c \Psi_c^{-1},$$

with Λ_c a diagonal matrix, (2.7), (2.9) is decoupled by putting $T = \Psi_c$:

$$\frac{dx_m(t)}{dt} = \Lambda_c x_m(t) + B_c u(t)$$

$$y(t) = \Phi_c x_m(t) + D_c u(t)$$

where the subscript m denotes *modal* and Λ_c, Φ_c are the matrices containing the eigenvalues and mode shapes from A_c and C_c, respectively [PDR99].

Discrete-time state-space model: Since for a given input $u(t)$, solving (2.6) or (2.8) analytically is usually impossible in the time domain, it seems natural to convert these models to discrete time. The discrete-time state-space model is considered as

$$x_{k+1} = A x_k + B u_k \tag{2.10}$$

$$y_k = Cx_k + Du_k. \tag{2.11}$$

Different discretization strategies exist for converting (2.7), (2.9) into (2.10), (2.11), including numerical integration of the right-hand side of (2.7) using a forward, backward, or trapezoid rule, zero-pole matching, or assuming that the input is constant (i.e., equal to $u(kT)$) or linear in $[kT, (k+1)T)$, known as the zero-order-hold (ZOH) or first-order-hold assumptions, respectively [FPW98]. These discretization schemes generally do not preserve the state-space basis, and the direct transmission term is not preserved either: $D \neq D_c$.

However, when the inputs are identically zero, the system of equations (2.7), (2.9) is easily solved using (2.8):

$$x((k+1)T) = e^{A_c T} x(kT)$$

$$y(kt) = C_c x(kT).$$

This leads to an exact discretization, where $(A, C) = (e^{A_c T}, C_c)$, and where the state-space basis is preserved. When solving the inverse modal analysis problem by fitting a discrete-time state-space model (2.10)–(2.11) to measured sampled data, the inverse map therefore allows computing exact continuous-time equivalents of the discrete poles and mode shapes [Rey12].

In this context, it is tempting to make a zero-order hold (ZOH) assumption, since it follows from (2.8) that, when $u(t) = u(kT)$ in $[kT, (k+1)T)$, the following map is obtained:

$$A = e^{A_c T},$$

$$B = \int_{kT}^{(k+1)T} e^{A_c((k+1)T-\tau)} d\tau B_c = (A - I) A_c^{-1} B_c,$$

$$C = C_c, \quad D = D_c.$$

A proof for the second equality in the expression for B can be found in [Jua94]. The map is exact when $u(t) = 0$, and the direct transmission term D is preserved. However, due to the ZOH assumption, the input matrix B_c, that is computed through the inverse map, is not a good approximation of the true B_c when the sampling frequency is not much larger than twice the largest important frequency that is present in the spectra of the input and output signals.

The state equations (2.10)–(2.11) can be solved as

$$y_k = CA^k x_0 + \sum_{l=1}^{k} CA^{l-1} B u_{k-l} + Du_k.$$

from where the impulse response is then readily obtained as

$$H_0 = D, \quad H_k = CA^{k-1}B, \quad k > 1.$$

By taking the z-transform of both sides of (2.10)–(2.11), a parametrization of the transfer function is obtained:

$$y(z) = (C(zI - A)^{-1}B + D)u(z) = H(z)u(z)$$

and then, similarly to the continuous-time state-space model, it follows from Cramer's rule that the poles are the eigenvalues of A.

As in the continuous-time case, one has that the input-output map provided by the discrete-time state-space description is preserved when $(A, B, C, D) \mapsto (T^{-1}AT, T^{-1}B, CT, D)$. When A has a similarity transform,

$$A = \Psi_d \Lambda_d \Psi_d^{-1} \tag{2.12}$$

where Λ_d is a diagonal matrix, (2.10), (2.11) is decoupled by putting $T = \Psi_d$

$$x_{m,k+1} = \Lambda_d x_{m,k} + B u_k,$$

$$y_k = \Phi_d x_{m,k} + D u_k.$$

Measurement noise: To obtain a more realistic description for the measured input-output behavior of real structures, the electronic noise generated by the measurement system should be considered. Then, the excitation $u(t)$ previously described is splitted into two parts: a part that can be measured in an operational vibration test, and a part that can not be measured. Loads that can not be measured have to be identified together with the system, from the measured response. The concerned discipline is called *output-only system identification*, blind system identification or blind deconvolution [Rey12]. When identifying the input and the system at the same time, a problem of identifiability occurs: the system description cannot be determined unambiguously unless extra assumptions are made concerning the unknown inputs.

When a system is driven by a unmeasured and stochastic inputs that need to be identified, an assumption is to consider this system stationary, ergodic and with zero mean. Wide sense stationarity, which means that the covariance between two time samples depends only on the time difference, not on the time instances at which the samples were taken, and quadratic mean ergodicity, (i.e., ensemble averaging can be replaced by time averaging, are common assumptions) [Dou99]. The zero mean assumption holds exactly when the constant trend is removed from the outputs (hence also from the unmeasured inputs) and from the measured inputs. In this case, the covariance functions of the inputs and outputs equal their correlation functions.

A common assumption is that the stochastic unobserved input $u^s(t)$ is a white noise vector. *Continuous-time White Noise* (CWN) means that its correlation function is of the form [Dou99]

$$R_{u^s u^s}(\tau) = \mathcal{I}\delta(\tau) \tag{2.13}$$

with $\mathcal{I}$ the intensity of the CWN. When $u^s(t)$ is a force in N, $\mathcal{I}$ has dimensions N^2/Hz. Two samples of a CWN process are not correlated when they are taken at different time instances; and when they are taken at the same time instance, their variance is infinite. When $u^s(t)$ is a CWN process (i.e., (2.13) holds) its *Power Spectral Density* (PSD) equals

$$S_{uu}(s) = \mathcal{I}.$$

This means that the PSD of a CWN process is real and constant, and has an infinite bandwidth. The latter property is clearly not feasible for describing most physical processes.

Therefore, a *Band-limited Continuous-time White Noise* (BCWN) sequence $u^s(t)$ is defined as a random process that has a real and constant PSD within a finite frequency bandwidth $[-f_B, f_B]$ [Å70]:

$$S_{uu}(\omega) = \begin{cases} \frac{\tilde{\mathcal{I}}}{2f_B}, & |f| \leq f_B \\ 0 \ , & |f| > f_B \end{cases} .$$

When $u^s(t)$ is a force in N, $\tilde{\mathcal{I}}$ has dimensions N^2. The corresponding correlation function is found with the inverse Fourier transform:

$$R_{u^s u^s}(\tau) = \tilde{\mathcal{I}} sinc(2\pi f_B \tau),$$

then

$$R_{u^s u^s}(0) = \tilde{\mathcal{I}}.$$

The sampled, stationary stochastic input sequence (u_k^s) is said to be a zero-mean *Discrete-time White Noise* (DWN) sequence when its correlation function obeys [Dou99]

$$R_{u^s u^s, j} = \epsilon(u_{k+j}^s u_k^{sT}) = \begin{cases} \text{cov}(u_k^s), & j = 0 \\ 0 \ , & j \neq 0 \end{cases} ,$$

where cov denotes the covariance operator. From (2.4), one has that the discrete PSD of (u_k^s), which is defined as the DFT of $R_{u^s u^s, j}$, obeys

$$S_{u^s u^s, j} = R_{u^s u^s, 0}.$$

Using (2.3), it follows that the discrete and continuous PSD of (u_k^s) are equal, even for a non-infinitesimal sampling period T. Therefore, if CWN is filtered with an ideal anti-alias filter with cut-off frequency $2/T$ and then sampled with sampling frequency $1/T$, the resulting sequence is a DWN sequence.

Based on this fact, it was shown in [PSG08] that if the unmeasured forces are indeed BCWN, a continuous-time model should preferably be identified, since then the measured output DFT is exactly related to the unmeasured force DFT by a continuous-time model, i.e., no discretization error is made despite the data sampling. However, most system identification algorithms identify discrete-time models.

Continuous combined deterministic-stochastic state-space model: When the observed outputs $y(t)$ are corrupted by additive sensor noise, denoted as $y^n(t) \in \mathbb{R}^r$, and when unobserved stochastic inputs $u^s(t) \in \mathbb{R}^{n_u^s}$ are present, the state-space model (2.7), (2.9) can be extended to

$$\frac{dx(t)}{dt} = A_c x(t) + B_c u(t) + w(t), \tag{2.14}$$

$$y(t) = C_c x(t) + D_c u(t) + v(t), \tag{2.15}$$

where

$$w(t) \stackrel{\text{def}}{=} B_c^s u^s(t),$$

$$v(t) \stackrel{\text{def}}{=} D_c^s u^s(t) + y^n(t),$$

$$B_c^s = \begin{bmatrix} 0 \\ M^{-1}B_4 \end{bmatrix}$$

and

$$D_c^s = C_{\ddot{v}} M^{-1} B_4$$

with $B_4 \in \mathbb{R}^{n/2 \times n_u^s}$ a selection matrix.

Discrete combined deterministic-stochastic state-space model: Applying for instance one of the discretization schemes listed in the beginning of this chapter, (2.14)–(2.15) can be converted to

$$x_{k+1} = Ax_k + Bu_k + w_k, \tag{2.16}$$

$$y_k = Cx_k + Du_k + v_k, \tag{2.17}$$

When it is assumed that the samples of $y^n(t)$, and $u^s(t)$ make up discrete-time white noise sequences, w_k and v_k are DWN sequences as well:

$$\epsilon \left(\begin{bmatrix} w_{k+l} \\ v_{k+l} \end{bmatrix} \begin{bmatrix} w_k \\ v_k \end{bmatrix}^T \right) = \begin{bmatrix} Q & S \\ S^T & R \end{bmatrix} \delta_1(l)$$

where $\delta_1(\bullet)$ is the unit impulse function, i.e., $\delta_1(0) = 1$ and $\delta_1(\bullet) = 0$ if $\bullet \neq 0$. With the decomposition of the states and outputs in a deterministic and a stochastic part,

$$x_k = x_k^d + x_k^s,$$

$$y_k = y_k^d + y_k^s,$$

and (2.16)–(2.17) is decomposed in a deterministic system

$$x_{k+1}^d = Ax_k^d + Bu_k,$$

$$y_k^d = Cx_k^d + Du_k,$$

and a stochastic subsystem

$$x_{k+1}^s = Ax_k^s + w_k, \tag{2.18}$$

$$y_k^s = Cx_k^s + v_k. \tag{2.19}$$

Just as for the deterministic subsystem, the eigenvalue decomposition of A, (2.12), decouples the stochastic subsystem:

$$x_{m,k+1}^s = \Lambda_d x_{m,k}^s + w_{m,k},$$

$$y_k^s = \Phi_d x_{m,k}^s + v_{m,k},$$

where $w_{m,k} = \Psi_d^{-1} w_k$.

Correlation matrices: The following definitions of correlation matrices of the stochastic subsystem (2.18)–(2.19) and the relationships between them are very frequently used, both in solving forward and inverse problems:

$$\Sigma^s \stackrel{\text{def}}{=} \epsilon(x_{k+1}^s \; x_{k+1}^{sT}) = A\Sigma^s A^T + Q,$$

$$G \stackrel{\text{def}}{=} \epsilon(x_{k+1}^s y_k^{sT}) = A\Sigma^s C^T + S,$$

$$\Lambda_l \stackrel{\text{def}}{=} \epsilon(y_{k+l}^s y_k^{sT}),$$

$$= \begin{cases} C\Sigma^s C^T + R, & l = 0 \\ CA^{l-1}G, & l > 0 \\ G^T(A^{l-1})^T C^T, & l < 0 \end{cases},$$

where, as before, stationarity and ergodicity of all stochastic sequences was assumed as well as the fact that x_k is independent of w_k and v_k, which follows immediately from (2.16)–(2.17) [Rey12].

2.3 The Stochastic Dynamic Damage Location Vector (SDDLV) approach

The SDDLV approach [Ber10] is an output-only damage localization method based on interrogating changes $\delta G(s)$ in the transfer matrix $G(s)$ of a system, performed between two data sets: one from the undamaged (reference) state and another from the damaged state. Vectors in the null space of $\delta G(s)$ are obtained from system identification results using output-only measurements of both states. Then, they are applied as *load vectors* to a FEM for the computation of a *stress field* over the structure in order to indicate the damage location, since it has been shown that damaged elements induce zero stress (or close to zero in practice) [Ber02, Ber06, Ber07, Ber10]. To gain robustness in this localization approach, the stress field is computed for different values of the Laplace variable s of the transfer matrix, and the results are aggregated. This section summarizes the deterministic computation of the stress field and the aggregation of the results.

2.3.1 Models and parameters

First, vectors in the null space of $\delta G(s)$ are computed using output-only measurements of the structure. The behavior of a mechanical structure is assumed to be described by a linear time-invariant (LTI) dynamical system as in (2.6) with $M, C, K \in \mathbb{R}^{d\times d}$ as the mass, damping and stiffness matrices respectively collected by the displacements of the d degrees of freedom (DOF) of the structure, where the external force $u(t)$ is unmeasured and modeled as white noise.

Then, let the system (2.6) be observed at r coordinates (the outputs). As $u(t)$ is unmeasured, it can be replaced with a fictive force $e(t) \in \mathbb{R}^r$ acting only in the measured coordinates and that re-produce the measured output. The corresponding *continuous-time state-space model* from equations (2.7) and (2.9) is

$$\begin{cases} \frac{dx(t)}{dt} = A_c x + B_c e \\ y(t) = C_c x + D_c e \end{cases}, \tag{2.20}$$

where only system matrices A_c and C_c can be obtained from output-only system identification. Matrices B_c and D_c in model (2.20) are only relevant for the following developments.

2.3.2 Influence matrix derivation

Matrices A_c and C_c can be obtained from output measurements, as outlined previously. However, input influence matrix B_c is related to noise inputs e, and is consequently unknown. An expression for B_c as a function of the direct transmission matrix is derived in the following lines using matrices that are known in the output-only identification.

Consider the output equation of model (2.20), where $y(t)$ is the output. Depending on the used sensors, y can be measured displacements $\eta(t)$, velocities $\frac{dy(t)}{dt}$ or accelerations $\frac{d^2y(t)}{dt^2}$, which makes a difference for the following derivations. Then, the output equations for displacement (dis), velocity (vel) or acceleration (acc) measurements are

$$y(t) = C_c^{\text{dis}} x, \tag{2.21}$$

$$\frac{dy(t)}{dt} = C_c^{\text{vel}} x, \tag{2.22}$$

$$\frac{d^2y(t)}{dt^2} = C_c^{\text{acc}} x + D_c e, \tag{2.23}$$

where C_c^{dis}, C_c^{vel}, and $C_c^{\text{acc}} \in \mathbb{R}^{r\times n}$ are the respective output mapping matrices. Differentiating (2.21) and (2.22) and combining the result with $\frac{dx(t)}{dt}$ from (2.20) leads to [Ber10]

$$C_c A_c^{-b} B_c = 0, \tag{2.24}$$

$$C_c A_c^{1-b} B_c = D_c, \tag{2.25}$$

where C_c is the output mapping matrix for either displacement, velocity, or acceleration and $b = 0$, 1 or 2 depending on whether the measured output y is displacement, velocity, or acceleration. Equations (2.24) and (2.25) can be combined as

$$HB_c = LD_c,$$

where $H \in \mathbb{R}^{2r\times n}$ and $L \in \mathbb{R}^{2r\times r}$ are given by

$$H \overset{\text{def}}{=} \begin{bmatrix} C_c A_c^{1-b} \\ C_c A_c^{-b} \end{bmatrix}, \; L \overset{\text{def}}{=} \begin{bmatrix} I \\ 0 \end{bmatrix}. \tag{2.26}$$

Then, it follows

$$B_c = H^{\dagger} L D_c,$$

where † denotes the Moore-Penrose pseudoinverse. To ensure that the pseudoinverse provides a unique solution in a least square sense it is necessary to ensure that $2r \geq n$. Note that in practice this is often an inactive constraint since the number of identified modes n is, in fact, less than 2 times the number of measurements.

2.3.3 Damage localization strategy

Depending on the kind of output measurements $y(t)$ (displacements, velocities, or accelerations; $b \overset{\text{def}}{=} 0, 1, 2$, respectively), the transfer matrix $G(s) \in \mathcal{C}^{r\times r}$ of system (2.20) can be expressed without the input influence matrix B_c for $2r \geq n$ as

$$G(s) \overset{\text{def}}{=} R(s) D_c, \quad \text{with} \quad R(s) \overset{\text{def}}{=} C_c A_c^{-b} (sI - A_c)^{-1} H^{\dagger} L \tag{2.27}$$

as derived in detail in [Ber06, Ber10], where I denotes the identity matrix and H and L are defined in (2.26). With the property $(A^{-b})^\dagger = A^b$ and the relation $A_c^{-b}(sI - A_c)^{-1}A_c^b = (sI - A_c)^{-1}$, the expression for $R(s)$ in (2.27) is equivalent to

$$R(s) = C_c(sI - A_c)^{-1} \begin{bmatrix} C_cA_c \\ C_c \end{bmatrix}^\dagger \begin{bmatrix} I \\ 0 \end{bmatrix}, \tag{2.28}$$

which is a helpful simplification and generalization. Equation (2.28) holds for displacement, velocity and acceleration measurements at the same time.

Let the variables in (2.27) be given in the damaged (variables with tilde) and reference states, respectively. The difference in the transfer matrices between both states is $\delta G(s) = \tilde{G}(s) - G(s)$. Then, assuming $\delta D_c = \tilde{D}_c - D_c = 0$ (corresponding to no mass change) and D_c being invertible, the matrices $\delta G(s)$ and $\delta R(s)^T = \tilde{R}(s)^T - R(s)^T$ have the same null space [Ber10]. Thus, the desired load vector can be equivalently found in the *null space* of $\delta R(s)^T$, which can be obtained from the Singular Value Decomposition (SVD)

$$\delta R(s)^T = U\Sigma V^H = \begin{bmatrix} U_1 & U_2 \end{bmatrix} \begin{bmatrix} \Sigma_1 & 0 \\ 0 & \Sigma_2 \end{bmatrix} \begin{bmatrix} V_1 & V_2 \end{bmatrix}^H, \tag{2.29}$$

where $U, \Sigma, V \in \mathcal{C}^{r\times r}$, $\Sigma_2 \approx 0$ and ^{H} denotes the conjugate transpose. The desired load vector $v(s)$ in the null space of $\delta R(s)^T$ can be chosen as any linear combination of the vectors in V_2, in particular as the vector corresponding to the smallest singular value. Note that only output-only measurement data is necessary for the computation of an estimate of $v(s)$.

The computation of the stress from the (dynamic) load vector $v(s)$ implies knowledge of FEM of the structure. Let d be the number of its DOFs let e be the number of stresses that are computed at the elements of the FEM. First, define the sensor mapping matrix $P \in \mathbb{R}^{d\times r}$, containing zeros and ones, where the column and the row of an entry 1 relate to a sensor position and its corresponding degree of freedom (DOF) in the model, respectively. From the load $Pv(s)$ at all DOF's the displacement $G_{\text{model}}(s)Pv(s)$ can be computed, where $G_{\text{model}}(s) \stackrel{\text{def}}{=} (Ms^2 + Cs + K)^{-1}$ is the transfer matrix from the FEM in the reference state. Finally, stress (or stress resultants) are computed at the elements of the FEM from the displacements. The function corresponding to this operation is linear and denoted by the matrix $Q \in \mathbb{R}^{e\times d}$, which is usually obtained from a FEM software. Combining the operations, the stress vector $S(s) \in \mathcal{C}^e$ that is computed from the load vector $v(s)$ can be expressed as [Ber10]

$$S(s) = \mathcal{L}_{\text{model}}(s)v(s) \tag{2.30}$$

where $\mathcal{L}_{\text{model}}(s) \stackrel{\text{def}}{=} Q\, G_{\text{model}}(s)\, P \in \mathcal{C}^{e\times r}$ is entirely obtained from the FEM of the structure. Theoretically, the components of the stress vector $S(s)$ corresponding to a damaged element are zero [Ber02, Ber10] and hence entries in $S(s)$ close to zero indicate potentially (but not necessarily) damaged elements. In practice these stresses are not exactly zero but small due to modal truncation, model errors and uncertainties from the measurement data. Note that while the load vector $v(s)$ is only defined at the sensor coordinates, damage can be localized at any element of the structure because the stress vector generated from $v(s)$ covers the full domain.

2.3.4 Multiple stress vectors and aggregation

Since damaged elements lead to stress values that are (close to) zero, but zero stress does not necessarily indicate damage [Ber02] on one side, and due to truncation and model errors on the other side, it is recommended to compute the load vector $v(s)$ and subsequently the stress vector $S(s)$ for several values of the Laplace variable s. Robustness of the damage localization approach is then achieved by aggregating the results.

Let the Laplace variables s_i, $i = 1, \ldots, \kappa$, be given. To minimize modal truncation errors, they should be chosen within a vicinity of the identified poles of the structure in the complex plane, but not too close to them [Ber10]. After the identification of the system matrices A_c and C_c in the reference and $\tilde{A}_c$ and $\tilde{C}_c$ in the damaged states, the computations (2.28)–(2.30) are repeated for each value s_i to obtain the respective stress vectors $S(s_i)$.

To decide if an element is damaged, the information of the corresponding entries in the stress vector $S(s_i)$ for all $i = 1, \ldots, \kappa$ can be used now. In [Ber10] the aggregation

$$\bar{S}_j = \sum_{i=1}^{\kappa} |S_j(s_i)| \tag{2.31}$$

for each entry j was suggested.

2.4 The Influence Lines Damage Localization (ILDL) approach

An influence line (IL) is a function that graphs the variation at a specific point on a mechanical structure in a predefined direction caused by a unit load [Hib09]. Any discontinuity in that predefined direction represents a potential damaged location in the displacement field. In this sense, the difference in the displacement field between the reference (undamaged) and damaged states can be viewed as a discontinuity, leading to potentially damaged locations [Ber13].

It is shown in [Ber13] that if a structure is loaded by some arbitrary static distribution and damage appears, while the load remains constant, then the change in the deformation field, given some assumptions on the nature of the damage, will be identical to that due to the action of a stress resultant acting on a discontinuity at the damage location. From this result and the previous argument it is concluded that the change in the deformation field due to the damage has the shape of the IL for the stress resultant at the location of the damage, and the deformation field is in the span of the ILs for multiple damage locations.

The step that completes the logical sequence in ILDL is to note that the image of the change in flexibility matrix $\delta F = \tilde{F} - F$ between damaged and reference states (variables with and without tilde) is the span for all possible differences in the displacement field due to damage. Thus the image of δF is identical to the span of the influence lines associated with all the damaged locations. In the implementation of the ILDL strategy δF and the influence lines only need to be evaluated at the sensor coordinates of the structure.

Therefore, damage localization based on the ILDL theorem consists of computing the ILs of stress resultants at the sensor coordinates for all elements from a finite element model

(FEM) that will be checked for damage, and computing the image of δF from output-only measurement data. The localization itself is performed by checking each element of the FEM if its respective IL lies in the image of δF. The ILDL does not directly specify the position of the damage. Instead, it provides a scheme to decide, given any postulated damage position, if it is correct or not.

Note that the ILDL approach is complementary to the Stochastic Dynamic Damage Location Vector (SDDLV) approach [Ber10], as detailed in 2.3, where loads in the kernel of δF are applied to a FEM to compute the stress field and damage is localized where the stress is (close to) zero.

2.4.1 Models, parameters and flexibility matrix

Similarly to subsection 2.3, the behavior of a structure is assumed to be described by a linear time-invariant (LTI) dynamical system (2.6) and the equivalent continuous-time state-space model is such as in (2.20), where the state vector of the structure is $x(t) \in \mathbb{R}^n$, $y(t) \in \mathbb{R}^r$ is the output vector, the state transition matrix is $A_c \in \mathbb{R}^{n\times n}$ and $C_c \in \mathbb{R}^{r\times n}$ is the output mapping matrix. The parameter n is the system order and parameter r is the number of outputs. Remember that only matrices A_c and C_c can be obtained from output-only system identification. The input influence matrix $B_c \in \mathbb{R}^{n\times r}$ and the direct transmission matrix $D_c \in \mathbb{R}^{r\times r}$ are used for theoretical purposes.

The flexibility matrix F cannot be obtained from output-only data since system matrices B_c and D_c are not available. However, not the change in flexibility δF itself is needed for the ILDL, but only the image of δF, which can be obtained only from A_c and C_c in the damaged and reference states as follows [Ber13]. By applying the same transfer matrix in (2.28)

$$R(s) = C_c(sI - A_c)^{-1} \begin{bmatrix} C_c A_c \\ C_c \end{bmatrix}^{\dagger} \begin{bmatrix} I \\ 0 \end{bmatrix}$$

and assuming that damage does not change the mass of the system ($D = \tilde{D}$) and that D is invertible, it follows that $\delta F = \delta R D$ (with $\delta R = \tilde{R} - R$) and thus that the image of δF is the same as the image of δR.

Then, the *image* of δR is obtained from the Singular Value Decomposition (SVD)

$$\delta R = U\Sigma V^H = \begin{bmatrix} U_1 & U_2 \end{bmatrix} \begin{bmatrix} \Sigma_1 & 0 \\ 0 & \Sigma_2 \end{bmatrix} \begin{bmatrix} V_1 & V_2 \end{bmatrix}^H, \tag{2.32}$$

where $U, \Sigma, V \in \mathcal{C}^{r\times r}$, $\Sigma_1 > 0$ and $U = (u_1, \ldots, u_r) = [U_1 \quad U_2]$ the left singular vectors. Note that U_1: $(u_1, u_2, ..., u_t)$ correspond to the nonzero singular values Σ_1, and U_2: $(u_{t+1}, u_{t+2}, ..., u_r)$ correspond to the zero singular values (in practice small) Σ_2, where a desired image of δR is the matrix (or vector depending on the rank of Σ) in U_1. For any chosen value s, matrix U_1 in the image of $\delta F(s)$ can be computed as described above, where only model (2.20) has been used without information about the geometry of the structure.

2.4.2 Influence line computation and damage localization

Although either the ILDL or the SDDLV methods suffice to extract all the information for the damage locations computation in theory, in real situations the flexibility change δR is approximated and the use of both methods can prove advantageous [Ber13]. In fact, practical implementation of the SDDLV method demands decision on the effective dimension of the null space and specific guidelines for this and other implementation issues appear in the [Ber10]. The desired load vector in the null space of (2.32) for the SDDLV is any linear combination of vectors in V_2. Since the rank is usually low, U_1 is related to less noisy information and the image in the ILDL method can provide more precise information to find damaged locations in the structure [Ber13].

Such as in 2.3.3, let $v(s)$ be any load vector at the sensor coordinates of the structure. From such a load stress resultants can be computed from a FEM. The relation between loads $v(s)$ and the vector of stress resultants $S(s)$ at the desired elements is linear and can be described by a matrix model $L_{\text{model}}(s)$ obtained from the FEM, such that model $S(s) = L_{\text{model}}(s)v(s)$.

For the ILDL approach the IL of each stress resultant in $S(s)$ is required at the sensor coordinates. Thus, applying the respective unit loads at the sensor coordinates to obtain the influence for an element j (corresponding to an entry $S_j(s)$ in vector $S(s)$), it is clear that the jth row $l^T_{j(s)}$ of model $L_{\text{model}}(s)$ is the IL of the stress resultant for element j, which is denoted by the column vector $l_j(s)$.

Damage localization with the ILDL approach consists then of checking if an IL l_j (computed from the FEM) is contained in the subspace U_1 (computed from the data in [Ber13]) for each element. The quantity used in [Ber13] that measures how well $l_j(s)$ fits into the image U_1 is the subspace angle

$$\theta_j = \cos^{-1} \left\| \left(\frac{(l_j(s))^H U_1}{\|l_j(s)\|} \right) \right\| \tag{2.33}$$

where $\theta_j = 0$ indicates the perfect fit. If j is a damaged element, θ_j will be close to zero. Since the subspace angle is not derivable at $\theta_j = 0$ for the subsequent sensitivity analysis for uncertainty quantification, the alternative quantity

$$\Gamma_j(s) = \frac{\|(l_j(s))^H \ U_1\|^2}{\|l_j(s)\|^2} \tag{2.34}$$

is proposed as an indicator of a fit. Note that $0 \leq \Gamma_j(s) \leq 1$, where $\Gamma_j(s) = 0$ indicates orthogonality between the subspaces and $\Gamma_j(s) = 1$ indicates the perfect fit.

2.4.3 Multiple aggregation

As an extension from [Ber13] to aggregate multiple quantities $\Gamma_j(s)$ in (2.34), consider that different Laplace variables s_i, $i = 1, \ldots, \kappa$, be given. To minimize modal truncation errors, they should be chosen within a vicinity of the identified poles of the structure in the complex plane, but not too close to them [Ber10]. After the identification of the system matrices A_c and C_c in the reference and $\tilde{A}_c$ and $\tilde{C}_c$ in the damaged states, the computations (2.28),

(2.32) and (2.34) are repeated for each value s_i to obtain the respective vectors $\Gamma(s_i)$. Following the instructions in [Ber10] to decide if an element is damaged, the information of the corresponding entries in the stress vector $\Gamma(s_i)$ for all $i = 1, \ldots, \kappa$ can be used in the aggregation

$$\bar{\Gamma}_j = \sum_{i=1}^{\kappa} \Gamma_j(s_i) \tag{2.35}$$

for each element j.

Chapter 3

System identification and uncertainty quantification

3.1 Introduction

Early research in modal testing resulted in an approach later described as *Experimental Modal Analysis* (EMA). In EMA, the structure is excited by one or several measured dynamic forces. Then, the response of the structure to these forces is recorded and the modal parameters in the frequency range of interest are extracted from the measurements. The first EMA techniques were Single Degree Of Freedom (SDOF) methods like Peak Picking (PP) or Circle Fitting [KP47]. An early review of SDOF techniques is presented in [BG63]. It is assumed in these methods that each mode can be estimated independently from the other modes, and consequently they are not useful when some modes of interest are closely spaced. This disadvantage was later removed with the introduction of Multiple Degree Of Freedom (MDOF) methods for EMA. Nowadays EMA is a well-established and often-used approach in mechanical engineering [HLS97, MS97, Ewi00].

EMA methods are in general not suitable for large structures as these are often inherently tested in operational rather that in laboratory conditions and the contribution of the measured excitation to the total structural response is usually low (e.g. A bridge cannot be isolated from its environment and tested in the laboratory, and it can only be excited to a limited vibration level when compact, practical actuators are used). This implies that the ever-present ambient excitation, also called operational loading, due to for example wind or traffic, can most often not be neglected. *Output-only* or *Operational Modal Analysis* (OMA) techniques have therefore been developed where the modal parameters are extracted from the dynamic response to operational forces [RHDR12]. There, ambient forces are usually modeled as stochastic quantities with unknown parameters but with known behavior, for instance, as white noise time series with zero mean and unknown covariance.

The OMA approach has two disadvantages when compared to EMA: the mode shapes can not be scaled in an absolute way and the frequency content of the excitation is usually narrow-banded. For these reasons, there has been an increasing interest during the last few years towards combined modal testing techniques, also called hybrid vibration testing or *Operational Modal Analysis with eXogenous inputs* (OMAX) [GDTDDS06], where an artificial force is used in operational conditions. The main difference between OMAX and the traditional EMA approach is that the operational forces are included in the identified system model: they are not considered as noise but as useful excitation. As a consequence, the amplitude of the artificial forces can be equal to, or even lower than the amplitude of the operational forces. This is of crucial importance for the modal testing of large structures. It allows to use actuators that are small and practical when compared to the ones needed for EMA testing of such structures, which are heavy and difficult to transport.

The modal analysis process consists of three distinct steps: data collection; system identification; and extracting and validating a set of modal parameters. The collection and preprocessing of the data are not treated explicitly herean overview of standard techniques is given in [HLS97, MS97, Ewi00]. System Identification can be defined as the field where mathematical models are estimated from measured data. The identified model can be parametric, in which case it contains a limited number of parameters like the matrix entries of a state-space model, or nonparametric, in which case the system is described in tabulated form, for instance as numerical Frequency Response Function (FRF) data.

System identification and modal analysis developed mainly along different paths. Modal analysis has its roots in mechanical engineering and focused originally on the identification of SDOF systems, which contain one mode only, but which can have multiple outputs or even multiple inputs while system identification has its roots in electrical and mathematical engineering and focused originally on the identification of systems that have a single input and a single output, but that can have multiple modes. Control of dynamic "systems" in the broad sense was historically the first motive for developing system identification algorithms, because of the need for an accurate model of the system to be controlled.

With the exception of realization algorithms [JP85], the interaction between the research fields of system identification and modal testing remained limited, chiefly because the main concern in modal testing was computational efficiency, as tens to hundreds of outputs need to be processed at the same time, while the main concern in system identification was the statistical performance of the methods. This changed gradually from the late 1980s on, partly due to the increasing computational power that became available, and partly because OMA, where a structure is tested in operational rather than in laboratory conditions, became an active field of research. With the development of operational modal analysis, the advantages of using system identification methods that can deal well with the high "noise" levels that are met in operational conditions, became clear [PDR01]. However, the interaction between both research domains remains rather low.

In the context of system identification, the stochastic subspace-based system identification methods are efficient tools for the identification of linear time-invariant systems (LTI), fitting a linear model to input/output or output-only measurements taken from a system. The excitation of the system is assumed to be noise with certain properties. In 1985, Benveniste and Fuchs [BF85] proved that the Instrumental Variable (IV) method and what was called the

Balanced Realization method for linear system eigenstructure identification are consistent under (unmeasured) non-stationary excitation. This result was obtained before Van Overschee and De Moor [VODM96] introduced their own formalism and popularized subspace methods in their data-driven form. Since then, the family of subspace algorithms is growing in size and popularity [Lar83, VODM94, Ver94, Vib95, MAL96], mostly for its capacity to deal with problems of large scale under realistic excitation assumptions. In [BM07], many subspace algorithms from literature are put in a common framework and their non-stationary consistency for eigenstructure identification is proven.

Concerning the theoretical properties of subspace methods, there are a number of convergence studies in a stationary context in the literature, see [DPS95, BDS99, BL02, Pin02, CP04b, CP04c, Bau05] to mention just a few of them. These papers provide deep and technically difficult results including convergence rates. They typically address the problem of identifying the system matrices or the transfer matrix, i.e. both the pole and zero parts of the system.

There is a broad range of applications of subspace algorithms in the identification of processes in automatic control, see e.g. [BNSR98, JSL01, SPG03, Pan08]. During the last decade, subspace methods found a special interest in mechanical, civil and aeronautical engineering for the identification of *vibration modes* (eigenvalues) and *mode shapes* (corresponding eigenvectors) of structures. Therefore, identifying an LTI from measurements is a basic service in vibration monitoring, see e.g. [HdAH99, MBG03, MBB$^+$06].

In this chapter, the theoretical background of subspace-based system identification is introduced from literature, on which the subsequent chapters are based. This chapter is organized as follows. In section 3.2, the general subspace identification algorithm is presented and examples of popular identification algorithms are given in section 3.3. In section 3.4, derivations for subspace identification algorithms under uncertainties is explained.

3.2 The general Stochastic Subspace Identification (SSI) algorithm

Consider LTI systems described by a discrete-time state-space model such as in (2.16) and (2.17)

$$\begin{cases} x_{k+1} &= Ax_k + Bu_k + w_{k+1} \\ y_k &= Cx_k + Du_k + v_k \end{cases} \tag{3.1}$$

with the state $x \in \mathbb{R}^n$, the observed input $u \in \mathbb{R}^m$, the output $y \in \mathbb{R}^r$ and the unobserved input and output disturbances w and v. The matrices $A \in \mathbb{R}^{n\times n}$ and $C \in \mathbb{R}^{r\times n}$ are the state transition and observation matrices, respectively. The parameter n denotes the system order and r the number of observed outputs, which is usually the number of sensors.

Throughout this work, we are interested in identifying only the system matrices A and C. In many cases, e.g. in Operational Modal Analysis, no observed inputs are available ($B = 0$, $D = 0$) and identification is done using the output-only data (y_k). When some inputs (u_k) are observed, combined deterministic-stochastic subspace identification algorithms can be used. There exist many Stochastic Subspace Identification algorithms in the literature, see

e.g. [VODM96, PDR99, BM07] and the related references for an overview. They all fit in the following general framework for the identification of the system matrices A and C of system (2.20) and its eigenstructure.

Denote a matrix $\mathcal{H}_{p+1,q}$ as subspace matrix, whose estimate $\widehat{\mathcal{H}}_{p+1,q}$ is built from the output or input/output data of the system (3.1) according to a chosen subspace algorithm. The subspace matrix enjoys the factorization property

$$\mathcal{H}_{p+1,q} = W\mathcal{O}_{p+1}\mathcal{Z}_q \tag{3.2}$$

into the matrix of observability

$$\mathcal{O}_{p+1} \stackrel{\text{def}}{=} \begin{bmatrix} C \\ CA \\ \vdots \\ CA^p \end{bmatrix} \in \mathbb{R}^{(p+1)r\times n},$$

and a matrix $\mathcal{Z}_q$, with an invertible weighting matrix W depending on the selected subspace algorithm. However, W is the identity matrix for many subspace algorithms.

Note that a subset of the r sensors can be used for reducing the size of the matrices in the identification process, see e.g. [PDR99, RDR08]. These sensors are called projection channels or reference sensors. Let r_0 be the number of reference sensors ($r_0 \leq r$). The parameters p and q are chosen such that $pr \geq qr_0 \geq n$. The subspace matrix has $(p+1)r$ rows and in many cases qr_0 columns.

The observation matrix C is then found in the first block-row of the observability matrix $\mathcal{O}_{p+1}$. The state transition matrix A is obtained from the shift invariance property of $\mathcal{O}_{p+1}$, namely as the least squares solution of

$$\mathcal{O}_{p+1}^{\uparrow}A = \mathcal{O}_{p+1}^{\downarrow}, \text{ where } \mathcal{O}_{p+1}^{\uparrow} \stackrel{\text{def}}{=} \begin{bmatrix} C \\ CA \\ \vdots \\ CA^{p-1} \end{bmatrix}, \ \mathcal{O}_{p+1}^{\downarrow} \stackrel{\text{def}}{=} \begin{bmatrix} CA \\ CA^2 \\ \vdots \\ CA^{p} \end{bmatrix} \tag{3.3}$$

and $\mathcal{O}_{p+1}^{\uparrow}, \mathcal{O}_{p+1}^{\downarrow} \in \mathbb{R}^{pr\times n}$.

Let the pairs (λ, ϕ_λ) be the eigenvalues and eigenvectors of matrix A and define the mode shape φ_λ with

$$\det(A - \lambda I) = 0, \quad A\phi_\lambda = \lambda\phi_\lambda, \quad \varphi_\lambda = C\phi_\lambda. \tag{3.4}$$

Assume that the system has no multiple eigenvalues and, thus, that the λ's and φ_λ's are pairwise complex conjugate. In particular, 0 is not an eigenvalue of state transition matrix A. The collection of pairs $(\lambda, \varphi_\lambda)$ form a canonical parameterization (invariant w.r.t. changes in the state basis) of the pole part of system (3.1), which is referred to as the system eigenstructure.

The actual implementation of this generic subspace identification algorithm uses a consistent estimate $\widehat{\mathcal{H}}_{p+1,q}$ obtained from the output or input/output data according to the selected

subspace identification algorithm. The SVD

$$\widehat{\mathcal{H}}_{p+1,q} = \begin{bmatrix} \widehat{U}_1 & \widehat{U}_0 \end{bmatrix} \begin{bmatrix} \widehat{\Delta}_1 & 0 \\ 0 & \widehat{\Delta}_0 \end{bmatrix} \begin{bmatrix} \widehat{V}_1^T \\ \widehat{V}_0^T \end{bmatrix} \tag{3.5}$$

and its truncation at the model order n yields an estimate

$$\widehat{\mathcal{O}}_{p+1} = \widehat{W}^{-1} \widehat{U}_1 \widehat{\Delta}_1^{1/2} \tag{3.6}$$

for the observability matrix, from which $(\widehat{C}, \widehat{A})$ and $(\widehat{\lambda}, \widehat{\varphi}_\lambda)$ are recovered as sketched above. Also, the estimate $\widehat{\mathcal{Z}}_q = \widehat{\Delta}_1^{1/2} \widehat{V}_1^T$ can be obtained. Note that the singular values in $\widehat{\Delta}_1$ are non-zero and $\widehat{\mathcal{O}}_{p+1}$ is of full column rank.

3.3 Popular SSI algorithms

Two well-known output-only subspace identification algorithms are covariance-driven subspace identification [BF85] and the data-driven Unweighted Principal Component algorithm [VODM96]. Here, they are defined using a subset of the recorded sensors at some point in the computation, so-called *reference sensors* or *projection channels* [PDR99], in order to reduce the computation effort.

Let $N + p + q$ be the number of available samples and let $y_k^{(\mathrm{ref})} \in \mathbb{R}^{r_0}$ $(r_0 \leq r)$ be the vector containing the reference sensor data, which is a subset of y_k for all samples. Then, define the data matrices

$$\mathcal{Y}^+ \stackrel{\mathrm{def}}{=} \frac{1}{\sqrt{N}} \begin{bmatrix} y_{q+1} & y_{q+2} & \vdots & y_{N+q} \\ y_{q+2} & y_{q+3} & \vdots & y_{N+q+1} \\ \vdots & \vdots & \vdots & \vdots \\ y_{q+p+1} & y_{q+p+2} & \vdots & y_{N+p+q} \end{bmatrix}, \; \mathcal{Y}^- \stackrel{\mathrm{def}}{=} \frac{1}{\sqrt{N}} \begin{bmatrix} y_q^{(\mathrm{ref})} & y_{q+1}^{(\mathrm{ref})} & \vdots & y_{N+q-1}^{(\mathrm{ref})} \\ y_{q-1}^{(\mathrm{ref})} & y_q^{(\mathrm{ref})} & \vdots & y_{N+q-2}^{(\mathrm{ref})} \\ \vdots & \vdots & \vdots & \vdots \\ y_1^{(\mathrm{ref})} & y_2^{(\mathrm{ref})} & \vdots & y_N^{(\mathrm{ref})} \end{bmatrix}. \tag{3.7}$$

For *covariance-driven* subspace identification, let $R_i \stackrel{\mathrm{def}}{=} \mathbf{E}(y_k y_{k-i}^{(\mathrm{ref})T})$ and the block Hankel matrix

$$\mathcal{H}_{p+1,q}^{\mathrm{cov}} \stackrel{\mathrm{def}}{=} \begin{bmatrix} R_0 & R_1 & \dots & R_{q-1} \\ R_1 & R_2 & \dots & R_q \\ \vdots & \vdots & \ddots & \vdots \\ R_p & R_{p+1} & \dots & R_{p+q-1} \end{bmatrix} \stackrel{\mathrm{def}}{=} \mathrm{Hank}(R_i) \tag{3.8}$$

be the theoretical output-correlation and subspace matrices for some parameters p and q. Then, introducing the cross-correlation between the state and the outputs $G \stackrel{\mathrm{def}}{=} \mathbf{E}(x_k y_k^{(\mathrm{ref})T})$, the correlations R_i yield $R_i = CA^iG$. In factorization property (3.2) W is the identity matrix and

$$\mathcal{Z}_q = \mathcal{C}_q(A, G) \stackrel{\mathrm{def}}{=} \begin{bmatrix} G & AG & \dots & A^{q-1}G \end{bmatrix} \tag{3.9}$$

is the well-known controllability matrix. From the output data (y_k), the empirical correlations can be estimated from

$$\widehat{R}_i = \frac{1}{N-i} \sum_{k=i+1}^{N} y_k y_{k-i}^{(\mathrm{ref})T}, \tag{3.10}$$

which are used to fill the estimate of the subspace matrix $\widehat{\mathcal{H}}_{p+1,q}^{\mathrm{cov}} \overset{\mathrm{def}}{=} \mathrm{Hank}(\widehat{R}_i)$ as in (3.8). Another variant of this algorithm uses the subspace matrix

$$\widehat{\mathcal{H}}_{p+1,q}^{\mathrm{covdat}} \overset{\mathrm{def}}{=} \mathcal{Y}^{+}\mathcal{Y}^{-T} \tag{3.11}$$

instead of $\widehat{\mathcal{H}}_{p+1,q}^{\mathrm{cov}}$ [BM07].

For the *Unweighted Principal Component* (UPC) algorithm, the estimate of the subspace matrix is defined as

$$\widehat{\mathcal{H}}_{p+1,q}^{\mathrm{UPC}} \overset{\mathrm{def}}{=} \mathcal{Y}^{+}\mathcal{Y}^{-T}(\mathcal{Y}^{-}\mathcal{Y}^{-T})^{\dagger}\mathcal{Y}^{-}, \tag{3.12}$$

where † denotes the pseudoinverse. Then, factorization property (3.2) holds asymptotically for $N \to \infty$ where W is the identity matrix and $\mathcal{Z}$ the Kalman filter state matrix [GVL96, KSH99]. A numerically efficient and stable way to obtain an estimate of the observability matrix avoids the explicit computation of $\widehat{\mathcal{H}}_{p+1,q}^{\mathrm{UPC}}$. Instead, the partitioning of the LQ decomposition [GVL96] of

$$\begin{bmatrix} \mathcal{Y}^{-} \\ \mathcal{Y}^{+} \end{bmatrix} = \begin{bmatrix} R_{11} & 0 \\ R_{21} & R_{22} \end{bmatrix} \begin{bmatrix} Q_1 \\ Q_2 \end{bmatrix} \tag{3.13}$$

is used, from which the relation $\widehat{\mathcal{H}}_{p+1,q}^{\mathrm{UPC}} = R_{21}Q_1$ follows. As Q_1 is an orthogonal matrix, the estimate of the observability matrix $\widehat{\mathcal{O}}_{p+1}$ can be obtained directly from R_{21} in the implementation of the algorithm. In this sense, the subspace matrix can also be defined by

$$\widehat{\mathcal{H}}_{p+1,q}^{\mathrm{UPC},R} \overset{\mathrm{def}}{=} R_{21},$$

where R_{21} is obtained from (3.13).

3.4 Uncertainty Quantification

As explained in Sections 2.3 and 2.4, Chapter 2, the system matrices A_c and C_c are needed for the damage localization in both the reference and damaged state of the system. When estimated from a finite number of data samples (e.g. using Stochastic Subspace Identification (SSI) methods [VODM96, PDR99]), not the "true" system matrices A_c and C_c are obtained, but estimates $\widehat{A}_c$ and $\widehat{C}_c$ of the matrices of the reduced order model that represents the identified bandwidth. As the input of system (2.20) is unmeasured noise, $\widehat{A}_c$ and $\widehat{C}_c$ are naturally subject to variance errors depending on the data and the estimation method. A variance analysis of the system matrices obtained from Stochastic Subspace Identification is made e.g. in [CP04a] and expressions for their computation in the context of structural vibration analysis are given in [RPDR08, DLM11].

There are number of reasons why the SSI does not yield the exact system matrices (A_c, C_c), but only estimates $(\hat{A}_c, \hat{C}_c)$. From the statistical point of view, there are three types of errors:

1. Bias of the model: The identified system may contain not only modes of the system under test, but also spurious modes.
2. Bias of the modes: The identified modes of the true system might be biased.
3. Variance of the modes: The modes of the identified system may be subject to variance errors.

While some procedures exist to remove part of the bias errors, the variance errors can only be estimated, but not removed. In the following, the uncertainty propagation is done by a sensitivity analysis of the covariances of the system matrices, based on the works of [PGS07, RPDR08]. The latter depend on the used system identification method and are assumed to be provided for the system matrices A_c and C_c of the *continuous-time* system (2.20).

3.4.1 Definitions

The following notation and properties are defined and will be used in the following sections. The operator $\otimes$ denotes the Kronecker product, having the property $\mathrm{vec}(AXB) = (B^T \otimes A)\mathrm{vec}(X)$. I_a denotes the identity matrix of size $a \times a$, and $0_{a,b}$ denotes the zero matrix of size $a \times b$. $e_j^a \in \mathbb{R}^a$ denotes the j-th unit vector (being column j of I_a). The permutation matrix $\mathcal{P}_{a,b} \stackrel{\text{def}}{=} \begin{bmatrix} I_a \otimes e_1^b & I_a \otimes e_2^b & \dots & I_a \otimes e_b^b \end{bmatrix} \in \mathbb{R}^{ab \times ab}$ is defined with the property

$$\mathrm{vec}(X^T) = \mathcal{P}_{a,b}\,\mathrm{vec}(X) \tag{3.14}$$

for any matrix $X \in \mathbb{R}^{a \times b}$ [DM13]. Finally, for dealing with the uncertainties of complex-valued matrices we introduce an equivalent real-valued notation by defining

$$M_{\mathrm{Re}} \stackrel{\text{def}}{=} \begin{bmatrix} \mathrm{Re}(M) & -\mathrm{Im}(M) \\ \mathrm{Im}(M) & \mathrm{Re}(M) \end{bmatrix}, \quad M_{\mathrm{re}} \stackrel{\text{def}}{=} \begin{bmatrix} \mathrm{Re}(M) \\ \mathrm{Im}(M) \end{bmatrix} \tag{3.15}$$

for any matrix M as in [PGS07]. Then, for example, a complex-valued equation $Ax = b$ is equivalent to $A_{\mathrm{Re}}\, x_{\mathrm{re}} = b_{\mathrm{re}}$, and the sensitivities of the real-valued matrices can be derived.

3.4.2 Sensitivities on singular values and singular vectors

The perturbation propagation to singular values and singular vectors for real and complex numbers are presented here, based in [PGS07].

Real case: Let $\sigma_i > 0$, u_i and v_i be the i-th singular value, left and right singular vector of some real matrix $X \in \mathbb{R}^{a,b}$ and ΔX a small perturbation on X. For the same X, then

$$\Delta\sigma_i = (v_i \otimes u_i)^T \mathrm{vec}(\Delta X), \quad \begin{bmatrix} \Delta u_i \\ \Delta v_i \end{bmatrix} = B_i^{\dagger} C_i \mathrm{vec}(\Delta X),$$

where

$$B_i \stackrel{\text{def}}{=} \begin{bmatrix} I_a & \frac{-X}{\sigma_i} \\ \frac{-X^T}{\sigma_i} & I_b \end{bmatrix}, \; C_i \stackrel{\text{def}}{=} \frac{1}{\sigma_i} \begin{bmatrix} v_i^T \otimes (I_a - u_i u_i^T) \\ (u_i^T \otimes (I_b - v_i v_i^T))\mathcal{P}_{a,b} \end{bmatrix},$$

I_n is identity matrix of size $n \times n$ and $\mathcal{P}_{a,b}$ is defined in Definition 3.4.1.

Complex case: Let $\sigma_i > 0$, $\tilde{u}_i$ and $\tilde{v}_i$ be the i-th singular value, left and right singular vector of some complex matrix $X \in \mathcal{C}^{a,b}$ with $t = \operatorname{rank}(X)$, and ΔX a small perturbation. In the SVD

$$X = U\Sigma V^H = \sum_{i=1}^{r} \sigma_i \tilde{u}_i \tilde{v}_i^H = \sum_{i=1}^{r} \sigma_i (\mathrm{e}^{\mathrm{i}\phi_i}\tilde{u}_i)(\mathrm{e}^{\mathrm{i}\phi_i}\tilde{v}_i)^H,$$

let the phase ϕ_i be chosen such that the imaginary part of the first entry of $\mathrm{e}^{\mathrm{i}\phi_i}\tilde{v}_i$ is zero and denote the respective left and right singular vectors by $u_i = \mathrm{e}^{\mathrm{i}\phi_i}\tilde{u}_i$, $v_i = \mathrm{e}^{\mathrm{i}\phi_i}\tilde{v}_i$. Then, perturbations on the singular vectors yield

$$\begin{bmatrix} \Delta(u_i)_{\mathrm{re}} \\ \Delta(v_i)_{\mathrm{re}} \end{bmatrix} = B_i^{\dagger} C_i \, (\operatorname{vec}(\Delta X))_{\mathrm{re}},$$

where

$$B_i \overset{\text{def}}{=} \begin{bmatrix} I_{2a} & \frac{(-X)_{\mathrm{Re}}}{\sigma_i} \\ \frac{(-X^T)_{\mathrm{Re}}}{\sigma_i} & I_{2b} \end{bmatrix} (I_{4r} - E^{4r,4r}_{3r+1,3r+1}),$$

$$C_i \overset{\text{def}}{=} \frac{1}{\sigma_i} \begin{bmatrix} (v_i^T \otimes I_a)_{\mathrm{Re}} - (u_i)_{\mathrm{re}}((\overline{v}_i \otimes u_i)_{\mathrm{re}})^T \\ ((u_i^T \otimes I_b)_{\mathrm{Re}} - (v_i)_{\mathrm{re}}((\overline{u}_i \otimes v_i)_{\mathrm{re}})^T)P_1 \end{bmatrix},$$

$$P_1 \overset{\text{def}}{=} \begin{bmatrix} \mathcal{P}_{a,b} & 0 \\ 0 & -\mathcal{P}_{a,b} \end{bmatrix}.$$

Note that the multiplication by $(I_{4r} - E^{4r,4r}_{3r+1,3r+1})$ sets the column in B_i to zero that corresponds to the imaginary part of the first entry of v_i.

3.4.3 Covariance estimation of identified discrete-time system matrices

The covariance estimation of the matrices A and C is done in three steps: First, a perturbation $\Delta\mathcal{H}$ of the subspace matrix in (3.8) is propagated to a perturbation $\Delta\mathcal{O}$ of the observability matrix, and second, a perturbation $\Delta\mathcal{O}$ is propagated to perturbations ΔA and ΔC in the system matrices. Finally, the covariances of the vectorized system matrices are computed. In order to obtain $\Delta\mathcal{O}$, the sensitivities of the singular values and vectors in (3.5) are necessary. They have been derived in [PGS07] and are detailed in [DM13].

The sensitivity of the observability matrix is derived in [RPDR08] and the perturbation $\Delta\mathcal{O} = U_1\Delta\Sigma_1^{1/2} + \Delta U_1 \Sigma_1^{1/2}$. Let B_i and C_i be given like in Section 3.4.2. Then,

$$\operatorname{vec}(\Delta\mathcal{O}) = \mathcal{J}_{\mathcal{O},\mathcal{H}} \operatorname{vec}(\Delta\mathcal{H})$$

where $\mathcal{J}_{\mathcal{O},\mathcal{H}} \in \mathbb{R}^{(p+1)rn\times(p+1)rqr}$ with

$$\mathcal{J}_{\mathcal{O},\mathcal{H}} \stackrel{\text{def}}{=} \frac{1}{2}\left(I_n \otimes U_1\Sigma_1^{-1/2}\right) S_4 \begin{bmatrix} (v_1 \otimes u_1)^T \\ \vdots \\ (v_n \otimes u_n)^T \end{bmatrix} + \left(\Sigma_1^{1/2} \otimes \begin{bmatrix} I_{(p+1)r} & 0_{(p+1)r\times qr} \end{bmatrix}\right) \begin{bmatrix} B_1^\dagger C_1 \\ \vdots \\ B_n^\dagger C_n \end{bmatrix},$$

$$S_4 \stackrel{\text{def}}{=} \sum_{k=1}^{n} E^{n^2,n}_{(k-1)n+k,k}, \quad (3.16)$$

Now, let the system matrix A be obtained from $\mathcal{O}$ in (3.3) and C from the first block row of $\mathcal{O}$ from Section 3.2. Then, a perturbation in $\mathcal{O}$ is propagated to A and C where sensitivity of the system matrices are collected by [RPDR08]

$$\operatorname{vec}(\Delta A) = \mathcal{J}_{A,\mathcal{O}} \operatorname{vec}(\Delta\mathcal{O}), \quad \operatorname{vec}(\Delta C) = \mathcal{J}_{C,\mathcal{O}} \operatorname{vec}(\Delta\mathcal{O}),$$

with $\mathcal{J}_{A,\mathcal{O}} \in \mathbb{R}^{n^2\times(p+1)rn}$, $\mathcal{J}_{C,\mathcal{O}} \in \mathbb{R}^{rn\times(p+1)rn}$, and

$$\begin{aligned} \mathcal{J}_{A,\mathcal{O}} &\stackrel{\text{def}}{=} (I_n \otimes \mathcal{O}^{\uparrow\dagger} S_2) - (A^T \otimes \mathcal{O}^{\uparrow\dagger} S_1) + ((\mathcal{O}^{\downarrow T} S_2 - A^T \mathcal{O}^{\uparrow T} S_2) \otimes (\mathcal{O}^{\uparrow T}\mathcal{O}^{\uparrow})^{-1})\mathcal{P}_{(p+1)r,n}, \\ \mathcal{J}_{C,\mathcal{O}} &\stackrel{\text{def}}{=} I_n \otimes \begin{bmatrix} I_r & 0_{r,pr} \end{bmatrix}. \end{aligned} \quad (3.17)$$

Note that the product rule for the sensitivity of $A = \mathcal{O}^{\uparrow\dagger}\mathcal{O}^{\downarrow} = (\mathcal{O}^{\uparrow T}\mathcal{O}^{\uparrow})^{-1}\mathcal{O}^{\uparrow T}\mathcal{O}^{\downarrow}$ and Kronecker algebra leads to the assertion. Note also that $\mathcal{J}_{A,\mathcal{O}} = \mathcal{A}_1$ and $\mathcal{J}_{C,\mathcal{O}} = \mathcal{A}_2$ in [RPDR08].

Finally, the covariances of the estimated system matrices $(\widehat{A}, \widehat{C})$ are obtained from

$$\Sigma_{\widehat{A},\widehat{C}} \stackrel{\text{def}}{=} \operatorname{cov}\left(\begin{bmatrix} \operatorname{vec}(\widehat{A}) \\ \operatorname{vec}(\widehat{C}) \end{bmatrix}\right) = \begin{bmatrix} \mathcal{J}_{\widehat{A},\mathcal{O}} \\ \mathcal{J}_{\widehat{C},\mathcal{O}} \end{bmatrix} \mathcal{J}_{\mathcal{O},\mathcal{H}}\, \widehat{\Sigma}_{\mathcal{H}}\, \mathcal{J}_{\mathcal{O},\mathcal{H}}^T \begin{bmatrix} \mathcal{J}_{\widehat{A},\mathcal{O}}^T & \mathcal{J}_{\widehat{C},\mathcal{O}}^T \end{bmatrix}, \quad (3.18)$$

where $\widehat{\Sigma}_{\mathcal{H}}$ is the covariance of (3.8) such that

$$\widehat{\Sigma}_{\mathcal{H}} = \frac{1}{n-1}\sum_{j=1}^{n} \operatorname{vec}\left(\widehat{\mathcal{H}}^{(j)} - \widehat{\mathcal{H}}\right) \operatorname{vec}\left(\widehat{\mathcal{H}}^{(j)} - \widehat{\mathcal{H}}\right)^T.$$

An efficient covariance estimation $\widehat{\Sigma}_{\mathcal{H}}$ of the subspace matrix can be obtained like in [DM13].

3.4.4 Covariance of the identified modal parameters

The sensitivity derivations for the eigenvalues and eigenvectors of a matrix and subsequently for the modal parameters are stated in [RPDR08] and its detailed derivations are in [GVL96, PGS07].

Let λ_i, ϕ_i and χ_i be the i-th eigenvalue, left eigenvector and right eigenvector of A with

$$A\phi_i = \lambda_i\phi_i, \quad \chi_i^* A = \lambda_i \chi_i^*, \quad (3.19)$$

where * denotes the complex conjugate transpose. Their respective sensitivities are

$$\Delta\lambda_i = \mathcal{J}_{\lambda_i,A}\text{vec}(\Delta A), \quad \Delta\phi_i = \mathcal{J}_{\phi_i,A}\text{vec}(\Delta A),$$

where $\mathcal{J}_{\lambda_i,A} \in \mathbb{C}^{1\times n^2}$ and $\mathcal{J}_{\phi_i,A} \in \mathbb{C}^{n\times n^2}$ are described as

$$\mathcal{J}_{\lambda_i,A} \stackrel{\text{def}}{=} \frac{1}{\chi_i^*\phi_i}(\phi_i^T \otimes \chi_i^*), \quad \mathcal{J}_{\phi_i,A} \stackrel{\text{def}}{=} (\lambda_i I_n - A)^\dagger \left(\phi_i^T \otimes \left(I_n - \frac{\phi_i\chi_i^*}{\chi_i^*\phi_i}\right)\right). \tag{3.20}$$

Now, let λ_i and ϕ_i be the i-th eigenvalue and left eigenvector of A be transformed into their equivalent continuous-time eigenvalue that $\lambda_i^c \stackrel{\text{def}}{=} \ln(\lambda_i)/\tau$ (τ as the time step). Then, the i-th eigenvalue sensitivity $\Delta\lambda_i^c$ is described as

$$\Delta\tilde{\lambda}_i^c = \mathcal{J}_{\lambda_i^c,A}\Delta\lambda_i$$

where

$$\mathcal{J}_{\lambda_i^c,A} = \frac{1}{\Delta t\,|\lambda_i|^2}\begin{bmatrix} \text{Re}(\mathcal{J}_{\lambda_i}) & \text{Im}(\mathcal{J}_{\lambda_i}) \\ -\text{Im}(\mathcal{J}_{\lambda_i}) & \text{Re}(\mathcal{J}_{\lambda_i}) \end{bmatrix}. \tag{3.21}$$

Now, suppose that the element k of the mode shape φ_i is scaled to unity (i.e. $\varphi_i = C\phi_i/(C\phi_i)_k$). Then, its sensitivity is described as

$$\Delta\varphi_i = \mathcal{J}_{\varphi_i,A,C}\begin{bmatrix}\text{vec}(\Delta A)\\ \text{vec}(\Delta C)\end{bmatrix},$$

where $\mathcal{J}_{\varphi_i,A,C} \in \mathbb{C}^{r\times(n^2+rn)}$ is

$$\mathcal{J}_{\varphi_i,A,C} \stackrel{\text{def}}{=} \frac{1}{(C\phi_i)_k}\left(I_r - \begin{bmatrix}0_{r,k-1} & \varphi_i & 0_{r,r-k}\end{bmatrix}\right)\begin{bmatrix}C\mathcal{J}_{\phi_i,A} & \phi_i^T \otimes I_r\end{bmatrix}. \tag{3.22}$$

Finally, the covariances of the eigenvalues and the mode shapes can be obtained, respectivelly, using (3.18), (3.20), (3.21) and (3.22) as

$$\begin{aligned}\widehat{\Sigma}_{\lambda_i^c} &= (\mathcal{J}_{\lambda_i^c}\mathcal{J}_{\lambda_{i,A}})_{\text{Re}} \;\; \widehat{\Sigma}_A \;\; ((\mathcal{J}_{\lambda_i^c}\mathcal{J}_{\lambda_i,A})_{\text{Re}})^T, \\ \widehat{\Sigma}_{\varphi_i,A,C} &= (\mathcal{J}_{\varphi_i,A,C})_{\text{re}} \;\; \widehat{\Sigma}_{A,C} \;\; ((\mathcal{J}_{\varphi_j,A,C})_{\text{re}})^T.\end{aligned} \tag{3.23}$$

Part III

Contributions

Chapter 4

Statistical decision making for damage localization with stochastic load vectors

This Chapter is dedicated to the first contribution of this thesis, consisting on the innovative development of a new statistical decision making method for damage localization in civil structures, based on the sensitivity-based rules (Chapter 3, Section 3.4) to overcome the inherent uncertainties in the Stochastic Dynamic Damage Location Vector (SDDLV) approach (Chapter 2, Section 2.3) and restricted for only one chosen Laplace variable. The new method is validated in a numerical simulation of a truss experiment.

4.1 Introduction

The SDDLV approach [Ber10] is an output-only damage localization technique that uses both finite element information and modal parameters, assuming that some damage has occurred. From estimates of the system matrices in both reference and damaged states, the null space of the difference between the respective transfer matrices is obtained. Then, damage is related to a residual derived from this null space and located where the residual is close to zero.

On one hand, these SDDLV does not take into account the intrinsic uncertainty of the problem due to the unknown noise exciting the system. The lack of uncertainty consideration proves to be critical considering no information is available on the choice of threshold for deciding whether the lowest residual is zero or not in practical situations. Empirical thresholds are currently used for decision. On the other hand, the identification of system matrices is afflicted by uncertainty, due to noise and limited data length. Sensitivity based methods such as presented in [PGS07] and [RPDR08] provide some guidelines to derive uncertainty estimates for modal parameters. An efficient sensitivity computation of these quantities has

been derived in [DM11, DLM11].

The current Chapter aims to replace empirical rules by sensitivity-based rules for applying some damage localization criterion, and is organized as follows. In Section 4.2 the SDDLV approach is introduced as a method for stochastic damage localization of mechanical structures from output-only signals. In Section 4.3, the covariance of the system matrices is propagated to the damage localization residuals and a hypothesis test is derived to test if an element is potentially damaged or not. In Section 4.4, numerical examples are provided. Finally, some conclusions of this work are presented in Section 4.5.

4.2 The SDDLV approach

The considered damage localization strategy, described in details in Chapter 2 (Section 2.3), is based on the works of [Ber06, Ber10] and is performed by interrogating changes in the transfer matrix G of a system. These changes δG are linked to physical properties of the structure. A structural failure is indicated by losses of *stiffness* (resistance of deformation of an elastic body to an applied force) and the consequent damage in some part (specific element or region) of the structure, affecting the *flexibility* of the system, which is linked to δG.

The change δG in the transfer matrix cannot be obtained experimentally using ambient vibration data recorded at the monitored structure. However, the null space of δG can be computed. *Load vectors* in this null space are then used for the computation of a *stress field* over the structure in order to indicate the damage location: *Stresses* are measures of internal reactions to external forces applied on a deformable body, where (in the method to be described) zero stress over elements of a structure indicates changes in the flexibility and consequently damage. The resulting damage localization method is the SDDLV method [Ber06, Ber10]. In this section, the underlying models and the basic principles of the SDDLV are introduced.

4.2.1 Dynamical equation and state-space model

The behavior of a mechanical structure is assumed to be described by a linear time-invariant (LTI) system and represented by the corresponding *continuous-time state-space model* (2.20)

$$\left\{ \begin{array}{rcl} \frac{dx(t)}{dt} & = & A_c x + B_c e \\ y & = & C_c x + D_c e \end{array} \right. , \tag{4.1}$$

where $\frac{dx(t)}{dt} \in \mathbb{R}^n$ is the state, $y \in \mathbb{R}^r$ is the output, $A_c \in \mathbb{R}^{n \times n}$ is the state transition matrix, $B_c \in \mathbb{R}^{n \times r}$ is the input influence matrix, $C_c \in \mathbb{R}^{r \times n}$ is the output mapping matrix, $D_c \in \mathbb{R}^{r \times r}$ is the direct transmission matrix. The fictive force $e(t)$ acts only in the measured coordinates and that re-produce the measured output, n is the system order and r is the observed outputs coordinates. If all the modes of the LTI system were identified then $n = 2d$. In practice this is seldom the case, so what one gets from identification is a reduced model order $n \ll 2d$. Since SDDLV is an output-only method, the non-identified matrices B_c and D_c are used in order to derive properties of the transfer matrix [Ber10].

4.2.2 Damage localization procedure

The damage localization in mechanical structures with output-only data can be determined with the null space vectors for the SDDLV technique. Like this, damage localization information from structural changes (stress over elements) is extracted with the underlying idea of detecting changes in the flexibility. Note that while the transfer matrix is defined at the coordinates defined by the sensors, damage can be localized at any point of the structure because the stress field generated from the sensor coordinate loads covers the full domain.

Consider now the transfer matrix of model (4.1), which is given by

$$G(s) \stackrel{\text{def}}{=} R(s)D_c, \tag{4.2}$$

where

$$R(s) \stackrel{\text{def}}{=} C_c A_c^{-b}[sI - A_c]^{-1} \begin{bmatrix} C_c A_c^{1-b} \\ C_c A_c^{-b} \end{bmatrix}^{\dagger} \begin{bmatrix} I \\ 0 \end{bmatrix} \tag{4.3}$$

with $G(s) \in \mathcal{C}^{r\times r}$, $b = 0, 1, 2$ the output measurements (displacements, velocities, or accelerations respectively) and I the identity matrix.

Using (4.2) for the damaged (variables with tilde) and reference states, respectively, and dropping the Laplace variables s for simplicity, gives the difference in the transfer matrices $\delta G = \tilde{G} - G$. Neglecting D_c in (4.2) in both damaged and reference states (see [Ber10] for more details), the desired null space of δG has the same null space of $\delta R^T = \tilde{R}^T - R^T$. Then, the null space of δR^T is finally obtained from the Singular Value Decomposition (SVD)

$$\delta R^T = \begin{bmatrix} U_1 & U_2 \end{bmatrix} \begin{bmatrix} \Sigma_1 & 0 \\ 0 & \Sigma_2 \end{bmatrix} \begin{bmatrix} V_1 & V_2 \end{bmatrix}^H, \tag{4.4}$$

where $U, \Sigma, V \in \mathcal{C}^{r\times r}$, $\Sigma_2 \approx 0$ and $V = (v_1, \ldots, v_r) = [V_{(1)} \;\; V_{(2)}]$ the right singular vectors. Note that $V_{(1)}$: $(v_1, v_2, ..., v_t)$ is the nonzero singular vectors and $V_{(2)}$: $(v_{t+1}, v_{t+2}, ..., v_r)$ is the ideally zero singular vectors (in practice small), where a desired load vector v in the null space of δR^T is then any linear combination of the vectors in $V_{(2)}$, e.g. $v = v_r$. For any chosen value s, the load vector $v = v(s)$ in the null space of $\delta G(s)$ can be computed as described above, where only model (4.1) has been used without using information about the geometry of the structure.

The computation of the stress implies knowledge of the model of the structure (coming e.g. from a FEM) and is a linear function of displacement. The function that maps the displacement to the stress resultant is denoted as matrix $Q \in \mathbb{R}^{d\times d}$, the transfer matrix is $G_{\text{model}}(s) \stackrel{\text{def}}{=} (Ms^2 + Cs + K)^{-1}$ of model of LTI system in the reference state, and the sensors mapping matrix $P \in \mathbb{N}^{d\times r}$ with 1's where each line (position in the structure) and each column (sensor number) agree and zeros elsewhere. Let this function be given by $\mathcal{L}_{\text{model}}(s) = QG_{\text{model}}(s)P$, such that the stresses $S(s) \in \mathcal{C}^d$ for a chosen value s write as [Ber10]

$$S(s) = \mathcal{L}_{\text{model}}(s)v(s). \tag{4.5}$$

If an element at some degree of freedom j is completely damaged, the resulting stress $S_j(s)$ at coordinate j from the load $v(s)$ is zero [Ber10]. Thus, the stresses in $S(s)$ are considered as damage localization residuals, where the entries close to zero correspond to elements that are potentially (but not necessarily) damaged. In this Chapter, the following derivations and details are described considering the case where just one Laplace variable (s) is used.

4.3 Uncertainties on damage localization residuals

The system matrices A_c and C_c are needed for the damage localization both in the reference and damaged state of the system as explained in the previous section. When estimated from a finite number of data samples e.g. using Stochastic Subspace Identification methods [VODM96, PDR99], not the "true" system matrices A_c and C_c are obtained, but estimates $\widehat{A}_c$ and $\widehat{C}_c$ of the matrices of the reduced order model that represents the identified bandwidth. As the input of system (4.1) is unmeasured noise, $\widehat{A}_c$ and $\widehat{C}_c$ are naturally subject to variance errors depending on the data and the estimation method. A variance analysis of the system matrices obtained from Stochastic Subspace Identification is made e.g. in [CP04a] and expressions for their computation in the context of structural vibration analysis are given in [RPDR08, DLM11].

When estimating the load vectors in the null space of δG and the related stress field, the uncertainty of the system matrices is propagated to the uncertainty in the damage localization results. In this section, the variances of damage localization results are evaluated in order to support the decision between undamaged and damaged elements: In theory, the stress over a damaged element is zero, but it will be non-zero when computed on noisy data with an approximate reduced order model and an empirical threshold needs to be set. Then, the decision if the stress $S_j(s)$ at element j is zero or not – and thus if the corresponding element j is potentially damaged or not – is facilitated when knowing the variance of the estimate.

In the following, the uncertainty propagation to the damage localization results is done by a sensitivity analysis, starting from the covariances of the system matrices. The latter depend on the used system identification method and are assumed to be provided for the system matrices A_c and C_c of the *continuous-time* system (4.1).

4.3.1 Definitions

First, the notation of perturbations is defined. Let θ be some parameter vector and $\hat{\theta}_N$ its estimate based on N data samples, whose expected value $\bar{\theta}_N \overset{\text{def}}{=} \mathbf{E}\hat{\theta}_N$ tends to θ_* as N goes to infinity. Define the estimated covariance $\text{cov}(\hat{\theta}_N) = \mathbf{E}\left((\hat{\theta}_N - \bar{\theta}_N)(\hat{\theta}_N - \bar{\theta}_N)^T\right)$ and let $\hat{\theta}_N$ fulfill the Central Limit Theorem

$$\sqrt{N}(\hat{\theta}_N - \theta_*) \xrightarrow{d} \mathcal{N}(0, \Sigma) \tag{4.6}$$

for $N \to \infty$, where Σ is the asymptotic covariance. As the number of data samples N is usually large, the distribution of $\hat{\theta}_N$ is approximated to be Gaussian with $\text{cov}(\hat{\theta}_N) \approx \frac{1}{N}\Sigma$. Property (4.6) is fulfilled for estimates e.g. from subspace methods, maximum likelihood or prediction error methods [CP04a, Lju99, BBM00, PGS07].

Let $f(\theta) \in \mathbb{R}^k$ be a vector-valued function of the parameter. Suppose that its first derivative $\mathcal{J}_f \stackrel{\text{def}}{=} \mathcal{J}_f(\theta_*) = [\nabla f_1(\theta_*)\ \nabla f_2(\theta_*)\ \ldots\ \nabla f_k(\theta_*)]^T$ exists in θ_* and that $\nabla f_j(\theta_*) \neq 0$ for all j. Using the Taylor approximation

$$f(\hat{\theta}_N) = f(\theta_*) + \mathcal{J}_f(\hat{\theta}_N - \theta_*) + O(||\hat{\theta}_N - \theta_*||^2),$$

it follows

$$\sqrt{N}(f(\hat{\theta}_N) - f(\theta_*)) \xrightarrow{d} \mathcal{N}(0, \mathcal{J}_f\, \Sigma\, \mathcal{J}_f^T), \tag{4.7}$$

which is known as the *delta method* [CB02], and the covariance of $f(\hat{\theta}_N)$ can be approximated by

$$\operatorname{cov}(f(\hat{\theta}_N)) \approx \mathcal{J}_f \operatorname{cov}(\hat{\theta}_N)\, \mathcal{J}_f^T. \tag{4.8}$$

Note that $\mathcal{J}_f = \mathcal{J}_f(\theta_*)$ in the derivation above. A consistent estimate of the sensitivity is then obtained from $\mathcal{J}_f(\hat{\theta}_N)$.

We assume the covariances of the system matrices to be known from the used system identification procedure, and

$$\hat{\theta}_N = \begin{bmatrix} \operatorname{vec}(\widehat{A}_c) \\ \operatorname{vec}(\widehat{C}_c) \end{bmatrix}, \quad \theta_* = \begin{bmatrix} \operatorname{vec}(A_c) \\ \operatorname{vec}(C_c) \end{bmatrix},$$

where vec is the *vectorization operator* stacking the columns of a matrix into a vector. Then it is the objective to compute the sensitivities of the stress vector $S(s)$ with respect to $\operatorname{vec}(A_c)$ and $\operatorname{vec}(C_c)$ to obtain $\operatorname{cov}(\hat{S}(s))$ from $\operatorname{cov}\left(\begin{bmatrix} \operatorname{vec}(\widehat{A}_c) \\ \operatorname{vec}(\widehat{C}_c) \end{bmatrix}\right)$ as in (4.8).

A *first-order perturbation* Δf of the function f (at the true parameter θ_*) is defined from the Taylor approximation for some θ close to θ_* as $\Delta f \stackrel{\text{def}}{=} \mathcal{J}_f\, \Delta\theta$, where $\Delta\theta = \theta - \theta_*$.

The following definitions are needed for the derivation of the sensitivities. First, some properties of the vectorization operator are stated.

Definition 1 *For $a, b \in \mathbb{N}$ define the permutation*

$$\mathcal{P}_{a,b} = \sum_{k=1}^{a} \sum_{l=1}^{b} E_{k,l}^{a,b} \otimes E_{l,k}^{b,a},$$

where $E_{k,l}^{a,b}$ is a matrix of size $a \times b$ that is equal to 1 at position (k, l) and zero elsewhere, and $\otimes$ denotes the Kronecker product.

Then, for any matrix $X \in \mathbb{R}^{a,b}$ it holds [PGS07]

$$\operatorname{vec}(X^T) = \mathcal{P}_{a,b} \operatorname{vec}(X). \tag{4.9}$$

Related to the vectorization operator, Kronecker products are used [Bre78], particularly the relation $\operatorname{vec}(EFG) = (G^T \otimes E) \operatorname{vec}(F)$ for compatible matrices E, F and G.

Notice that some of the involved matrices and vectors, e.g. δR^T in (4.4) or the null space vector v, are complex-valued variables. In order to use derivations for real matrices, we introduce the notation similar to [PGS07] as

$$M_{\mathrm{Re}} \stackrel{\mathrm{def}}{=} \begin{bmatrix} \mathrm{Re}(M) & -\mathrm{Im}(M) \\ \mathrm{Im}(M) & \mathrm{Re}(M) \end{bmatrix}, \quad M_{\mathrm{re}} \stackrel{\mathrm{def}}{=} \begin{bmatrix} \mathrm{Re}(M) \\ \mathrm{Im}(M) \end{bmatrix} \tag{4.10}$$

for any matrix M. Then, for example, the relation $\delta R^T v = 0$ is equivalent to $(\delta R^T)_{\mathrm{Re}}\, v_{\mathrm{re}} = 0$, and the sensitivities for the real-valued matrices will be derived.

Now, results from [PGS07] are presented on the perturbation propagation to singular values and vectors for real matrices in Lemma 2 and complex matrices in Lemma 3, before deriving the sensitivities for the pseudoinverse in Lemma 4.

Lemma 2 ([PGS07]) *Let $\sigma_i > 0$, u_i and v_i be the i-th singular value, left and right singular vector of some real matrix $X \in \mathbb{R}^{a,b}$ and ΔX a small perturbation on X. For the same X, then*

$$\Delta\sigma_i = (v_i \otimes u_i)^T \mathrm{vec}(\Delta X), \quad \begin{bmatrix} \Delta u_i \\ \Delta v_i \end{bmatrix} = B_i^{\dagger} C_i \mathrm{vec}(\Delta X),$$

where

$$B_i \stackrel{\mathrm{def}}{=} \begin{bmatrix} I_a & \frac{-X}{\sigma_i} \\ \frac{-X^T}{\sigma_i} & I_b \end{bmatrix}, \; C_i \stackrel{\mathrm{def}}{=} \frac{1}{\sigma_i} \begin{bmatrix} v_i^T \otimes (I_a - u_i u_i^T) \\ (u_i^T \otimes (I_b - v_i v_i^T))\mathcal{P}_{a,b} \end{bmatrix},$$

I_n is identity matrix of size $n \times n$ and $\mathcal{P}_{a,b}$ is defined in Definition 3.4.1.

Lemma 3 ([PGS07]) *Let $\sigma_i > 0$, $\tilde{u}_i$ and $\tilde{v}_i$ be the i-th singular value, left and right singular vector of some complex matrix $X \in \mathcal{C}^{a,b}$ with $t = \mathrm{rank}(X)$, and ΔX a small perturbation. In the SVD*

$$X = U\Sigma V^H = \sum_{i=1}^{r} \sigma_i \tilde{u}_i \tilde{v}_i^H = \sum_{i=1}^{r} \sigma_i (\mathrm{e}^{\mathrm{i}\phi_i}\tilde{u}_i)(\mathrm{e}^{\mathrm{i}\phi_i}\tilde{v}_i)^H,$$

let the phase ϕ_i be chosen such that the imaginary part of the first entry of $\mathrm{e}^{\mathrm{i}\phi_i}\tilde{v}_i$ is zero and denote the respective left and right singular vectors by $u_i = \mathrm{e}^{\mathrm{i}\phi_i}\tilde{u}_i$, $v_i = \mathrm{e}^{\mathrm{i}\phi_i}\tilde{v}_i$. Then, perturbations on the singular vectors yield

$$\begin{bmatrix} \Delta(u_i)_{\mathrm{re}} \\ \Delta(v_i)_{\mathrm{re}} \end{bmatrix} = B_i^{\dagger} C_i \, (\mathrm{vec}(\Delta X))_{\mathrm{re}},$$

where

$$B_i \stackrel{\mathrm{def}}{=} \begin{bmatrix} I_{2a} & \frac{(-X)_{\mathrm{Re}}}{\sigma_i} \\ \frac{(-X^T)_{\mathrm{Re}}}{\sigma_i} & I_{2b} \end{bmatrix} (I_{4r} - E^{4r,4r}_{3r+1,3r+1}),$$

$$C_i \stackrel{\mathrm{def}}{=} \frac{1}{\sigma_i} \begin{bmatrix} (v_i^T \otimes I_a)_{\mathrm{Re}} - (u_i)_{\mathrm{re}}((\overline{v}_i \otimes u_i)_{\mathrm{re}})^T \\ ((u_i^T \otimes I_b)_{\mathrm{Re}} - (v_i)_{\mathrm{re}}((\overline{u}_i \otimes v_i)_{\mathrm{re}})^T)P_1 \end{bmatrix},$$

$$P_1 \stackrel{\text{def}}{=} \begin{bmatrix} \mathcal{P}_{a,b} & 0 \\ 0 & -\mathcal{P}_{a,b} \end{bmatrix}.$$

Note that the multiplication by $(I_{4r} - E^{4r,4r}_{3r+1,3r+1})$ *sets the column in* B_i *to zero that corresponds to the imaginary part of the first entry of* v_i*.*

In the following lemma, the sensitivities of the pseudoinverse computation are derived.

Lemma 4 *Let* $X \in \mathbb{R}^{a,b}$*,* $c = \operatorname{rank}(X)$ *and* ΔX *a small perturbation on* X*. Let the SVD* $X = U\Sigma V^T$ *be given with*

$$U = \begin{bmatrix} u_1 & \dots & u_c \end{bmatrix}, V = \begin{bmatrix} v_1 & \dots & v_c \end{bmatrix}, \Sigma = \operatorname{diag}\{\sigma_1, \dots, \sigma_c\},$$

where Σ *is invertible. Then,*

$$\operatorname{vec}(\Delta X^\dagger) = \mathcal{J}_{X^\dagger} \operatorname{vec}(\Delta X),$$

where

$$\mathcal{J}_{X^\dagger} = \mathcal{B} + (U\Sigma^{-1} \otimes \begin{bmatrix} 0_{b,a} & I_b \end{bmatrix})\mathcal{C} + (I_a \otimes V\Sigma^{-1})\mathcal{P}_{a,c}(I_c \otimes \begin{bmatrix} I_a & 0_{a,b} \end{bmatrix})\mathcal{C},$$

$$\mathcal{B} \stackrel{\text{def}}{=} -\sum_{i=1}^{c} \sigma_i^{-2}(u_i v_i^T \otimes v_i u_i^T), \quad \mathcal{C} \stackrel{\text{def}}{=} \begin{bmatrix} B_1^\dagger C_1 \\ \vdots \\ B_c^\dagger C_c \end{bmatrix},$$

$\mathcal{P}_{a,c}$ *as in Definition 3.4.1 and* B_i*,* C_i *as in Lemma 2.*

Proof: The pseudoinverse of X is given by $X^\dagger = V\Sigma^{-1}U^T$ and thus

$$\Delta(X^\dagger) = \Delta(V)\Sigma^{-1}U^T - V\Sigma^{-1}\Delta(\Sigma)\Sigma^{-1}U^T + V\Sigma^{-1}\Delta(U^T).$$

The assertion follows from vectorizing this equation, using Definition 3.4.1, Lemma 2 and Kronecker algebra. □

4.3.2 Covariance of system matrices

In this section, the sensitivity of the matrix R in (4.3) with respect to the system matrices A_c and C_c is derived, which is needed for the damage localization in (4.4).

For simplicity, assume that the data is given by acceleration sensors ($b = 2$). Derivations for displacement and velocity data ($b = 0, 1$) follow analogously. Then, R is defined in (4.3) as $R = ZH^\dagger L$ with

$$Z = C_c A_c^{-2}(sI - A_c)^{-1}, \quad H = \begin{bmatrix} C_c A_c^{-1} \\ C_c A_c^{-2} \end{bmatrix}. \tag{4.11}$$

Lemma 5 *A perturbation of $R = ZH^{\dagger}L$ is linked to a perturbation of A_c and C_c by the relation*

$$\mathrm{vec}(\Delta R) = \begin{bmatrix} \mathcal{J}_{A_c} & \mathcal{J}_{C_c} \end{bmatrix} \begin{bmatrix} \mathrm{vec}(\Delta A_c) \\ \mathrm{vec}(\Delta C_c) \end{bmatrix}, \tag{4.12}$$

where

$$\begin{aligned} \mathcal{J}_{A_c} &\stackrel{\text{def}}{=} -\left((A_c^{-2}M)^T \otimes C_c A_c^{-1}\right) - \left((A_c^{-1}M)^T \otimes C_c A_c^{-2}\right) + \left(M^T \otimes Z\right) \\ &\quad -(L^T \otimes Z)\left[\mathcal{J}_{H^{\dagger},1}(A_c^{-T} \otimes C_c A_c^{-1}) + \mathcal{J}_{H^{\dagger},2}\left(((A_c^{-2})^T \otimes C_c A_c^{-1}) + (A_c^{-T} \otimes C_c A_c^{-2})\right)\right], \\ \mathcal{J}_{C_c} &\stackrel{\text{def}}{=} \left((A_c^{-2}M)^T \otimes I_r\right) + (L^T \otimes Z)\left[\mathcal{J}_{H^{\dagger},1}(A_c^{-T} \otimes I_r) + \mathcal{J}_{H^{\dagger},2}((A_c^{-2})^T \otimes I_r)\right], \end{aligned}$$

$$M \stackrel{\text{def}}{=} (sI - A_c)^{-1}H^{\dagger}L, \tag{4.13}$$

with the sensitivities $\mathcal{J}_{H^{\dagger},1}$, $\mathcal{J}_{H^{\dagger},2}$ related to the pseudoinverse of H defined in (4.17).

Proof:

Deriving the first-order perturbation ΔR using the product rule yields

$$\Delta R = \Delta(Z)H^{\dagger}L + Z\Delta(H^{\dagger})L, \tag{4.14}$$

where

$$Z = C_c A_c^{-2}(sI - A_c)^{-1}, \; H = \begin{bmatrix} C_c A_c^{-1} \\ C_c A_c^{-2} \end{bmatrix}$$

for $b = 2$. Now, ΔZ and $\Delta(H^{\dagger})$ are derived as a function of ΔA_c and ΔC_c. Using the relation

$$\Delta X^{-1} = -X^{-1}\Delta(X)X^{-1}$$

for an arbitrary invertible matrix X, we derive

$$\Delta(C_c A_c^{-1}) = \Delta(C_c)A_c^{-1} - C_c A_c^{-1}\Delta(A_c)A_c^{-1}, \tag{4.15}$$

and

$$\Delta(C_c A_c^{-2}) = \Delta(C_c)A_c^{-2} - C_c A_c^{-1}\Delta(A_c)A_c^{-2} - C_c A_c^{-2}\Delta(A_c)A_c^{-1}. \tag{4.16}$$

Then, the perturbation ΔZ is obtained as

$$\begin{aligned} \Delta Z &= \Delta(C_c A_c^{-2})(sI - A_c)^{-1} - (C_c A_c^{-2})(sI - A_c)^{-1}\Delta(A_c)(sI - A_c)^{-1} \\ &= \Delta(C_c A_c^{-2})(sI - A_c)^{-1} - Z\Delta(A_c)(sI - A_c)^{-1}. \end{aligned}$$

The perturbation of the pseudoinverse $H^{\dagger}$ in (4.14) yields

$$\mathrm{vec}(\Delta H^{\dagger}) = \mathcal{J}_{H^{\dagger}}\mathrm{vec}(\Delta H),$$

where the sensitivity $\mathcal{J}_{H^{\dagger}}$ is derived in Lemma 4. Define the selection matrices

$$S_1 \stackrel{\text{def}}{=} I_n \otimes [I_r \;\; 0_{r,r}], \quad S_2 \stackrel{\text{def}}{=} I_n \otimes [0_{r,r} \;\; I_r],$$

where I_n is the identity matrix of size n and $0_{r,r}$ is the zero matrix of size $r \times r$. Then,

$$\begin{bmatrix} S_1 \\ S_2 \end{bmatrix} \operatorname{vec}(\Delta H) = \begin{bmatrix} \operatorname{vec}(\Delta(C_c A_c^{-1})) \\ \operatorname{vec}(\Delta(C_c A_c^{-2})) \end{bmatrix}$$

and define

$$\mathcal{J}_{H^\dagger,1} \stackrel{\text{def}}{=} \mathcal{J}_{H^\dagger} S_1^T, \quad \mathcal{J}_{H^\dagger,2} \stackrel{\text{def}}{=} \mathcal{J}_{H^\dagger} S_2^T, \tag{4.17}$$

such that

$$\operatorname{vec}(\Delta H^\dagger) = \mathcal{J}_{H^\dagger,1} \operatorname{vec}(\Delta(C_c A_c^{-1})) + \mathcal{J}_{H^\dagger,2} \operatorname{vec}(\Delta(C_c A_c^{-2})), \tag{4.18}$$

where $\Delta(C_c A_c^{-1})$ and $\Delta(C_c A_c^{-2})$ are given in (4.15) and (4.16).

In order to obtain relations for the vectorized perturbation $\operatorname{vec}(\Delta R)$, (4.14) is vectorized and Equations (4.15)–(4.18) are plugged in. Collecting the terms for ΔA_c and ΔC_c then leads to

$$\operatorname{vec}(\Delta R) = \mathcal{J}_{A_c} \operatorname{vec}(\Delta A_c) + \mathcal{J}_{C_c} \operatorname{vec}(\Delta C_c)$$

and thus to the assertion, where $\mathcal{J}_{A_c}$ and $\mathcal{J}_{C_c}$ are defined in (4.13). □

Corollary 6 *With the notations of Lemma 5 and of* (4.10)*, the relation*

$$\operatorname{cov}\left((\operatorname{vec}(R^T))_{\text{re}}\right) = \mathcal{J}_R \operatorname{cov}\left(\begin{bmatrix} \operatorname{vec}(A_c) \\ \operatorname{vec}(C_c) \end{bmatrix}\right) \mathcal{J}_R^T$$

holds for the asymptotic covariance of the real and imaginary parts of R^T, where $\mathcal{J}_R$ is defined as

$$\mathcal{J}_R = \begin{bmatrix} \mathcal{P}_{r,r} & 0_{r^2,r^2} \\ 0_{r^2,r^2} & \mathcal{P}_{r,r} \end{bmatrix} \begin{bmatrix} \operatorname{Re}(\mathcal{J}_{A_c}) & \operatorname{Re}(\mathcal{J}_{C_c}) \\ \operatorname{Im}(\mathcal{J}_{A_c}) & \operatorname{Im}(\mathcal{J}_{C_c}) \end{bmatrix}.$$

Proof: From (4.9) it follows $\operatorname{vec}(\Delta R^T) = \mathcal{P}_{r,r} \operatorname{vec}(\Delta R)$. Stacking the real and the imaginary part of this relation and plugging in (4.12) leads to the assertion. □

4.3.3 Covariance of damage localization residuals

In order to compute the covariance of the damage localization residual – the stresses $S(s)$ from (4.5) for a chosen value s –, the covariance of the load vector v is needed, which is a singular vector in the null space of $\delta R^T = \tilde{R}^T - R^T$ in (4.4). In the following proposition the first-order perturbation of right singular vectors v in the null space is provided in order to obtain the covariance of the stresses $S(s)_{\text{re}}$ in Theorem 8.

Proposition 7 *Let t be the rank of δR^T and let v be a vector in the null space of δR^T. Suppose that the complex singular vectors u_j and v_j, $j = 1, \ldots, t$, are defined such that the imaginary part of the first entry of each v_j is zero. Then, the sensitivity $\mathcal{J}_v$ of v yields*

$$\mathcal{J}_v = -((v_{\text{re}})^T \otimes V_{(1)\text{Re}}) P_1 \left(I_t \otimes \begin{bmatrix} 0_{2r,2r} & I_{2r} \end{bmatrix}\right) \begin{bmatrix} B_1^\dagger C_1 \\ \vdots \\ B_t^\dagger C_t \end{bmatrix}, \tag{4.19}$$

such that $\Delta v_{\mathrm{re}} = \mathcal{J}_v \ (\mathrm{vec}\,\Delta(\delta R^T))_{\mathrm{re}}$, *where for* $j = 1, \ldots, t$

$$B_j \stackrel{\mathrm{def}}{=} \begin{bmatrix} I_{2r} & -\frac{1}{\sigma_j}(\delta R^T)_{\mathrm{Re}} \\ -\frac{1}{\sigma_j}(\delta R^T)_{\mathrm{Re}}^T & I_{2r} \end{bmatrix} (I_{4r} - E_{3r+1,3r+1}^{4r,4r}),$$

$$C_j \stackrel{\mathrm{def}}{=} \frac{1}{\sigma_j} \begin{bmatrix} (v_j^T \otimes I_r)_{\mathrm{Re}} - (u_j)_{\mathrm{re}}((\overline{v}_j \otimes u_j)^T)_{\mathrm{re}} \\ [(u_j^T \otimes I_r)_{\mathrm{Re}} - (v_j)_{\mathrm{re}}((\overline{u}_j \otimes v_j)^T)_{\mathrm{re}}]P_2 \end{bmatrix},$$

and

$$P_1 \stackrel{\mathrm{def}}{=} \mathcal{P}_{2r,2t} \begin{bmatrix} I_{2rt} \\ I_t \otimes \begin{bmatrix} 0_{r,r} & -I_r \\ I_r & 0_{r,r} \end{bmatrix} \end{bmatrix}, \ P_2 \stackrel{\mathrm{def}}{=} \begin{bmatrix} \mathcal{P}_{r,r} & 0_{r^2,r^2} \\ 0_{r^2,r^2} & -\mathcal{P}_{r,r} \end{bmatrix}.$$

Proof: Recall that the right singular vectors in $V \in \mathcal{C}^{r\times r}$ of (δR^T) are considered as $V = \begin{bmatrix} V_{(1)} & V_{(2)} \end{bmatrix}$, where $V_{(1)}$ contains the right singular vectors $(v_1, v_2, ..., v_t)$ corresponding to the nonzero singular values, and $V_{(2)}$ contains the right singular vectors $(v_{t+1}, v_{t+2}, ..., v_r)$ corresponding to the singular values that are considered as zero. The sensitivity computation for $\Delta V_{(1)}$ for non-zeros singular values can be obtained from Lemma 3 as

$$\mathrm{vec}(\Delta(V_{(1)})_{\mathrm{re}}) = \left(I_t \otimes \begin{bmatrix} 0_{2r,2r} & I_{2r} \end{bmatrix}\right) \begin{bmatrix} B_1^\dagger C_1 \\ \vdots \\ B_t^\dagger C_t \end{bmatrix} (\mathrm{vec}\,\Delta(\delta R^T))_{\mathrm{re}}, \tag{4.20}$$

but a relation for Δv_{re} is needed, where v is a vector in the null space of (δR^T). Such a vector is a linear combination of the vectors in $V_{(2)}$, where

$$v = \sum_{k=t+1}^{r} \alpha_k v_k \tag{4.21}$$

with some coefficients $\alpha_k \in \mathcal{C}$. In the following, sensitivities for $v_k \in V_{(2)}$ are derived. It holds

$$V_{(1)}^H V_{(2)} = 0_{t,r-t}, \quad V_{(2)}^H V_{(2)} = I_{r-t}$$

and consequently

$$(V_{(1)}^H)_{\mathrm{Re}} V_{(2)\mathrm{re}} = 0_{2t,r-t}, \quad (V_{(2)}^H)_{\mathrm{Re}} V_{(2)\mathrm{re}} = \begin{bmatrix} I_{r-t} \\ 0_{r-t,r-t} \end{bmatrix}. \tag{4.22}$$

A first-order perturbation on the first equation in (4.22) yields

$$(V_{(1)}^H)_{\mathrm{Re}}\, \Delta V_{(2)\mathrm{re}} + \Delta(V_{(1)}^H)_{\mathrm{Re}}\, V_{(2)\mathrm{re}} = 0_{2t,r-t},$$

which leads to

$$(I_{r-t} \otimes (V_{(1)}^H)_{\mathrm{Re}})\, \mathrm{vec}(\Delta V_{(2)\mathrm{re}}) = -((V_{(2)\mathrm{re}})^T \otimes I_{2t})\, \mathrm{vec}(\Delta(V_{(1)}^H)_{\mathrm{Re}}). \tag{4.23}$$

using the properties of the vectorization operator. Now, $\mathrm{vec}(\Delta(V_{(1)}^H)_{\mathrm{Re}})$ is expressed in terms of $\mathrm{vec}(\Delta V_{(1)\mathrm{re}})$, which is given in (4.20). It holds

$$\Delta(V_{(1)}^H)_{\mathrm{Re}} = \begin{bmatrix} \mathrm{Re}\,\Delta(V_{(1)}^T) & \mathrm{Im}\,\Delta(V_{(1)}^T) \\ -\mathrm{Im}\,\Delta(V_{(1)}^T) & \mathrm{Re}\,\Delta(V_{(1)}^T) \end{bmatrix} = \begin{bmatrix} \mathrm{Re}\,\Delta(V_{(1)}) & -\mathrm{Im}\,\Delta(V_{(1)}) \\ \mathrm{Im}\,\Delta(V_{(1)}) & \mathrm{Re}\,\Delta(V_{(1)}) \end{bmatrix}^T = (\Delta(V_{(1)})_{\mathrm{Re}})^T,$$

and after vectorizing and using (4.9),

$$\mathrm{vec}(\Delta(V_{(1)}^H)_{\mathrm{Re}}) = \mathrm{vec}((\Delta(V_{(1)})_{\mathrm{Re}})^T) = \mathcal{P}_{2r,2t}\ \mathrm{vec}(\Delta V_{(1)\mathrm{Re}}).$$

From the definition of the operators $(\cdot)_{\mathrm{Re}}$ and $(\cdot)_{\mathrm{re}}$ in (4.10) follows then

$$\mathrm{vec}(\Delta(V_{(1)}^H)_{\mathrm{Re}}) = \mathcal{P}_{2r,2t} \begin{bmatrix} I_{2rt} \\ I_t \otimes \begin{bmatrix} 0_{r,r} & -I_r \\ I_r & 0_{r,r} \end{bmatrix} \end{bmatrix} \mathrm{vec}(\Delta V_{(1)\mathrm{re}}) = P_1\ \mathrm{vec}(\Delta V_{(1)\mathrm{re}}),$$

where P_1 is defined in Proposition 7. Plugging this into the right part of (4.23) leads to

$$(I_{r-t} \otimes (V_{(1)}^H)_{\mathrm{Re}})\,\mathrm{vec}(\Delta V_{(2)\mathrm{re}}) = -((V_{(2)\mathrm{re}})^T \otimes I_{2t})\,P_1\ \mathrm{vec}(\Delta V_{(1)\mathrm{re}}). \tag{4.24}$$

Now, repeating the steps (4.23)–(4.24) for a first-order perturbation of the second equation in (4.22) yields analogously

$$(I_{r-t} \otimes (V_{(2)}^H)_{\mathrm{Re}})\,\mathrm{vec}(\Delta V_{(2)\mathrm{re}}) + ((V_{(2)\mathrm{re}})^T \otimes I_{2(r-t)})\,P_3\ \mathrm{vec}(\Delta V_{(2)\mathrm{re}}) = 0, \tag{4.25}$$

where

$$P_3 \overset{\mathrm{def}}{=} \mathcal{P}_{2r,2(r-t)} \begin{bmatrix} I_{2r(r-t)} \\ I_{r-t} \otimes \begin{bmatrix} 0_{r,r} & -I_r \\ I_r & 0_{r,r} \end{bmatrix} \end{bmatrix}.$$

Consider the term $((V_{(2)\mathrm{re}})^T \otimes I_{2(r-t)})\,P_3$ separately. Using the properties of the Kronecker product [Fac05, Dï1] it follows

$$\begin{aligned}
((V_{(2)\mathrm{re}})^T \otimes I_{2(r-t)})\,P_3 &= \mathcal{P}_{r-t,2(r-t)}\,(I_{2(r-t)} \otimes (V_{(2)\mathrm{re}})^T) \begin{bmatrix} I_{r-t} \otimes I_{2r} \\ I_{r-t} \otimes \begin{bmatrix} 0_{r,r} & -I_r \\ I_r & 0_{r,r} \end{bmatrix} \end{bmatrix} \\
&= \mathcal{P}_{r-t,2(r-t)} \begin{bmatrix} I_{r-t} \otimes (V_{(2)\mathrm{re}})^T \\ I_{r-t} \otimes (V_{(2)\mathrm{re}})^T \begin{bmatrix} 0_{r,r} & -I_r \\ I_r & 0_{r,r} \end{bmatrix} \end{bmatrix} \\
&= \mathcal{P}_{r-t,2(r-t)}\,(P_4^T P_4) \begin{bmatrix} I_{r-t} \otimes \begin{bmatrix} \mathrm{Re}(V_{(2)}^T) & \mathrm{Im}(V_{(2)}^T) \end{bmatrix} \\ I_{r-t} \otimes \begin{bmatrix} -\mathrm{Im}(V_{(2)}^T) & \mathrm{Re}(V_{(2)}^T) \end{bmatrix} \end{bmatrix} \\
&= \mathcal{P}_{r-t,2(r-t)}\,P_4^T\,(I_{r-t} \otimes (V_{(2)}^H)_{\mathrm{Re}}),
\end{aligned} \tag{4.26}$$

where P_4 is the permutation matrix

$$P_4 \stackrel{\text{def}}{=} \begin{bmatrix} I_{r-t} \otimes \begin{bmatrix} I_{r-t} \\ 0_{r-t,r-t} \end{bmatrix} & \vdots & I_{r-t} \otimes \begin{bmatrix} 0_{r-t,r-t} \\ I_{r-t} \end{bmatrix} \end{bmatrix}.$$

Plugging (4.26) into (4.25) yields

$$(I_{2(r-t)^2} + \mathcal{P}_{r-t,2(r-t)}\, P_4^T)\, (I_{r-t} \otimes (V_{(2)}^H)_{\text{Re}})\, \text{vec}(\Delta V_{(2)\text{re}}) = 0.$$

Finally, assembling (4.24) and (4.25) gives

$$\begin{bmatrix} I_{2(r-t)^2} & 0 \\ 0 & I_{2(r-t)^2} + \mathcal{P}_{r-t,2(r-t)}\, P_4^T \end{bmatrix} \begin{bmatrix} (I_{r-t} \otimes (V_{(1)}^H)_{\text{Re}}) \\ (I_{r-t} \otimes (V_{(2)}^H)_{\text{Re}}) \end{bmatrix} \text{vec}(\Delta V_{(2)\text{re}}) =$$

$$\begin{bmatrix} -((V_{(2)\text{re}})^T \otimes I_{2t})\, P_1 \\ 0 \end{bmatrix} \text{vec}(\Delta V_{(1)\text{re}}). \tag{4.27}$$

The solution for $\text{vec}(\Delta V_{(2)\text{re}})$ may not be unique, as the matrix $(I_{2(r-t)^2} + \mathcal{P}_{r-t,2(r-t)}\, P_4^T)$ is in general rank deficient for $t \leq r-2$. One solution is given by

$$\text{vec}(\Delta V_{(2)\text{re}}) = -(I_{r-t} \otimes V_{(1)\text{Re}})((V_{(2)\text{re}})^T \otimes I_{2t})\, P_1\, \text{vec}(\Delta V_{(1)\text{re}}), \tag{4.28}$$

as can be verified by plugging it in (4.27). Note that $(V_{(1)}^H)_{\text{Re}} V_{(1)\text{Re}} = I$ and $(V_{(1)}^H)_{\text{Re}} V_{(2)\text{Re}} = 0$. Then, from comparing the blocks in the solution (4.28) it follows

$$\Delta(v_k)_{\text{re}} = -(((v_k)_{\text{re}})^T \otimes V_{(1)\text{Re}})\, P_1\, \text{vec}(\Delta V_{(1)\text{re}})$$

for any singular vector $v_k \in V_{(2)}$, and for an arbitrary vector v in the null space it follows

$$\Delta v_{\text{re}} = -((v_{\text{re}})^T \otimes V_{(1)\text{Re}})\, P_1\, \text{vec}(\Delta V_{(1)\text{re}})$$

from (4.21). The assertion follows by substituting $\text{vec}(\Delta V_{(1)\text{re}})$ from (4.20). □

Theorem 8 *Let* $\text{cov}((\text{vec}\, R^T)_{\text{re}})$ *and* $\text{cov}((\text{vec}\, \tilde{R}^T)_{\text{re}})$ *from the reference and damaged state be given in Corollary 6 and* $\mathcal{J}_v$ *in Proposition 7. Then,*

$$\Sigma_S \stackrel{\text{def}}{=} \text{cov}(S(s)_{\text{re}}) = \mathcal{J}_{S(s)} \left(\text{cov}((\text{vec}\, \tilde{R}^T)_{\text{re}}) + \text{cov}((\text{vec}\, R^T)_{\text{re}}) \right) \mathcal{J}_{S(s)}^T,$$

where

$$\mathcal{J}_{S(s)} = (\mathcal{L}_{\text{model}}(s))_{\text{Re}}\, \mathcal{J}_v$$

with $\mathcal{L}_{\text{model}}(s)$ *defined in Section 4.2.2.*

Proof: As R and $\tilde{R}$ are computed on two different data sets from the reference and damaged states, they are statistically independent and it follows

$$\operatorname{cov}\left((\operatorname{vec}\,\delta R^T)_{\mathrm{re}}\right) = \operatorname{cov}((\operatorname{vec}\tilde{R}^T)_{\mathrm{re}}) + \operatorname{cov}((\operatorname{vec}R^T)_{\mathrm{re}}) \tag{4.29}$$

From Proposition 7 follows

$$\operatorname{cov}(v_{\mathrm{re}}) = \mathcal{J}_v \operatorname{cov}\left((\operatorname{vec}\,\delta R^T)_{\mathrm{re}}\right)\,\mathcal{J}_v^T, \tag{4.30}$$

and from (4.5) follows

$$\operatorname{cov}(S(s)_{\mathrm{re}}) = (\mathcal{L}_{\mathrm{model}}(s))_{\mathrm{Re}}\,\operatorname{cov}(v_{\mathrm{re}})\,(\mathcal{L}_{\mathrm{model}}(s))_{\mathrm{Re}}^T. \tag{4.31}$$

Plugging (4.29) and (4.30) in (4.31) leads to the assertion. □

4.3.4 Hypothesis testing for damage localization

If the stress $\hat{S}_j(s)$ over a finite element j is close to zero, the element is a candidate for being classified as damaged. The values in the stress vector $\hat{S}(s)$ are complex values, whose real and imaginary parts can have different signs. One could for example test if the real parts are close to 0 (neglecting the imaginary part if it is small), or, more general, if both the real and imaginary parts are close to 0 for an element. For each element j, this corresponds to the hypotheses

$$\begin{cases} \mathbf{H}_0: \ \hat{S}_j(s) \neq 0 & \text{(element is undamaged)} \\ \mathbf{H}_1: \ \hat{S}_j(s) = 0 & \text{(element is potentially damaged)} \end{cases} \tag{4.32}$$

The elements in the vector $\hat{S}(s)_{\mathrm{re}}$ are asymptotically Gaussian distributed with non-zero mean under $\mathbf{H}_0$ and zero mean under $\mathbf{H}_1$. A consistent estimate of the covariance $\hat{\Sigma}_S$ of $\hat{S}(s)_{\mathrm{re}}$ can be obtained from Theorem 8. Then, testing $\mathbf{H}_0$ against $\mathbf{H}_1$ can be done by computing the variables

$$\hat{\chi}_j^2(1) \overset{\text{def}}{=} \frac{(\operatorname{Re}(\hat{S}_j(s)))^2}{\hat{\sigma}_j^2} \qquad \text{or} \qquad \hat{\chi}_j^2(2) \overset{\text{def}}{=} \begin{bmatrix} \operatorname{Re}(\hat{S}_j(s)) \\ \operatorname{Im}(\hat{S}_j(s)) \end{bmatrix}^T \hat{\Sigma}_j^{-1} \begin{bmatrix} \operatorname{Re}(\hat{S}_j(s)) \\ \operatorname{Im}(\hat{S}_j(s)) \end{bmatrix}, \tag{4.33}$$

where $\hat{\sigma}_j^2 = \hat{\Sigma}_S(j,j)$ is the entry (j,j) of $\hat{\Sigma}_S$ and $\hat{\Sigma}_j$ is the covariance of $\begin{bmatrix} \operatorname{Re}(\hat{S}_j(s)) & \operatorname{Im}(\hat{S}_j(s)) \end{bmatrix}^T$ consisting in the elements

$$\hat{\Sigma}_j = \begin{bmatrix} \hat{\Sigma}_S(j,j) & \hat{\Sigma}_S(j,j+r) \\ \hat{\Sigma}_S(j+r,j) & \hat{\Sigma}_S(j+r,j+r) \end{bmatrix}$$

of the matrix $\hat{\Sigma}_S$. The variables $\hat{\chi}_j^2(1)$ and $\hat{\chi}_j^2(2)$ are asymptotically χ^2-distributed with one and two degrees of freedom, respectively, and non-centrality parameter zero under $\mathbf{H}_1$. Some thresholds t_1 and t_2 are defined, such that

$$\int_0^{t_i} f_{\chi^2(i)}(x)dx = 1-\beta,$$

where $f_{\chi^2(i)}(x)$ is the probability density function of the central χ^2 distribution with i degrees of freedom ($i = 1, 2$) and β is the desired type II error of the hypothesis test (4.32), i.e. the probability of deciding that an element is undamaged while it is potentially damaged. Note that the type I error, i.e. the probability of deciding that an element is potentially damaged while it is in fact undamaged, cannot be assigned a priori as the distribution under $\mathbf{H}_0$ is unknown, but it is desired to be small. To obtain a small type I error (and to avoid that elements are falsely classified as potentially damaged) β cannot be chosen too small, e.g. $\beta = \frac{1}{3}$.

Then, using the test $\hat{\chi}_j^2(1)$, $\mathbf{H}_0$ is rejected and $\mathbf{H}_1$ is accepted for an element j (damage occurred), if $\hat{\chi}_j^2(1) \leq t_1$. Using test $\hat{\chi}_j^2(2)$, $\mathbf{H}_0$ is rejected and $\mathbf{H}_1$ is accepted for an element j, if $\hat{\chi}_j^2(2) \leq t_2$.

4.4 Numerical application

A numerical applications using a simulated 25 DOF truss structure in Figure 4.1 was used to validate the damage localization algorithm with the hypothesis test. Recall that the residual (the stress) is close to zero for damaged elements. Damage was simulated by a stiffness reduction in one or two of the elements. For both the undamaged and the damaged state, a data sample of length $N = 25{,}000$ of acceleration data ($b = 2$) was generated with added output noise using Gaussian white noise excitation. From the output-only data, first the system matrices and their covariances were estimated of the discrete-time state-space system corresponding to (4.1), using SSI and the uncertainty quantification in [RPDR08]. In order to obtain the matrices $\widehat{A}_c$ and $\widehat{C}_c$ of the continuous-time system and their respective covariances, a discrete to continuous transformation was made. The Laplace variable s was empirically chosen near a pole of $\widehat{A}_c$ to compute the stress $\hat{S}(s)$ in (4.5). The covariance $\hat{\Sigma}_S$ of $\hat{S}(s)_{\text{re}}$ was computed from Theorem 8.

First, the output was generated at six sensor positions in vertical direction at the lower chord (see Figure 4.1) with added 5% output noise. Damage was simulated by decreasing the stiffness of element 16 by 20%. From system identification, not all of the 25 theoretical modes could be identified at model order $n = 50$. Four well-estimated modes were chosen in both the undamaged and the damaged state using a stabilization diagram procedure [RPDR08], from where the matrices $\widehat{A}_c$ and $\widehat{C}_c$ and their covariances are obtained in both states. From these system matrices, the real and imaginary parts of the stress values and their covariance are computed for $s = 2\text{i}$. Once the identified modes are selected from the system identification

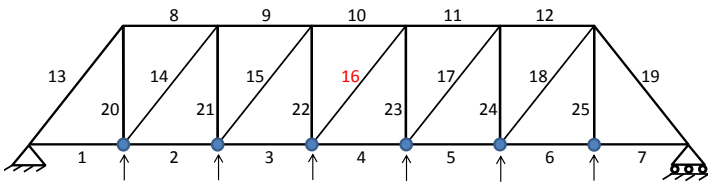

Figure 4.1 – Truss structure with six sensors.

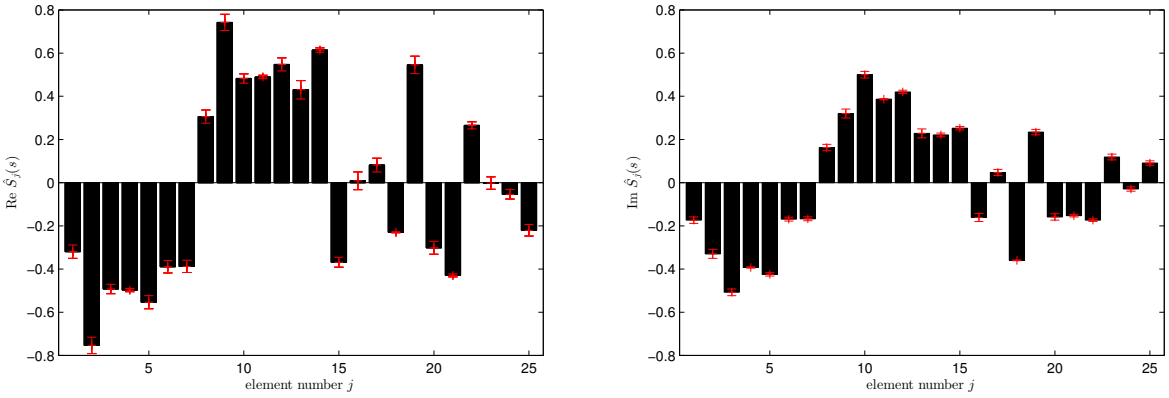

Figure 4.2 – Real parts (left) and imaginary parts (right) of localization residuals and their standard deviations.

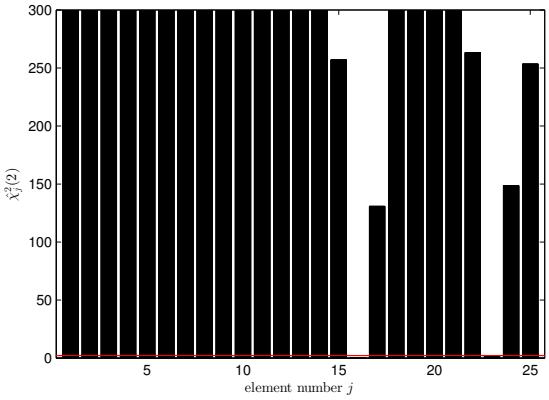

Figure 4.3 – χ^2-test values of the localization residuals with threshold to decide between both hypotheses – 6 sensors, 5% output noise, 20% stiffness reduction in bar 16.

for $\widehat{A}_c$ and $\widehat{C}_c$, the method is automated. Computational time was a few seconds after the uncertainty compuation of the system identification results is done. For the considered subspace identification method an efficient uncertainty computation procedure was used [DM13]. The overall computational time was around 30 seconds in this case.

In Figure 4.2, the real and imaginary parts of each of the stress values are shown with their standard deviation. Note that the imaginary parts of the stress are not negligible in this example. In Figure 4.3, the values $\hat{\chi}^2_j(2)$ in (4.33) are computed on the real and imaginary parts of the stress and their covariance. In order to decide if an element is potentially damaged or not, the threshold $t_2 = 2.16$ is computed at $\beta = 0.34$ (the horizontal line in Figure 4.3). Two elements are below this threshold: the damaged element 16 as well as the undamaged element 23 that is a neighboring element of 16 (see Figure 4.1). It can be shown, in fact, that for the used sensor set element 23 is inseparable from element 16 at $s = 0$ [Ber02], i.e. if the stress in 16 is zero, so it must be in 23. Although $s = 2\mathrm{i}$ (used here) is not zero, it is small and the noted behavior is clearly manifested. The corresponding χ^2-values are $\hat{\chi}^2_{16} = 0.30$ for

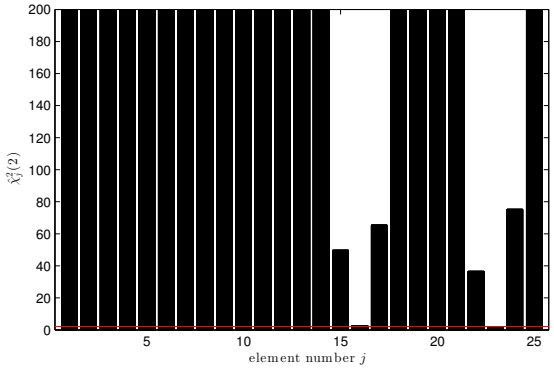

Figure 4.4 – χ^2-test values with different measurement noise – 10% measurement noise, 6 sensors, 20% stiffness reduction in bar 16.

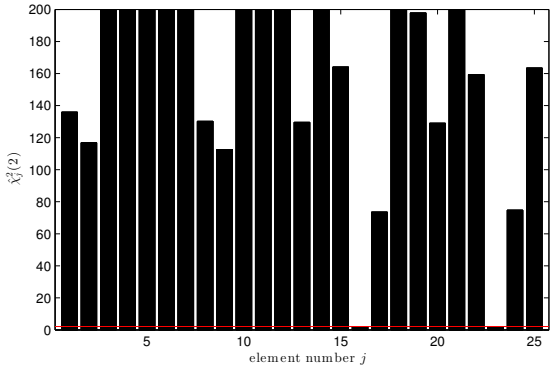

Figure 4.5 – χ^2-test values with different damage extent – 5% measurement noise, 6 sensors, 10% stiffness reduction in bar 16.

element 16 and $\hat{\chi}^2_{23} = 1.26$ for element 23. Thus, the lowest χ^2-value corresponds correctly to the damaged element. The elements 1–15, 17–22 and 24–25 are correctly classified as undamaged. In Figure 4.3, the χ^2-values are only displayed until the value 300, while some of them were at more than 10^5.

Several variations of this test case are examined with different levels of noise, sensor positions and damages in the following.

4.4.1 Measurement noise

With higher measurement noise and constant data length the variance of the identified modal parameters increases, leading to a higher variance of the localization residual and thus to a reduction of the contrast between the χ^2 values of the undamaged and damaged elements. This can be observed in Figure 4.4 where the previous simulation was repeated with 10% added output noise.

4.4.2 Damage extent

A smaller damage extent leads to a smaller difference between the transfer functions of the reference and the damaged states and thus to a smaller damage localization residual. However, its covariance is hardly dependent of the magnitude of the difference, but is the sum of covariances corresponding to both states as shown in Theorem 8. Hence, smaller damage leads to higher variation in the residual and thus to less contrast between the χ^2 values. Results with 10% stiffness reduction in bar 16 are shown in Figure 4.5. This damage can still be reliably localized. Note that the minimum damage that in general can be localized depends on many different factors, like the level of the noise, the length of the signals, the position of the damage and the sensors, the value of s etc., and that the presented result holds only for the particular setting.

4.4.3 Number of sensors and multiple damages

In the SDDLV the system order n is limited by $2r$, i.e. the number of mode pairs that are considered in the system matrices A_c and C_c must be smaller than the number of sensors. Thus, less sensors demand more modal truncation, which leads to more bias on the damage detection residuals, if the truncated higher modes are influenced by the damage. In Figure 4.6 results are presented with 4 sensors (number 1,3,4,6 from the left of the sensors in Figure 4.1), where only 3 mode pairs are used from the system identification. Using less sensors and less modes leads obviously to less contrast between the χ^2 values of the undamaged and damaged elements.

The theory shows that as the number of damaged bars increases the dimension of the theoretical null space decreases and thus the estimation of vectors in the null space under noisy conditions becomes more difficult. In this case, a more precise estimation of δR^T is necessary, which requires more modes to be estimated from the system identification and thus more sensors due to the constraint $2r \geq n$. In Figure 4.7, results are presented for two

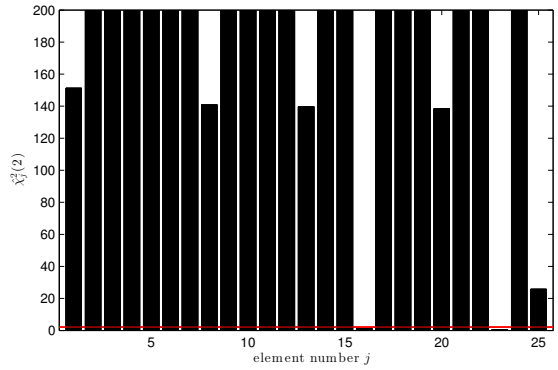

Figure 4.6 – χ^2-test values with different number of sensors – 5% output noise, 4 sensors, 20% stiffness reduction in bar 16.

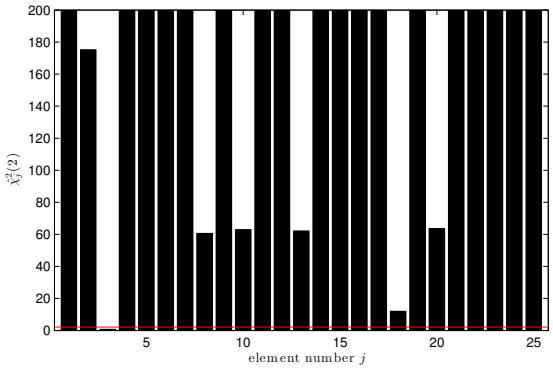

Figure 4.7 – χ^2-test values with multiple damages – 5% output noise, 12 sensors, 20% stiffness reduction in bars 3 and 18.

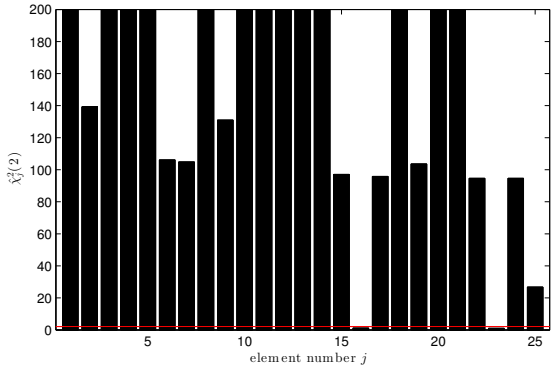

Figure 4.8 – χ^2-test values with model errors – 5% output noise, 6 sensors, 20% stiffness reduction in bar 16.

damages in bars 3 and 18, where now 12 mode pairs and 12 sensors (the present 6 sensors plus 6 sensors on the upper cord) were used. It should be noted that the estimated stresses in the damaged elements are small but different from zero due to modal truncation and noise, which become more important when multiple damages are present. While the resulting χ^2 values of the damaged elements are the lowest and the value of bar 3 is correctly under the threshold, the values of bar 18 exceeds it slightly.

4.4.4 Model errors

The considered structure is statically determinate. At $s = 0$ the stress field is entirely independent of the structural properties (other than the topology which is known with high precision). As $s \neq 0$, model errors play a role but their influence remains moderate in this case as can be observed in Figure 4.8. There, the model was created for a truss with a 5% perturbation of the area of the bars for the computation of $\mathcal{L}_{\text{model}}(s)$, compared to the model that was used for the data generation.

4.5 Conclusion

Deciding whether a damage localization residual is zero or not is no more based on empirical thresholds, but on uncertainty bounds, which are now obtained for each element that is tested for damage separately, unlike in [Ber10]. Thus, the intrinsic uncertainty from the data is propagated properly for each evaluated element in the damage localization residual $S(s)$. Then, it can be decided if an element is potentially damaged or undamaged using a hypothesis test that takes into account the uncertainties. This statistical test was successfully performed in a numerical application, where subspace identification was chosen as the underlying system identification method. Choosing a different identification method could yield a different performance.

The presented statistical framework for the SDDLV method is based on the uncertainty computation of the system identification results, which has been proven feasible in several case studies using field data [RPDR08, DHL$^+$11, DM13]. Also, the DLV framework has been used in real applications [GSJB07]. Hence, the proposed damage localization test appears to be a promising foundation for the application on field data. Future work includes the aggregation of the damage localization residual at different values of the Laplace variable s for the hypothesis test and the validation of the method on a real large-scale application example.

4.6 Dissemination

Parts of this chapter have been published in:

[MDBM12] L. Marin, M. Döhler, D. Bernal, and L. Mevel. Uncertainty quantification for stochastic damage localization for mechanical system. In *Proccedings of the 8th IFAC Safeprocess*, Mexico City, Mexico, 2012.

[DMBM13b] M. Döhler, L. Marin, D. Bernal, and L. Mevel. Statistical decision making for damage localization with stochastic load vectors. *Mechanical Systems and Signal Processing*, 37, 2013.

[MDBM13a] L. Marin, M. Döhler, D. Bernal, and L. Mevel. Damage localization using a statistical test on residuals from the sddlv approach. *Society for Experimental Mechanics Series*, 41:143–152, 2013.

[DMBM13a] M. Döhler, L. Marin, D. Bernal, and L. Mevel. Comparison of two statistical damage localization approaches. In *Proccedings of the 5th International Operational Modal Analysis Conference*, 2013.

Chapter 5

Robust statistical damage localization with stochastic load vectors

The contribution of the previous Chapter 4 is extended into a robust fashion in this current Chapter, consisting in the development of a statistical decision making method for damage localization in civil structures, based on the sensitivity-based rules (Chapter 3, Section 3.4) for the inherent uncertainties in the SDDLV approach (Chapter 2, Section 2.3) for different chosen Laplace variable. The constitution of real system matrices for the sensitivity-based rules is explained in details and the whole method is validated into numerical simulations and a real experiment of structures.

5.1 Introduction

The Stochastic Dynamic Damage Location Vector (SDDLV) approach [Ber10] is a damage localization technique using both finite element information and modal parameters from output-only vibration measurements. From estimates of the modes in both reference and damaged states, the null space of the difference between surrogates of the transfer matrices at the sensor positions for some Laplace variable s in the complex plane is obtained. Then, a vector in this null space is applied as a load to the FEM of the structure to compute the stress field, where only the FEM of the structure in its reference state is used. Damage is related to this stress field and is potentially located at elements where the stress is close to zero. A full description of the SDDLV is available in Chapter 2, Section 2.3.

The estimates from the output-only measurements that are used for damage localization are naturally subject to variance errors [PGS07, RPDR08, CM11]. Taking into account these uncertainties proves to be important for structural damage diagnosis [SM11, SM13]. Based

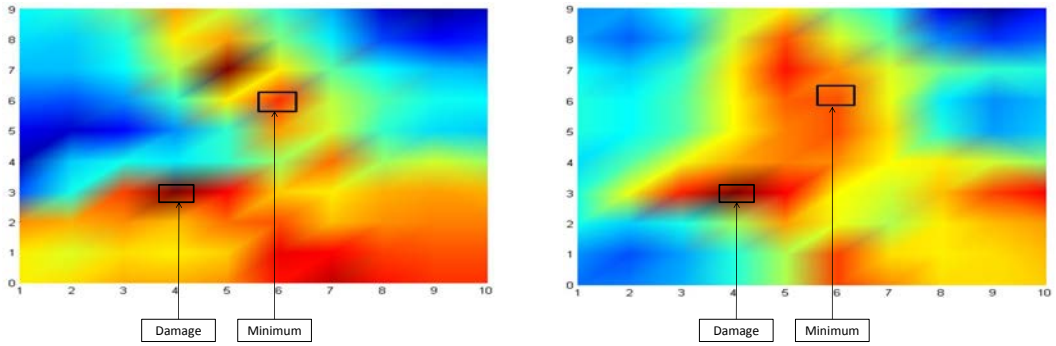

Figure 5.1 – Representation of damage test values for two different s-values on a simulated plate.

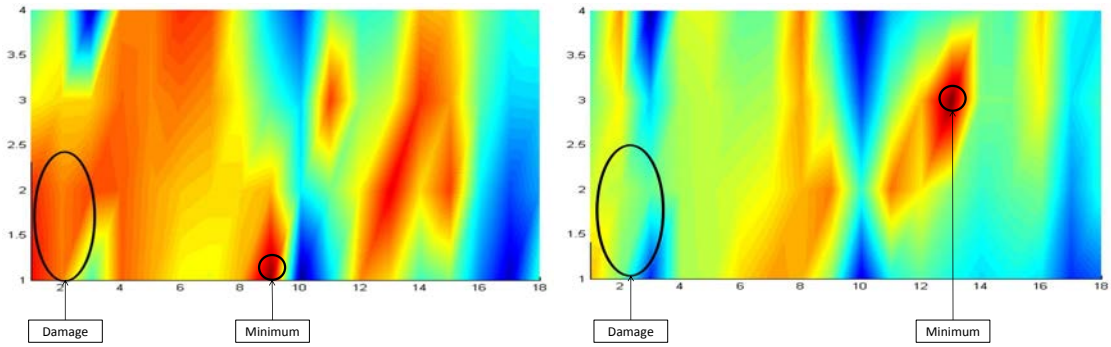

Figure 5.2 – Representation of damage test values for two different s-values on a real beam.

on these considerations, a statistical extension of the SDDLV method was developed for the actual decision if an element is damaged, which depends on very few parameters and takes the intrinsic uncertainty of the stress computation associated to the measurements into account. Still, one input to the algorithm is the Laplace domain variable s where the transfer function matrix difference is evaluated. Heuristic rules have been derived in [Ber10] for the optimal choice of this Laplace variable and the aggregation of results for different Laplace variables was suggested to increase the robustness of the approach. Different choices of s lead to different localization results due to a different impact of the modal truncation. As illustrated by the localization examples in Figures 5.1 and 5.2, bad choices of s provide erroneous results and consequently a wrong damage location at the minimum test values close to zero.

Taking into account uncertainties not only improves the statistical robustness of the approach, it also aims at decreasing the number of potential false alarms. Indeed, the SDDLV approach of [Ber10] only guarantees that elements whose damage index is significantly non zero are not afflicted with damage. Nonetheless, it can happen that because of noise, model reduction, sparse instrumentation or other limitations the ensemble of elements with close to zero damage index is too large to help decision making in real applications. It was seen in the previous Chapter 4 that using uncertainty information helps increasing the contrast between both ensembles. Using different Laplace variables s as explained above should fur-

ther increase the robustness of the approach and help the decision, which is an important extension of the previous Chapter 4 where just one Laplace variable is used.

The current Chapter extends the previous Chapter 4 by focusing on a robust statistical approach, where multiple damage localization results computed at different Laplace variables will be aggregated with respect to their statistical relevance. This will remove a part of the errors and uncertainty related to the choice of the Laplace domain variable. The underlying SDDLV approach using subspace identification and the statistical methodology are explained, before the robust statistical approach is derived. First, the SDDLV approach is introduced as an output-only method for damage localization in Section 5.2. In Section 5.3 the necessary system identification step with the construction of parametric system matrices from identified modes is explained. Then, the robust statistical approach for the aggregation of damage localization results is derived in Section 5.4. In Section 5.5 the new method is successfully applied on numerical and real cases. Finally, some conclusions of this work are presented in Section 5.6.

5.2 The SDDLV approach

The behavior of a mechanical structure is assumed to be described by a linear time-invariant (LTI) system and represented by the corresponding *continuous-time state-space model* (2.20)

$$\left\{ \begin{array}{rcl} \frac{dx(t)}{dt} & = & A_c x + B_c e \\ y & = & C_c x + D_c e \end{array} \right. , \tag{5.1}$$

where $\frac{dx(t)}{dt} \in \mathbb{R}^n$ is the state, $y \in \mathbb{R}^r$ is the output, $A_c \in \mathbb{R}^{n \times n}$ is the state transition matrix, $B_c \in \mathbb{R}^{n \times r}$ is the input influence matrix, $C_c \in \mathbb{R}^{r \times n}$ is the output mapping matrix, $D_c \in \mathbb{R}^{r \times r}$ is the direct transmission matrix. The fictive force $e(t)$ acts only in the measured coordinates and that re-produce the measured output, n is the system order and r is the observed outputs coordinates. If all the modes of the LTI system were identified then $n = 2d$. In practice this is seldom the case, so what one gets from identification is a reduced model order $n \ll 2d$. Since SDDLV is an output-only method, the non-identified matrices B_c and D_c are used in order to derive properties of the transfer matrix [Ber10].

Consider now the transfer matrix of model (5.1), which is given by

$$G(s) \stackrel{\text{def}}{=} R(s) D_c, \tag{5.2}$$

where

$$R(s) = C_c (sI - A_c)^{-1} \left[\begin{array}{c} C_c A_c \\ C_c \end{array} \right]^{\dagger} \left[\begin{array}{c} I \\ 0 \end{array} \right] \tag{5.3}$$

with $G(s) \in \mathcal{C}^{r \times r}$ and I the identity matrix.

Using (5.2) for the damaged (variables with tilde) and reference states, respectively, and dropping the Laplace variables s for simplicity, gives the difference in the transfer matrices $\delta G = \tilde{G} - G$. Neglecting D_c in (5.2) in both damaged and reference states (see [Ber10] for

more details), the desired null space of δG has the same null space of $\delta R^T = \tilde{R}^T - R^T$. Then, the null space of δR^T is finally obtained from the Singular Value Decomposition (SVD)

$$\delta R^T = \begin{bmatrix} U_1 & U_2 \end{bmatrix} \begin{bmatrix} \Sigma_1 & 0 \\ 0 & \Sigma_2 \end{bmatrix} \begin{bmatrix} V_1 & V_2 \end{bmatrix}^H, \tag{5.4}$$

where $U, \Sigma, V \in \mathcal{C}^{r \times r}$, $\Sigma_2 \approx 0$ and $V = (v_1, \ldots, v_r) = [V_{(1)} \;\; V_{(2)}]$ the right singular vectors. Note that $V_{(1)}$: $(v_1, v_2, ..., v_t)$ is the nonzero singular vectors and $V_{(2)}$: $(v_{t+1}, v_{t+2}, ..., v_r)$ is the ideally zero singular vectors (in practice small), where a desired load vector v in the null space of δR^T is then any linear combination of the vectors in $V_{(2)}$, e.g. $v = v_r$. For any chosen value s, the load vector $v = v(s)$ in the null space of $\delta G(s)$ can be computed as described above, where only model (5.1) has been used without using information about the geometry of the structure.

The computation of the stress implies knowledge of the model of the structure (coming e.g. from a FEM) and is a linear function of displacement. The function that maps the displacement to the stress resultant is denoted as matrix $Q \in \mathbb{R}^{d \times d}$, the transfer matrix is $G_{\text{model}}(s) \stackrel{\text{def}}{=} (Ms^2 + Cs + K)^{-1}$ of model of LTI system in the reference state, and the sensors mapping matrix $P \in \mathbb{N}^{d \times r}$ with 1's where each line (position in the structure) and each column (sensor number) agree and zeros elsewhere. Let this function be given by $\mathcal{L}_{\text{model}}(s) = QG_{\text{model}}(s)P$, such that the stresses $S(s) \in \mathcal{C}^d$ for a chosen value s write as [Ber10]

$$S(s) = \mathcal{L}_{\text{model}}(s)v(s). \tag{5.5}$$

If an element at some degree of freedom j is completely damaged, the resulting stress $S_j(s)$ at coordinate j from the load $v(s)$ is zero [Ber10]. Thus, the stresses in $S(s)$ are considered as damage localization residuals, where the entries close to zero correspond to elements that are potentially (but not necessarily) damaged.

Since damaged elements lead to stress values that are (close to) zero, but zero stress does not necessarily indicate damage [Ber02] on one side, and due to truncation and model errors on the other side, it is recommended to compute the load vector $v(s)$ and subsequently the stress vector $S(s)$ for several values of the Laplace variable s. Robustness of the damage localization approach is then achieved by aggregating the results.

Let the Laplace variables s_i, $i = 1, \ldots, \kappa$, be given. To minimize modal truncation errors, they should be chosen within a vicinity of the identified poles of the structure in the complex plane, but not too close to them [Ber10]. After the identification of the system matrices A_c and C_c in the reference and $\tilde{A}_c$ and $\tilde{C}_c$ in the damaged states, the computations (5.3)–(5.5) are repeated for each value s_i to obtain the respective stress vectors $S(s_i)$.

To decide if an element is damaged, the information of the corresponding entries in the stress vector $S(s_i)$ for all $i = 1, \ldots, \kappa$ can be used now. In [Ber10] the aggregation

$$\bar{S}_j = \sum_{i=1}^{\kappa} |S_j(s_i)| \tag{5.6}$$

for each entry j was suggested. In Section 5.4.5 we propose a new aggregation scheme based on the uncertainties of the system identification results.

5.3 SSI and system modes selection

This Section is developed using baselines on the background theory of Chapter 3 where procedures for the system identification and uncertainty quantification are described.

Estimates of the system matrices A_c and C_c from output-only measurements of the continuous-time system (5.1) are required for the damage localization strategy from the previous section. Stochastic subspace-based system identification methods are efficient tools for this task, identifying the *discrete-time state-space model*

$$\begin{cases} x_{k+1} &= A_d x_k + v_k \\ y_k &= C_d x_k + w_k, \end{cases}$$

where $A_d = \exp(A_c \tau)$, $C_d = C_c$, τ is the time step and v_k and w_k are process and measurement noise, respectively. In the first step, we identify estimates $\widehat{A}_d$ and $\widehat{C}_d$ of the system matrices at different model orders from the measurements using *covariance-driven subspace identification* [BF85, PDR99, DM12]. Due to noise, these model orders need to be relatively high and furthermore noise modes appear in the results. From these results at most r mode pairs are selected in a so-called stabilization diagram in the second step, such that the condition $2r \geq n$ is fulfilled. Finally, the corresponding eigenvalues of the continuous-time system and the mode shapes are used to build the desired estimates $\widehat{A}_c$ and $\widehat{C}_c$ in the last step, rejecting the noise modes.

5.3.1 Step 1: System identification

For reference-based subspace identification a subset of the sensors can be selected in order to reduce the computation effort, the so-called *reference sensors* or *projection channels* [PDR99] indicated by $^{(\mathrm{ref})}$. Define the theoretical cross-correlation between the state and the outputs $G \stackrel{\mathrm{def}}{=} \mathbf{E}(x_{k+1} y_k^{(\mathrm{ref})T})$, the output correlation $R_i \stackrel{\mathrm{def}}{=} \mathbf{E}(y_k y_{k-i}^{(\mathrm{ref})T}) = C_d A_d^{i-1} G$ and the block Hankel matrix

$$\mathcal{H} \stackrel{\mathrm{def}}{=} \begin{bmatrix} R_1 & R_2 & \dots & R_q \\ R_2 & R_3 & \dots & R_{q+1} \\ \vdots & \vdots & \ddots & \vdots \\ R_{p+1} & R_{p+2} & \dots & R_{p+q} \end{bmatrix} \stackrel{\mathrm{def}}{=} \mathrm{Hank}(R_i), \tag{5.7}$$

where the parameters p and q are given such that $pr \geq qr^{(\mathrm{ref})} \geq n$ with usually $p = q$. Then, matrix $\mathcal{H}$ possesses the well-known factorization property $\mathcal{H} = \mathcal{O}\mathcal{C}$ into the matrices of observability and controllability

$$\mathcal{O} \stackrel{\mathrm{def}}{=} \begin{bmatrix} C_d \\ C_d A_d \\ \vdots \\ C_d A_d^p \end{bmatrix} \quad \text{and} \quad \mathcal{C} \stackrel{\mathrm{def}}{=} \begin{bmatrix} G & A_d G & \dots & A_d^{q-1} G \end{bmatrix},$$

respectively. From $\mathcal{O}$, the observation matrix C_d is obtained in its first block row. Matrix A_d is obtained from the shift invariance property of $\mathcal{O}$ as the least squares solution

$$A_d = \mathcal{O}^{\uparrow\dagger}\mathcal{O}^{\downarrow}, \text{ where } \mathcal{O}^{\uparrow} \stackrel{\text{def}}{=} \begin{bmatrix} C_d \\ C_d A_d \\ \vdots \\ C_d A_d^{p-1} \end{bmatrix}, \ \mathcal{O}^{\downarrow} \stackrel{\text{def}}{=} \begin{bmatrix} C_d A_d \\ C_d A_d^2 \\ \vdots \\ C_d A_d^{p} \end{bmatrix}. \tag{5.8}$$

and † denotes the Moore-Penrose pseudoinverse.

Using measurement data, the correlation estimates $\widehat{R}_i = 1/N \sum_{k=1}^{N} y_k y_{k-i}^{(\text{ref})T}$, $i = 1, \ldots, p+q$, are computed to fill the Hankel matrix estimate $\widehat{\mathcal{H}} = \text{Hank}(\widehat{R}_i)$ in (5.7). The observability matrix estimate $\widehat{\mathcal{O}}$ is obtained from a thin SVD of $\widehat{\mathcal{H}}$ and its truncation at the desired model order as

$$\widehat{\mathcal{H}} = \begin{bmatrix} E_1 & E_2 \end{bmatrix} \begin{bmatrix} S_1 & 0 \\ 0 & S_2 \end{bmatrix} \begin{bmatrix} F_1^T \\ F_2^T \end{bmatrix}, \ \widehat{\mathcal{O}} = E_1 S_1^{1/2}. \tag{5.9}$$

Then, the system matrix estimates $\widehat{A}_d$ and $\widehat{C}_d$ are obtained from (5.8). For simplicity, Sections 5.3.2 and 5.3.3 are written for the true parameters without $\widehat{\ }$, but hold in the same way for the estimates.

5.3.2 Step 2: Mode selection

From the system matrices A_d and C_d, the eigenvalues λ_i^d and mode shapes φ_i for each mode i are retrieved from

$$\det(A_d - \lambda_i^d I) = 0, \quad A_d \phi_i = \lambda_i^d \phi, \quad \varphi_i = C_d \phi_i. \tag{5.10}$$

The eigenvalues λ_i^c of the system matrix A_c of the respective continuous-time system are then

$$\lambda_i^c = \frac{1}{\tau} \ln(\lambda_i^d) \tag{5.11}$$

and the natural frequencies f_i and damping ratios ξ_i are obtained from

$$f_i = \frac{|\lambda_i^c|}{2\pi\tau}, \quad \xi_i = \frac{-\text{Re}(\lambda_i^c)}{|\lambda_i^c|}. \tag{5.12}$$

The set of identified modes does not contain only physical (true) modes of the structure in practice, but also spurious modes due to non-white noise and non-stationary excitation, a low signal-to-noise ratio, or a wrong selection of the model order. The standard technique for discriminating spurious from physical modes is the use of a *stabilization diagram*, where the modes are computed at multiple subsequent over-estimated model orders and the identified frequencies are plotted versus the model order [PDR99, DM12]. This multi-order computation is done by truncating at the desired model orders in (5.9) and the subsequent computation of the modes at these orders in (5.8), (5.10)–(5.12) [PDR99]. A fast multi-order computation was described in [DM12]. Finally, under the premise that the true system modes remain quite constant at different model orders, while spurious modes vary, the true structural modes can be chosen in the stabilization diagram based on user-defined stabilization criteria [RHDR12].

5.3.3 Step 3: Final system matrices

The system modes appear in conjugated complex pairs. Let m be the number of mode pairs identified from the stabilization diagram, where $r \geq m$ to satisfy the constraint $2r \geq n = 2m$. Let (λ_i^c, φ_i) and $(\overline{\lambda_i^c}, \overline{\varphi}_i)$, $i = 1, \ldots, m$, be the identified modes. Then, the system matrices in the modal basis write as $A_c = \mathrm{diag}(\lambda_1^c, \ldots, \lambda_m^c, \overline{\lambda_1^c}, \ldots, \overline{\lambda_m^c})$ and $C_c = [\varphi_1 \ \ldots \ \varphi_m \ \overline{\varphi}_1 \ \ldots \ \overline{\varphi}_m]$. Since the system matrices (A_c, C_c) are defined up to a change of basis $(T^{-1}A_cT, C_cT)$, we can equivalently define the real-valued system matrices

$$A_c = \begin{bmatrix} \mathrm{Re}(\Lambda_c) & -\mathrm{Im}(\Lambda_c) \\ \mathrm{Im}(\Lambda_c) & \mathrm{Re}(\Lambda_c) \end{bmatrix}, \quad C_c = \begin{bmatrix} \mathrm{Re}(\Phi) & \mathrm{Im}(\Phi) \end{bmatrix}, \tag{5.13}$$

where $\Lambda_c = \mathrm{diag}(\lambda_1^c, \ldots, \lambda_m^c)$ and $\Phi = [\varphi_1 \ \ldots \ \varphi_m]$, obtained from the chosen modes.

5.4 Uncertainties and SDDLV robust statistical testing

For the SDDLV damage localization algorithm, estimates of the system matrices A_c and C_c are obtained in the reference and damaged states from a finite number of data samples. The identification of these matrices is subject to uncertainties due to the unknown excitation (being modeled as white noise), measurement noise and finite data length. Methods for the uncertainty quantification of the estimates from stochastic subspace identification in the context of structural vibration analysis are given in [RPDR08, DLM13, DM13].

Since the stress vector estimate $\widehat{S}(s_i)$ is computed from the estimates $\widehat{A}_c$ and $\widehat{C}_c$ in both reference and damaged states, the uncertainties from the system identification are propagated to uncertainties in the stress vector. These uncertainties may be crucial in deciding whether an element is potentially damaged, i.e. whether the stress of an element is in fact zero or not, while the computed stress value is just close to zero. The uncertainty propagation from system identification results in general to the stress $\widehat{S}(s_i)$ for a single value of the Laplace variable s_i was analyzed. In this section, the uncertainty propagation is made explicit for the chosen subspace identification algorithm from Section 5.3. Furthermore, expressions for the uncertainty propagation to the stress vector $\widehat{S}(s_i)$ computed at multiple values s_i, $i = 1, \ldots, \kappa$, are derived. With these means, the aggregation of the results and the test for damaged elements can be performed based on statistical criteria. Finally, the respective test is derived.

5.4.1 Principles of covariance computation and uncertainty propagation

The uncertainties in the measurement data are propagated to the damage localization results. The former can be quantified by a covariance estimate $\widehat{\Sigma}_{\mathcal{H}} = \mathrm{cov}(\mathrm{vec}(\widehat{\mathcal{H}}))$ of the Hankel matrix, where $\mathrm{vec}(\cdot)$ denotes the column stacking vectorization operator. The estimate $\widehat{\Sigma}_{\mathcal{H}}$ can be directly estimated from the data as described in [RPDR08, DM13] by separating the available data of length N into n_b blocks of length N_b, such that $N = n_b N_b$. Then, the Hankel matrix $\widehat{\mathcal{H}}^{(j)} = \mathrm{Hank}(\widehat{R}_i^{(j)})$ in (5.7) is computed on the correlations $\widehat{R}_i^{(j)} = 1/N_b \sum_{k=1+(j-1)N_b}^{jN_b} y_k y_{k-i}^{(\mathrm{ref})T}$ on each block. The Hankel matrix on the entire dataset

hence yields $\widehat{\mathcal{H}} = \frac{1}{n_b}\sum_{j=1}^{n_b}\widehat{\mathcal{H}}^{(j)}$, and the covariance estimate

$$\widehat{\Sigma}_{\mathcal{H}} = \frac{1}{n_b - 1}\sum_{j=1}^{n_b}\operatorname{vec}\left(\widehat{\mathcal{H}}^{(j)} - \widehat{\mathcal{H}}\right)\operatorname{vec}\left(\widehat{\mathcal{H}}^{(j)} - \widehat{\mathcal{H}}\right)^T.$$

is obtained.

All computed quantities in Sections 5.2 and 5.3 are ultimately functions of the Hankel matrix. Let f be such a vector valued function of $\widehat{\mathcal{H}}$. Its covariance can be calculated using the Taylor approximation as

$$f(\widehat{\mathcal{H}}) \approx f(\mathcal{H}) + \mathcal{J}_{f,\mathcal{H}}\operatorname{vec}(\widehat{\mathcal{H}} - \mathcal{H}) \;\Rightarrow\; \operatorname{cov}(f(\widehat{\mathcal{H}})) \approx \mathcal{J}_{f,\mathcal{H}}\,\widehat{\Sigma}_{\mathcal{H}}\,\mathcal{J}_{f,\mathcal{H}}^T \tag{5.14}$$

with the sensitivity matrix $\mathcal{J}_{f,\mathcal{H}} \overset{\text{def}}{=} \partial f(\mathcal{H})/\partial\operatorname{vec}(\mathcal{H})$, which can be obtained analytically [PGS07, RPDR08, DM13]. A consistent estimate is obtained by replacing the theoretical variables (such as $\mathcal{H}$) with consistent estimates obtained from the data (such as $\widehat{\mathcal{H}}$) in the computation of the sensitivity matrix. With the operator Δ we define (theoretical) first-order perturbations, yielding $\Delta f = \mathcal{J}_{f,\mathcal{H}}\operatorname{vec}(\Delta\mathcal{H})$. Using this relationship, the desired sensitivity matrix can be obtained and used for the covariance computation in (5.14). Like this, the covariance of the Hankel matrix can be propagated to any parameters that are dependent on the data, in particular to the modal parameters and the stress estimate $\widehat{S}(s_i)$.

In the following, the sensitivity and covariance computation is done for the theoretical values (like $\mathcal{H}$, A_c, C_c, $S(s_i)$). Estimates of the sensitivities and covariances are then obtained by plugging in the estimates obtained from the data (like $\widehat{\mathcal{H}}$, $\widehat{A}_c$, $\widehat{C}_c$, $\widehat{S}(s_i)$).

The following notation and properties will be used. $\otimes$ denotes the Kronecker product, having the property $\operatorname{vec}(AXB) = (B^T \otimes A)\operatorname{vec}(X)$. I_a denotes the identity matrix of size $a \times a$, and $0_{a,b}$ denotes the zero matrix of size $a \times b$. $e_j^a \in \mathbb{R}^a$ denotes the j-th unit vector (being column j of I_a). The permutation matrix $\mathcal{P}_{a,b} \overset{\text{def}}{=} \begin{bmatrix} I_a \otimes e_1^b & I_a \otimes e_2^b & \dots & I_a \otimes e_b^b \end{bmatrix} \in \mathbb{R}^{ab\times ab}$ is defined with the property

$$\operatorname{vec}(X^T) = \mathcal{P}_{a,b}\operatorname{vec}(X) \tag{5.15}$$

for any matrix $X \in \mathbb{R}^{a\times b}$. Finally, for dealing with the uncertainties of complex-valued matrices we introduce an equivalent real-valued notation by defining

$$M_{\text{Re}} \overset{\text{def}}{=} \begin{bmatrix} \operatorname{Re}(M) & -\operatorname{Im}(M) \\ \operatorname{Im}(M) & \operatorname{Re}(M) \end{bmatrix}, \quad M_{\text{re}} \overset{\text{def}}{=} \begin{bmatrix} \operatorname{Re}(M) \\ \operatorname{Im}(M) \end{bmatrix} \tag{5.16}$$

for any matrix M as in [PGS07]. Then, for example, a complex-valued equation $Ax = b$ is equivalent to $A_{\text{Re}}\,x_{\text{re}} = b_{\text{re}}$, and the sensitivities of the real-valued matrices can be derived.

5.4.2 Covariance of system matrices from subspace identification

For the covariance computation of A_c and C_c, a perturbation $\Delta\mathcal{H}$ of the Hankel matrix in (5.7) is propagated to a perturbation $\Delta\lambda_i^c$ and $\Delta\varphi_i$ in the selected modes $i = 1, \dots, m$ (see Section 5.3.2), yielding

$$\Delta\lambda_i^c = \mathcal{J}_{\lambda_i^c,\mathcal{H}}\operatorname{vec}(\Delta\mathcal{H}), \quad \Delta\varphi_i = \mathcal{J}_{\varphi_i,\mathcal{H}}\operatorname{vec}(\Delta\mathcal{H}),$$

where the sensitivities $\mathcal{J}_{\lambda_i^c,\mathcal{H}} \in \mathcal{C}^{1\times h}$ and $\mathcal{J}_{\varphi_i,\mathcal{H}} \in \mathcal{C}^{r\times h}$ with $h = (p+1)qrr^{(\mathrm{ref})}$ have been derived in detail in [RPDR08, DM13]. Plugging these expressions into (5.13) and vectorizing the system matrices leads to

$$\mathrm{vec}(\Delta A_c) = \mathcal{J}_{A_c,\mathcal{H}}\,\mathrm{vec}(\Delta\mathcal{H}), \quad \mathrm{vec}(\Delta C_c) = \mathcal{J}_{C_c,\mathcal{H}}\,\mathrm{vec}(\Delta\mathcal{H}), \tag{5.17}$$

where

$$\mathcal{J}_{A_c,\mathcal{H}} = P_1 \begin{bmatrix} \mathrm{Re}(\mathcal{J}_{\lambda_1^c,\mathcal{H}}) \\ \vdots \\ \mathrm{Re}(\mathcal{J}_{\lambda_m^c,\mathcal{H}}) \\ \mathrm{Im}(\mathcal{J}_{\lambda_1^c,\mathcal{H}}) \\ \vdots \\ \mathrm{Im}(\mathcal{J}_{\lambda_m^c,\mathcal{H}}) \end{bmatrix},\ \mathcal{J}_{C_c,\mathcal{H}} = \begin{bmatrix} \mathrm{Re}(\mathcal{J}_{\varphi_1,\mathcal{H}}) \\ \vdots \\ \mathrm{Re}(\mathcal{J}_{\varphi_m,\mathcal{H}}) \\ \mathrm{Im}(\mathcal{J}_{\varphi_1,\mathcal{H}}) \\ \vdots \\ \mathrm{Im}(\mathcal{J}_{\varphi_m,\mathcal{H}}) \end{bmatrix},\ P_1 = \begin{bmatrix} E_1 \\ \vdots \\ E_m \\ F_1 \\ \vdots \\ F_m \end{bmatrix},$$

and the selection matrix P_1 is composed of the matrices

$$E_j = \begin{bmatrix} e_j^m e_j^{m\,T} & 0_{m,m} \\ 0_{m,m} & e_j^m e_j^{m\,T} \end{bmatrix},\ F_j = \begin{bmatrix} 0_{m,m} & -e_j^m e_j^{m\,T} \\ e_j^m e_j^{m\,T} & 0_{m,m} \end{bmatrix}.$$

Then, the covariance of the system matrices can be obtained from (5.17) as

$$\Sigma_{A_c,C_c} \overset{\mathrm{def}}{=} \mathrm{cov}\left(\begin{bmatrix}\mathrm{vec}(A_c)\\ \mathrm{vec}(C_c)\end{bmatrix}\right) = \begin{bmatrix}\mathcal{J}_{A_c,\mathcal{H}}\\ \mathcal{J}_{C_c,\mathcal{H}}\end{bmatrix} \Sigma_{\mathcal{H}} \begin{bmatrix}\mathcal{J}_{A_c,\mathcal{H}}\\ \mathcal{J}_{C_c,\mathcal{H}}\end{bmatrix}^T. \tag{5.18}$$

5.4.3 Covariance of system matrices

In the next step, the sensitivity $\mathcal{J}_{R(s),A_c,C_c}$ of the matrix $R(s)$ with respect to the system matrices A_c and C_c is derived, which is needed for the stress computation in (5.4)–(5.6). In the following we generalize the sensitivity computation for acceleration data to the simplified and more general formula of $R(s)$ in (5.3). Define

$$Z(s) = C_c(sI - A_c)^{-1},\quad H = \begin{bmatrix} C_cA_c \\ C_c \end{bmatrix},\quad L = \begin{bmatrix} I \\ 0 \end{bmatrix},$$

such that $R(s) = Z(s)H^\dagger L$. Applying the product rule, a first-order perturbation of $R(s)$ yields

$$\Delta R(s) = [\Delta Z(s)]H^\dagger L + Z(s)[\Delta(H^\dagger)]L. \tag{5.19}$$

Both terms $\Delta Z(s)$ and $\Delta(H^\dagger)$ are now developed as functions of ΔA_c and ΔC_c, which are already given in (5.17).

Using the relation $\Delta(X^{-1}) = -X^{-1}[\Delta X]X^{-1}$, the first term yields

$$\begin{aligned} \Delta Z(s) &= [\Delta C_c](sI - A_c)^{-1} - C_c(sI - A_c)^{-1}[\Delta(sI - A_c)](sI - A_c)^{-1} \\ &= [\Delta C_c](sI - A_c)^{-1} + Z(s)[\Delta A_c](sI - A_c)^{-1}. \end{aligned} \tag{5.20}$$

For the second term, the perturbation of the pseudoinverse $H^\dagger$ yields

$$\mathrm{vec}(\Delta(H^\dagger)) = \mathcal{J}_{H^\dagger}\mathrm{vec}(\Delta H), \tag{5.21}$$

where the sensitivity $\mathcal{J}_{H^\dagger}$ is given in Chapter 4. Define the selection matrices $S_1 \stackrel{\text{def}}{=} I_n \otimes [I_r \;\; 0_{r,r}]$, $S_2 \stackrel{\text{def}}{=} I_n \otimes [0_{r,r} \;\; I_r]$ such that

$$\mathrm{vec}(\Delta H) = \begin{bmatrix} S_1^T & S_2^T \end{bmatrix} \begin{bmatrix} \mathrm{vec}(\Delta(C_cA_c)) \\ \mathrm{vec}(\Delta C_c) \end{bmatrix} = S_1^T\mathrm{vec}(\Delta(C_cA_c)) + S_2^T\mathrm{vec}(\Delta C_c),$$

and together with (5.21)

$$\mathrm{vec}(\Delta(H^\dagger)) = \mathcal{J}_{H^\dagger}S_1^T\mathrm{vec}(\Delta(C_cA_c)) + \mathcal{J}_{H^\dagger}S_2^T\mathrm{vec}(\Delta C_c),$$

where $\Delta(C_cA_c) = [\Delta C_c]A_c + C_c[\Delta A_c]$. Combining this result with (5.19) and (5.20) yields subsequently

$$\mathrm{vec}(\Delta R(s)) = \begin{bmatrix} \mathcal{J}_{R(s),A_c} & \mathcal{J}_{R(s),C_c} \end{bmatrix} \begin{bmatrix} \mathrm{vec}(\Delta A_c) \\ \mathrm{vec}(\Delta C_c) \end{bmatrix},$$

where

$$\begin{aligned} \mathcal{J}_{R(s),A_c} &\stackrel{\text{def}}{=} \left(M(s)^T \otimes Z(s)\right) + \left(L^T \otimes Z(s)\right)\mathcal{J}_{H^\dagger}S_1^T(I_n \otimes C_c), \\ \mathcal{J}_{R(s),C_c} &\stackrel{\text{def}}{=} \left(M(s)^T \otimes I_r\right) + \left(L^T \otimes Z(s)\right)\mathcal{J}_{H^\dagger}\left(S_1^T(A_c^T \otimes I_r) + S_2^T\right), \end{aligned}$$

with $M(s) \stackrel{\text{def}}{=} (sI - A_c)^{-1}H^\dagger L$. Stacking the real and imaginary parts of $\mathrm{vec}(\Delta R(s)^T)$, it follows from (5.15) and (5.16)

$$(\mathrm{vec}(\Delta R(s)^T))_{\mathrm{re}} = \mathcal{J}_{R(s)} \begin{bmatrix} \mathrm{vec}(\Delta A_c) \\ \mathrm{vec}(\Delta C_c) \end{bmatrix}, \tag{5.22}$$

where

$$\mathcal{J}_{R(s)} = \begin{bmatrix} \mathcal{P}_{r,r} & 0_{r^2,r^2} \\ 0_{r^2,r^2} & \mathcal{P}_{r,r} \end{bmatrix} \begin{bmatrix} \mathrm{Re}(\mathcal{J}_{R(s),A_c}) & \mathrm{Re}(\mathcal{J}_{R(s),C_c}) \\ \mathrm{Im}(\mathcal{J}_{R(s),A_c}) & \mathrm{Im}(\mathcal{J}_{R(s),C_c}) \end{bmatrix},$$

and finally with (5.18)

$$\mathrm{cov}\left((\mathrm{vec}(R(s)^T))_{\mathrm{re}}\right) = \mathcal{J}_{R(s)}\,\Sigma_{A_c,C_c}\,\mathcal{J}_{R(s)}^T.$$

5.4.4 Covariance of stress vector

With the computations in the previous section, the covariance associated to the matrices $R(s)$ and $\tilde{R}(s)$ can be obtained in the reference and damaged states of the structure for a chosen value s. In the next step, these covariances are propagated to the load vector $v(s)$ in the null space of $\delta R(s)^T = \tilde{R}(s)^T - R(s)^T$ and finally to the stress vector $S(s)$, as computed in (5.4)–(5.5).

The covariance propagation to the null space vector $v(s)$ is based on the relation $\Delta v(s)_{\mathrm{re}} = \mathcal{J}_{v(s)}\ (\mathrm{vec}(\Delta\delta R(s)^T))_{\mathrm{re}}$, where $\mathcal{J}_{v(s)}$ is derived in Chapter 4. Then, from (5.5) it follows

$$\Delta S(s)_{\mathrm{re}} = \mathcal{J}_{S(s)}\ (\mathrm{vec}(\Delta\delta R(s)^T))_{\mathrm{re}},$$

where

$$\mathcal{J}_{S(s)} = \mathcal{L}_{\mathrm{model}}(s)_{\mathrm{Re}}\ \mathcal{J}_{v(s)},$$

and together with (5.22) it follows

$$\Delta S(s)_{\mathrm{re}} = \mathcal{J}_{S(s)}\,\mathcal{J}_{\tilde{R}(s)} \begin{bmatrix} \mathrm{vec}(\Delta\tilde{A}_c) \\ \mathrm{vec}(\Delta\tilde{C}_c) \end{bmatrix} - \mathcal{J}_{S(s)}\,\mathcal{J}_{R(s)} \begin{bmatrix} \mathrm{vec}(\Delta A_c) \\ \mathrm{vec}(\Delta C_c) \end{bmatrix}. \tag{5.23}$$

Since the system matrices from the damaged and reference states are obtained on different statistically independent measurements, the covariance expression

$$\Sigma_{S(s)} \stackrel{\mathrm{def}}{=} \mathrm{cov}(S(s)_{\mathrm{re}}) = \mathcal{J}_{S(s)}\,\mathcal{J}_{\tilde{R}(s)}\,\Sigma_{\tilde{A}_c,\tilde{C}_c}\,\mathcal{J}_{\tilde{R}(s)}^T\,\mathcal{J}_{S(s)}^T + \mathcal{J}_{S(s)}\,\mathcal{J}_{R(s)}\,\Sigma_{A_c,C_c}\,\mathcal{J}_{R(s)}^T\,\mathcal{J}_{S(s)}^T \tag{5.24}$$

follows.

5.4.5 Statistical aggregation and evaluation of stress results

Since the computation of the stress $S(s_i)$ at multiple Laplace variables s_i, $i = 1, \ldots, \kappa$, increases the information content on the damage location (see Section 5.2), a joint evaluation of these stresses increases the robustness of the statistical approach, where only one Laplace variable s was considered. The joint statistical evaluation requires the covariance computation of the stacked (real-valued) stress results

$$\overline{S} \stackrel{\mathrm{def}}{=} \begin{bmatrix} S(s_1)_{\mathrm{re}} \\ \vdots \\ S(s_\kappa)_{\mathrm{re}} \end{bmatrix}. \tag{5.25}$$

Stacking (5.23) for each s_i accordingly leads to

$$\Delta\overline{S} = \begin{bmatrix} \mathcal{J}_{S(s_1)}\mathcal{J}_{\tilde{R}(s_1)} \\ \vdots \\ \mathcal{J}_{S(s_\kappa)}\mathcal{J}_{\tilde{R}(s_\kappa)} \end{bmatrix} \begin{bmatrix} \mathrm{vec}(\Delta\tilde{A}_c) \\ \mathrm{vec}(\Delta\tilde{C}_c) \end{bmatrix} - \begin{bmatrix} \mathcal{J}_{S(s_1)}\mathcal{J}_{R(s_1)} \\ \vdots \\ \mathcal{J}_{S(s_\kappa)}\mathcal{J}_{R(s_\kappa)} \end{bmatrix} \begin{bmatrix} \mathrm{vec}(\Delta A_c) \\ \mathrm{vec}(\Delta C_c) \end{bmatrix},$$

and, analogously to (5.24), to the covariance $\Sigma_{\overline{S}} \stackrel{\mathrm{def}}{=} \mathrm{cov}(\overline{S})$ with

$$\Sigma_{\overline{S}} = \begin{bmatrix} \mathcal{J}_{S(s_1)}\mathcal{J}_{\tilde{R}(s_1)} \\ \vdots \\ \mathcal{J}_{S(s_\kappa)}\mathcal{J}_{\tilde{R}(s_\kappa)} \end{bmatrix} \Sigma_{\tilde{A}_c,\tilde{C}_c} \begin{bmatrix} \mathcal{J}_{S(s_1)}\mathcal{J}_{\tilde{R}(s_1)} \\ \vdots \\ \mathcal{J}_{S(s_\kappa)}\mathcal{J}_{\tilde{R}(s_\kappa)} \end{bmatrix}^T + \begin{bmatrix} \mathcal{J}_{S(s_1)}\mathcal{J}_{R(s_1)} \\ \vdots \\ \mathcal{J}_{S(s_\kappa)}\mathcal{J}_{R(s_\kappa)} \end{bmatrix} \Sigma_{A_c,C_c} \begin{bmatrix} \mathcal{J}_{S(s_1)}\mathcal{J}_{R(s_1)} \\ \vdots \\ \mathcal{J}_{S(s_\kappa)}\mathcal{J}_{R(s_\kappa)} \end{bmatrix}^T. \tag{5.26}$$

While in previous works [Ber10] the stress values $S(s_i)$ at multiple Laplace variables were aggregated empirically as in (5.6), the covariance expression (5.26) allows a new statistical aggregation scheme for damage localization based on a statistical test for each element j of the structure. In this scheme, *all* stress values at the different Laplace variables in $\overline{S}$ corresponding to an element j are tested for being 0 (and thus possibly damaged) in a hypothesis test, where the computed stress values are pondered individually by their covariance. A scalar test variable χ_j^2 is computed for each element j in such a test as follows.

First, the selection matrix for retrieving all entries in vector $\overline{S}$ corresponding to an element j is described. Let $T_j \in \mathbb{R}^{n_j \times e}$ be the matrix that selects all entries computed for an element j in the stress vector $S(s)$. The number n_j of these stress resultants for an element j depends on the kind of the element and the way of the computation of the stress resultant(s), which is up to the user. Accounting for the real and imaginary parts of the stress vector, and the stacking for all Laplace variables in (5.25), the vector $\overline{S}_j$ containing all stress values corresponding to an element j is

$$\overline{S}_j = P_j \, \overline{S} \in \mathbb{R}^{2\kappa n_j} \quad \text{where} \quad P_j = I_\kappa \otimes \begin{bmatrix} T_j & 0_{n_j,e} \\ 0_{n_j,e} & T_j \end{bmatrix}.$$

Second, the covariance of vector $\overline{S}_j$ is selected from $\Sigma_{\overline{S}}$ accordingly as

$$\Sigma_j = P_j \, \Sigma_{\overline{S}} \, P_j^T.$$

Since an estimate of vector $\overline{S}_j$ is asymptotically Gaussian distributed, it can finally be tested for being 0 and thus potentially damaged with the χ^2-test variable

$$\chi_j^2 = \overline{S}_j^T \, \Sigma_j^{-1} \, \overline{S}_j, \tag{5.27}$$

which has $2\kappa n_j$ degrees of freedom and non-centrality parameter 0 in the damaged case. Thus, the scalar variable χ_j^2 contains a statistically meaningful aggregation of all stress results computed for an element j, and it can be decided if an element j is potentially damaged if χ_j^2 is below a threshold. Such a threshold can be theoretically obtained from the properties of the χ^2-distribution for a desired type I or type II error, but for practical purposes it is often sufficient to announce potential damage locations in the elements j with the lowest values of χ_j^2.

5.5 Applications

The damage localization algorithm with the statistical aggregation of the SDDLV results from Section 5.4.5 has been applied on two applications of increasing difficulty, first on a numerical simulation of a plate and second on measurements of a real beam in a lab experiment. For each application, the statistical aggregation of the computed stresses in Equation (5.27) from Section 5.4.5 is compared to the previously suggested deterministic aggregation in Equation (5.6) from Section 5.2. Stresses close to zero correspond to potentially damaged elements.

The different Laplace variables (s-values) considered in theses applications are empirically chosen within the range of the identified poles as suggested in [Ber10] and no criterion is

available for the pertinence of the choice of such values. For both applications, the presented results include the information coming from SDDLV at all different s-values mixed with the respective aggregations. Since damage localization with these methods corresponds to finding the elements with the lowest aggregated stress values, the absolute values of (5.6) and (5.27) are limited to some level to increase the scale contrast on the potentially damaged elements. All stress results are then normalized to a scale between 0 (possibly damaged, red) and 1 (not damaged, blue) for a visual presentation. The results were obtained in Matlab 2011b, where the entire computation time of the algorithms was less than a minute, and only a few seconds after the uncertainty computation of the system identification results.

5.5.1 Simulated plate

The considered plate model has the dimensions 150 cm × 100 cm × 1 cm. Its edges are fixed and it consists of 100 plate elements as depicted in Figure 5.3. Damage in the plate was simulated by decreasing the stiffness in element "P66" by 50%. For both the undamaged and the damaged states, acceleration data of length $N = 24{,}000$ with a sampling frequency of 400 Hz was generated at the ten sensor positions shown in Figure 5.3. The data was generated from band limited white noise excitation until 150 Hz, and 5% white measurement noise were added on the outputs.

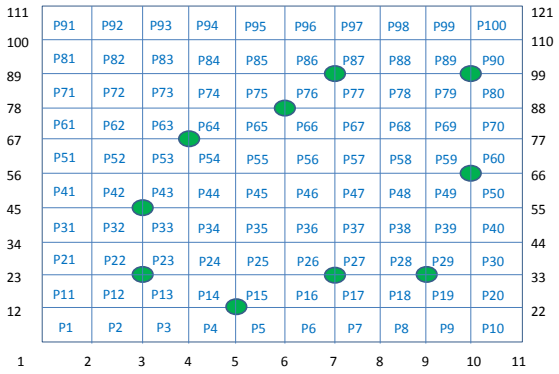

Figure 5.3 – Geometry of the plate with ten sensor positions.

From the system identification as described in Section 5.3, five well-estimated modes were chosen based on the frequencies in a stabilization diagram for both the undamaged and the damaged state, which are shown in Table 5.1. Then, matrices $\widehat{A}_c$ and $\widehat{C}_c$ in both states are filled and their uncertainty is obtained from the same dataset as described in Sections 5.4.1–5.4.2. The matrix $\mathcal{L}_{\text{model}}(s)$ in (5.5) is obtained from the FEM of the plate model, such that the moments m_{xx} and m_{yy} are computed as the stress resultants for each of the 100 plate elements from a load vector at the sensor coordinates. Then, the real and imaginary parts of the stress vector $S(s_i)$ containing these moments and their covariance is computed for the Laplace variables $s_1 = 1 + 40\text{i}$, $s_2 = 1 + 140\text{i}$, $s_3 = 1 + 200\text{i}$, $s_4 = 1 + 250\text{i}$. Thus, 16 stress related values are computed for each plate element j (real and imaginary parts of

Table 5.1 – Identified frequencies [Hz] of simulated plate in reference and damaged states.

Mode	1	2	3	4	5
Mode description	Bending	Bending	Torsion	Bending	Bending
Reference state	34.44	65.77	105.8	117.8	134.9
Damaged state	34.25	65.68	105.4	117.4	134.7

2 moments at 4 Laplace variables). These values are aggregated statistically in the variable χ_j^2 in (5.27) for each element j with the new method described in this Chapter. Also, the previous deterministic aggregation of these values in (5.6) is performed for a comparison. Both results are normalized and presented in Figures 5.4(a) and 5.4(b), respectively.

While the damage localization fails with deterministic aggregation in Figure 5.4(b), the damage is successfully localized with the statistical aggregation in Figure 5.4(a). Element P66 is well classified as damaged and indeed has the lowest χ^2 indicator value, close in the scale to 0. Also, elements in the vicinity of P66 have relatively low values, since close elements in the plate are hardly separable. Comparing the results of the statistical and deterministic aggregation in Figures 5.4(a) and 5.4(b), respectively, shows the importance of the statistical evaluation of the computed stress results, which leads to a significant improvement of the damage localization procedure.

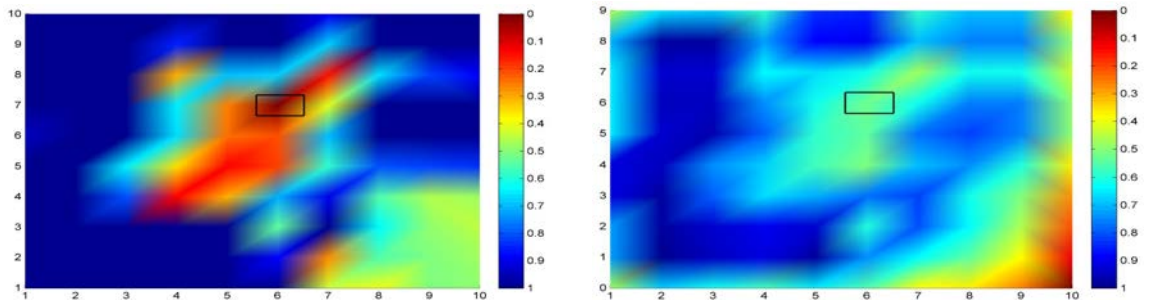

(a) Statistical aggregation – damage is found. (b) Deterministic aggregation – damage is not found.

Figure 5.4 – Damage localization in simulated plate. The black box contains the damaged element.

5.5.2 Real beam experiment

In a lab experiment, vibration tests were conducted on a beam (Figure 5.5) that was artificially damaged. The experiments were conducted by Brüel & Kjær as a benchmark for damage localization. The considered beam is made of PVC. Its dimensions are $50\,\text{cm} \times 8\,\text{cm} \times 1\,\text{cm}$ and it is fixed on one side. For both the undamaged and the damaged states, acceleration data of length $N = 295{,}936$ with a sampling frequency of 8192 Hz was recorded under white noise excitation by a shaker. The available data was downsampled and decimated by factor 6. The beam is equipped with 27 sensors on the top and on the bottom (see Figure 5.5) as follows:

- Sensors 1, 4, 7, ..., 25 are installed on the top of the beam and are vertical accelerometers.
- Sensors 2, 5, 8, ..., 26 are installed on the top of the beam and are horizontal accelerometers.
- Sensors 3, 6, 9, ..., 27 are installed on the bottom of the beam and are horizontal accelerometers.

Since the shaker acts in the horizontal direction, the vertical accelerometers are dismissed and only the 18 accelerometers in horizontal direction are used for the following damage localization.

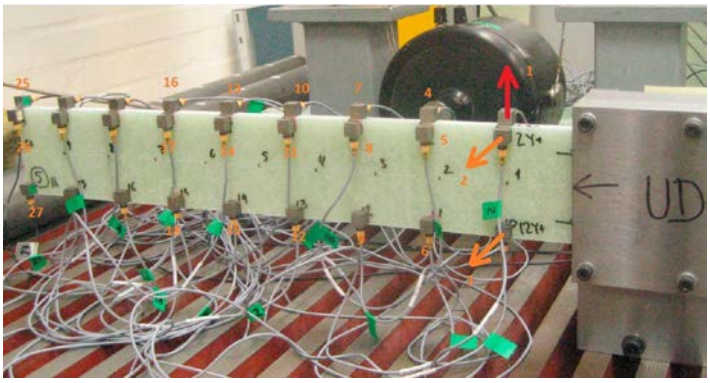

Figure 5.5 – Experimental setup of the beam.

A FEM of the beam in the reference state was made consisting of 72 plate elements as depicted in Figure 5.6, from which matrix $\mathcal{L}_{\text{model}}(s)$ is obtained. The computation of the stress resultant using the model is performed analogously to the previous section. Note that the beam from Figure 5.5 is rotated for convenience in the model in Figure 5.6, where the sensors on the top are now on the bottom and vice versa.

The beam was damaged by drilling holes, which are located around positions P02 and P20 in the model (see Figure 5.6). In a first scenario, three holes were drilled, and the damaged was increased to 5 holes in a second scenario around the same location. For drilling each new hole, the beam was removed and repositioned, where the the shaker position was also changed. Note that in the experiments the shaker influences the properties of the beam since it may change the mass at the shaker position, which is slightly different between the undamaged and the damaged states. Therefore, damage may also be localized in the vicinity of the shaker position and should be discarded. This effect would not appear in real operational cases.

From the measurement data, eight well-estimated modes were chosen in the undamaged and the two damaged states with the procedure described in Section 5.3. The corresponding frequencies for each chosen mode are presented in Table 5.2. Then, the matrices $\widehat{A}_c$ and $\widehat{C}_c$ and their covariances are obtained in the different states. The stress resultants and their covariances are computed for two different sets of Laplace variables s_i of different size, one

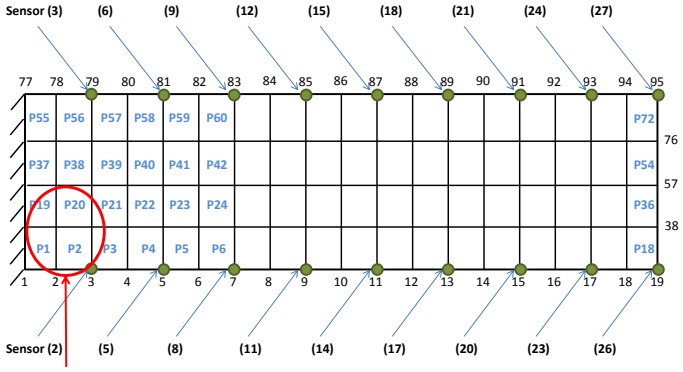

Figure 5.6 – Model of the beam with 18 sensors and the damage location.

Table 5.2 – Identified frequencies [Hz] of beam in reference and damaged states.

Mode	1	2	3	4	5	6	7	8
Mode description	Bending	Bending	Torsion	Torsion	Bending	Bending	Bending	Bending
Reference state	16.52	84.17	173.3	206.5	286.3	326.6	529.7	561.8
Damaged state: three holes	16.17	83.99	172.1	204.4	284.7	326.6	526.9	555.9
Damaged state: five holes	15.79	83.80	168.5	203.5	265.0	322.5	523.7	550.8

with four values $s_i \in \{1+3\mathrm{i}, 1+110\mathrm{i}, 1+520\mathrm{i}, 1+1600\mathrm{i}\}$ and another one with ten values $s_i \in \{1+3\mathrm{i}; 1+50\mathrm{i}; 1+110\mathrm{i}; 1+530\mathrm{i}; 1+560\mathrm{i}; 1+700\mathrm{i}; 1+855\mathrm{i}; 1+900\mathrm{i}; 1+940\mathrm{i}; 1+1600\mathrm{i}\}$. Then, the aggregation for the localization is performed with the new statistical method in (5.27) and compared to the deterministic aggregation in (5.6). The results are visualized in Figures 5.7 and 5.8 for both sets of Laplace variables, respectively.

In both figures it can be seen that the damage localization procedure with the new statistical aggregation (Figures (a), (c)) indicates strongly damage in the damaged elements P02 and P20, and sometimes in the directly adjacent elements, while the localization based on the deterministic aggregation of the stress results (Figures (b), (d)) is not successful. The aggregated results that are visualized in both figures often spread within the vertical direction of the beam, since damages at the same horizontal, but at different vertical coordinates are hard to distinguish with the used sensor and shaker layout. Note that the minimal test values are still found in the lower part of the beam, correctly indicating the damage location with the new procedure, while the small extent of the damage, its proximity to the fixed part of the beam and the lack of sensors on the vertical axis impose difficulties for the localization approach. Note also that change in the position of the shaker between the reference and damaged states is clearly visible as a damage in the middle of the beam (corresponding to elements in the vicinity of P23 and P41), which should be discarded.

An increase in the damage extent leads to localization results with a better contrast, as can be observed when comparing Figures 5.7(a) and (c), as well as Figures 5.8(a) and (c). The use of more Laplace variables for the statistical aggregation of the stress results leads also to clearer localization results in Figures 5.8(a) and 5.8(c), compared to Figures 5.7(a)

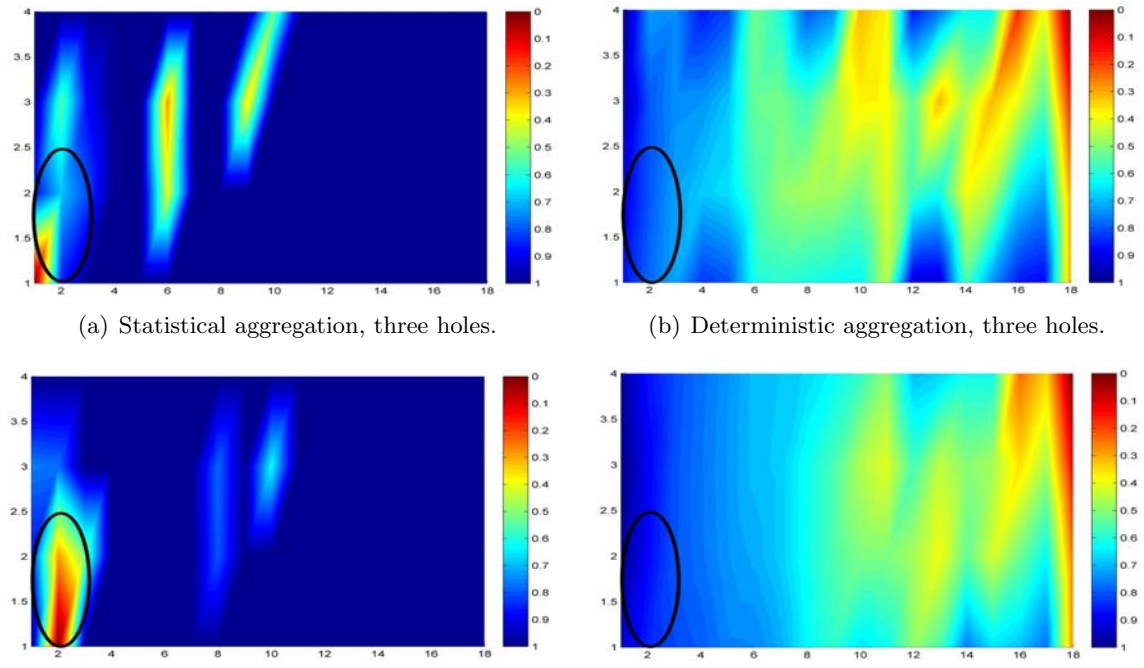

(a) Statistical aggregation, three holes.

(b) Deterministic aggregation, three holes.

(c) Statistical aggregation, five holes.

(d) Deterministic aggregation, five holes.

Figure 5.7 – Damage localization in beam using four s-values, with comparison of the new statistical aggregation (left) and the deterministic (right) aggregation, and different damage levels (top: three holes, bottom: five holes within the oval).

and 5.7(c), respectively.

Summarizing the results, it is found that the deterministic aggregation of the stress vectors from the SDDLV approach could not provide sufficient resolution for damage localization in this experiment, while the statistical evaluation and aggregation of the same stress vectors with the new method described here made a correct damage localization possible.

5.6 Conclusion

In this Chapter, we have formalized a damage localization approach combining structural model information and data driven uncertainties computation. The approach has been applied on some relevant examples, both numerical and measured in a real case study in the lab. The main focus of the Chapter has been the robustness of the method with respect to the fusion of damage localization results computed at different Laplace variables in the complex plane. The selection of these Laplace variables itself is not addressed here. It has been shown that the statistical aggregation of many values leads to a better localization information than a purely heuristic summation of values as previously done. Future works will focus on the testing of the method on structures in the field, where the FEM size and the identification parameterization are largely different.

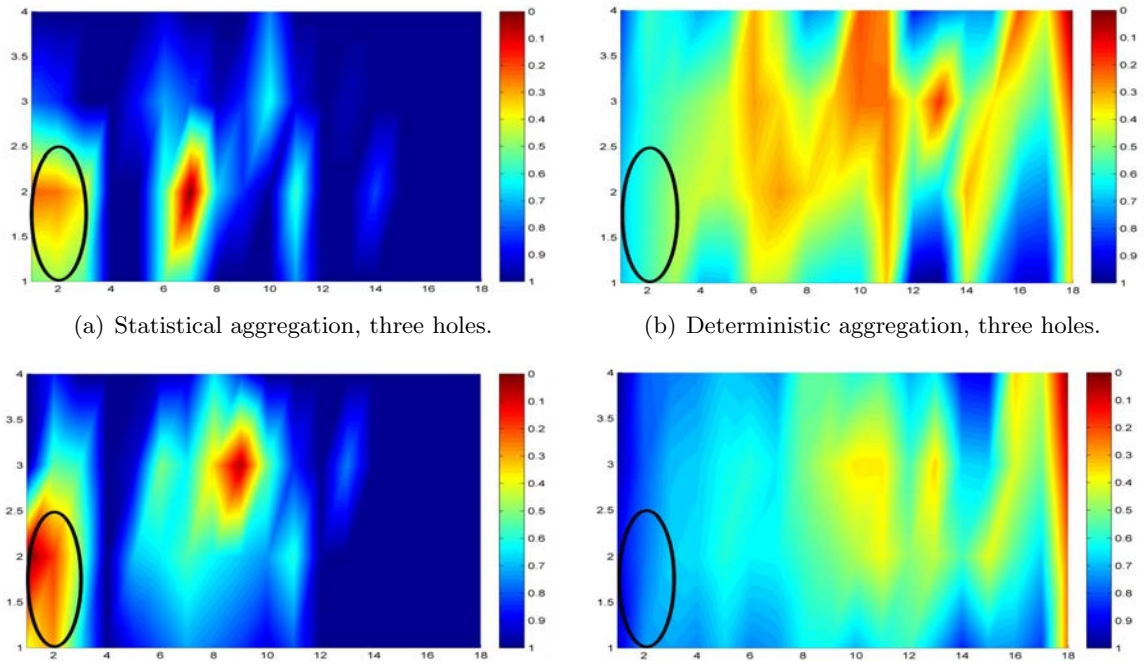

(a) Statistical aggregation, three holes.

(b) Deterministic aggregation, three holes.

(c) Statistical aggregation, five holes.

(d) Deterministic aggregation, five holes.

Figure 5.8 – Damage localization in beam using ten s-values, with comparison of the new statistical aggregation (left) and the deterministic (right) aggregation, and different damage levels (top: three holes, bottom: five holes within the oval).

5.7 Dissemination

Parts of this chapter have been submitted to:

[MDBM13b] L. Marin, M. Döhler, D. Bernal, and L. Mevel. Robust statistical damage localization with stochastic load vectors. *Structural Control and Health Monitoring*, 00:1–29, 2013. Under revision.

Chapter 6

Robust statistical decision making applied to influence lines damage localization

This Chapter is dedicated to the last contribution of this thesis, consisting on the development of a robust statistical decision making method for damage localization in civil structures based on the sensitivity-based rules (Chapter 3, Section 3.4) to overcome the inherent uncertainties in the Influence Lines Damage Localization (ILDL) approach (Chapter 2, Section 2.4) for different chosen Laplace variable. The whole method is validated in numerical simulations and real experiment of structures.

6.1 Introduction

Based on changes in the flexibility matrices δG between the reference and damaged states, a systematic approach for damage localization that interrogates these changes using output-only data is the Stochastic Dynamic Damage Location Vector (SDDLV) approach [Ber10]. Vectors in the kernel of δG, which can be obtained from the output-only data, are applied as loads to a finite element model (FEM) and lead to stress resultants that are zero over closed regions that contain the damage. Since the image and the kernel are complementary subspaces, the information on the damage location in the kernel is also contained in the image of δG.

The Influence Line Damage Location (ILDL) theorem, recently presented in [Ber13], shows that the image of δF is a basis for the influence lines (IL) for the damage location resultants. Damage is thus located at points where the subspace angle between the image and the IL computed from the FEM is zero (or small when δF is approximated). Although the kernel and the image contain the same complementary information from δF in theory, in

practice only an estimate of this matrix is available. Currently, empirical thresholds are used in the ILDL approach for deciding at which elements damage is located (i.e. where subspace angles are close to zero) and no stochastic approach is taken into account [Ber13].

In this chapter, the computation of the subspace angle is extended to the stochastic case and also to the uncertainty estimation originated from the measurement data with a sensitivity based method [RPDR08]. Then, statistical decision making on the damage locations replaces empirical thresholds. The chapter is organized as follows. In Section 6.2 the ILDL approach is introduced as a method for damage localization of mechanical structures from output-only signal. Then, in Section 6.3, the covariance of the system matrices is propagated to the damage localization residuals and a robust statistical approach for the aggregation of damage localization results is derived. Numerical and practical applications are provided in Section 6.4. Finally, in Section 6.5, some conclusions of this chapter are presented.

6.2 The ILDL approach

An influence line (IL) is a function that graphs the variation at a specific point on a mechanical structure in a predefined direction caused by a unit load [Hib09]. Any discontinuity in that predefined direction represents a potential damaged location in the displacement field. In this sense, the difference in the displacement field between the reference (undamaged) and damaged states can be viewed as a discontinuity, leading to potentially damaged locations [Ber13].

It is shown in [Ber13] that if a structure is loaded by some arbitrary static distribution and damage appears, while the load remains constant, then the change in the deformation field, given some assumptions on the nature of the damage, will be identical to that due to the action of a stress resultant acting on a discontinuity at the damage location. From this result and the previous argument it is concluded that the change in the deformation field due to the damage has the shape of the IL for the stress resultant at the location of the damage, and the deformation field is in the span of the ILs for multiple damage locations.

The step that completes the logical sequence in ILDL is to note that the image of the change in flexibility matrix $\delta F = \tilde{F} - F$ between damaged and reference states (variables with and without tilde) is the span for all possible differences in the displacement field due to damage. Thus the image of δF is identical to the span of the influence lines associated with all the damaged locations. In the implementation of the ILDL strategy δF and the influence lines only need to be evaluated at the sensor coordinates of the structure.

Therefore, damage localization based on the ILDL theorem consists of computing the ILs of stress resultants at the sensor coordinates for all elements from a finite element model (FEM) that will be checked for damage, and computing the image of δF from output-only measurement data. The localization itself is performed by checking each element of the FEM if its respective IL lies in the image of δF. The ILDL does not directly specify the position of the damage. Instead, it provides a scheme to decide, given any postulated damage position, if it is correct or not.

Note that the ILDL approach is complementary to the Stochastic Dynamic Damage Lo-

cation Vector (SDDLV) approach [Ber10], where loads in the kernel of δF are applied to a FEM to compute the stress field and damage is localized where the stress is (close to) zero.

6.2.1 Models, parameters and flexibility matrix

The behavior of a structure is assumed to be described by a linear time-invariant (LTI) dynamical system (2.6) and the equivalent continuous-time state-space model is such as in (2.20), where the state vector of the structure is $x(t) \in \mathbb{R}^n$, $y(t) \in \mathbb{R}^r$ is the output vector, the state transition matrix is $A_c \in \mathbb{R}^{n\times n}$ and $C_c \in \mathbb{R}^{r\times n}$ is the output mapping matrix. The parameter n is the system order and parameter r is the number of outputs. Remember that only matrices A_c and C_c can be obtained from output-only system identification. The input influence matrix $B_c \in \mathbb{R}^{n\times r}$ and the direct transmission matrix $D_c \in \mathbb{R}^{r\times r}$ are used for theoretical purposes.

The flexibility matrix F cannot be obtained from output-only data since system matrices B_c and D_c are not available. However, not the change in flexibility δF itself is needed for the ILDL, but only the image of δF, which can be obtained only from A_c and C_c in the damaged and reference states as follows [Ber13]. By applying the same transfer matrix in (2.28)

$$R(s) = C_c(sI - A_c)^{-1} \begin{bmatrix} C_c A_c \\ C_c \end{bmatrix}^{\dagger} \begin{bmatrix} I \\ 0 \end{bmatrix}$$

and assuming that damage does not change the mass of the system ($D = \tilde{D}$) and that D is invertible, it follows that $\delta F = \delta R D$ (with $\delta R = \tilde{R} - R$) and thus that the image of δF is the same as the image of δR.

Then, the *image* of δR is obtained from the Singular Value Decomposition (SVD)

$$\delta R = U\Sigma V^H = \begin{bmatrix} U_1 & U_2 \end{bmatrix} \begin{bmatrix} \Sigma_1 & 0 \\ 0 & \Sigma_2 \end{bmatrix} \begin{bmatrix} V_1 & V_2 \end{bmatrix}^H, \tag{6.1}$$

where $U, \Sigma, V \in \mathcal{C}^{r\times r}$, $\Sigma_1 > 0$ and $U = (u_1, \ldots, u_r) = [U_1 \quad U_2]$ the left singular vectors. Note that U_1: $(u_1, u_2, ..., u_t)$ correspond to the nonzero singular values Σ_1, and U_2: $(u_{t+1}, u_{t+2}, ..., u_r)$ correspond to the zero singular values (in practice small) Σ_2, where a desired image of δR is the matrix (or vector depending on the rank of Σ) in U_1. For any chosen value s, matrix U_1 in the image of $\delta F(s)$ can be computed as described above, where only model (2.20) has been used without information about the geometry of the structure.

6.2.2 Influence line computation and damage localization

Although either the ILDL or the SDDLV methods suffice to extract all the information for the damage locations computation in theory, in real situations the flexibility change δR is approximated and the use of both methods can prove advantageous [Ber13]. In fact, practical implementation of the SDDLV method demands decision on the effective dimension of the null space and specific guidelines for this and other implementation issues appear in the [Ber10]. The desired load vector in the null space of (6.1) for the SDDLV is any linear combination of

vectors in V_2 (see Chapters 2, Section 2.3). Since the rank is usually low, U_1 is related to less noisy information and the image in the ILDL method can provide more precise information to find damaged locations in the structure [Ber13].

Such as in 2.3.3, let $v(s)$ be any load vector at the sensor coordinates of the structure. From such a load stress resultants can be computed from a FEM. The relation between loads $v(s)$ and the vector of stress resultants $S(s)$ at the desired elements is linear and can be described by a matrix model $L_{\text{model}}(s)$ obtained from the FEM, such that model $S(s) = L_{\text{model}}(s)v(s)$.

For the ILDL approach the IL of each stress resultant in $S(s)$ is required at the sensor coordinates. Thus, applying the respective unit loads at the sensor coordinates to obtain the influence for an element j (corresponding to an entry $S_j(s)$ in vector $S(s)$), it is clear that the jth row $l^T_{j(s)}$ of model $L_{\text{model}}(s)$ is the IL of the stress resultant for element j, which is denoted by the column vector $l_j(s)$.

Damage localization with the ILDL approach consists then of checking if an IL l_j (computed from the FEM) is contained in the subspace U_1 (computed from the data in [Ber13]) for each element. The quantity used in [Ber13] that measures how well $l_j(s)$ fits into the image U_1 is the subspace angle

$$\theta_j = \cos^{-1} \left\| \left(\frac{(l_j(s))^H U_1}{\|l_j(s)\|} \right) \right\| \tag{6.2}$$

where $\theta_j = 0$ indicates the perfect fit. If j is a damaged element, θ_j will be close to zero. Since the subspace angle is not derivable at $\theta_j = 0$ for the subsequent sensitivity analysis for uncertainty quantification, the alternative quantity

$$\Gamma_j(s) = \frac{\|(l_j(s))^H \ U_1\|^2}{\|l_j(s)\|^2} \tag{6.3}$$

is proposed as an indicator of a fit. Note that $0 \leq \Gamma_j(s) \leq 1$, where $\Gamma_j(s) = 0$ indicates orthogonality between the subspaces and $\Gamma_j(s) = 1$ indicates the perfect fit.

6.2.3 Multiple aggregation

As an extension from [Ber13] to aggregate multiple quantities $\Gamma_j(s)$ in (6.3), consider that different Laplace variables s_i, $i = 1, \ldots, \kappa$, be given. To minimize modal truncation errors, they should be chosen within a vicinity of the identified poles of the structure in the complex plane, but not too close to them [Ber10]. After the identification of the system matrices A_c and C_c in the reference and $\tilde{A}_c$ and $\tilde{C}_c$ in the damaged states, the computations (2.28), (6.1) and (6.3) are repeated for each value s_i to obtain the respective vectors $\Gamma(s_i)$. Following the instructions in [Ber10] to decide if an element is damaged, the information of the corresponding entries in the stress vector $\Gamma(s_i)$ for all $i = 1, \ldots, \kappa$ can be used in the aggregation

$$\bar{\Gamma}_j = \sum_{i=1}^{\kappa} \Gamma_j(s_i) \tag{6.4}$$

for each element j.

6.3 Uncertainty quantification and robust statistical testing

As described in the previous section, system matrices A_c and C_c are necessary for the damage localization both in the reference and damaged states. However, not the "true" system matrices A_c and C_c are obtained, but estimates $\widehat{A}_c$ and $\widehat{C}_c$ of the matrices of the reduced order model that represents the identified bandwidth from a finite number of data samples . The estimated system matrices are obtained using the *covariance-driven subspace identification* [BF85, PDR99, DÏ1]. As the input of system (2.20) is unmeasured noise, $\widehat{A}_c$ and $\widehat{C}_c$ are naturally subject to variance errors depending on the data and the estimation method. A variance analysis of the estimated system matrices and expressions for their computation in the context of structural vibration analysis are given in [RPDR08, DLM11].

The uncertainties from the system identification are propagated to uncertainties in the estimated generalized cosine $\widehat{\Gamma}_j(s)$ computed from the estimates $\widehat{A}_c$ and $\widehat{C}_c$ in both reference and damaged states. These uncertainties may be crucial in deciding whether an element is potentially damaged. In this section, the uncertainty propagation is made explicit for the chosen subspace identification algorithm and expressions for the uncertainty propagation to the generalized cosine $\widehat{\Gamma}_j(s_i)$ computed at multiple values s_i, $i = 1, \ldots, \kappa$ are derived, based on Chapter 5. Then, the aggregation of the results and the test for damaged elements can be performed based on statistical criteria.

6.3.1 Definitions

The following notation and properties are defined based in Chapter 4 and will be used in the following sections. The operator $\otimes$ denotes the Kronecker product, having the property $\mathrm{vec}(AXB) = (B^T \otimes A)\mathrm{vec}(X)$. I_a denotes the identity matrix of size $a \times a$, and $0_{a,b}$ denotes the zero matrix of size $a \times b$. $e_j^a \in \mathbb{R}^a$ denotes the j-th unit vector (being column j of I_a). The permutation matrix $\mathcal{P}_{a,b} \overset{\text{def}}{=} \begin{bmatrix} I_a \otimes e_1^b & I_a \otimes e_2^b & \ldots & I_a \otimes e_b^b \end{bmatrix} \in \mathbb{R}^{ab \times ab}$ is defined with the property

$$\mathrm{vec}(X^T) = \mathcal{P}_{a,b}\,\mathrm{vec}(X) \tag{6.5}$$

for any matrix $X \in \mathbb{R}^{a \times b}$ [DM13]. Finally, for dealing with the uncertainties of complex-valued matrices we introduce an equivalent real-valued notation by defining

$$M_{\mathrm{Re}} \overset{\text{def}}{=} \begin{bmatrix} \mathrm{Re}(M) & -\mathrm{Im}(M) \\ \mathrm{Im}(M) & \mathrm{Re}(M) \end{bmatrix}, \quad M_{\mathrm{re}} \overset{\text{def}}{=} \begin{bmatrix} \mathrm{Re}(M) \\ \mathrm{Im}(M) \end{bmatrix} \tag{6.6}$$

for any matrix M as in [PGS07]. Then, for example, a complex-valued equation $Ax = b$ is equivalent to $A_{\mathrm{Re}}\, x_{\mathrm{re}} = b_{\mathrm{re}}$, and the sensitivities of the real-valued matrices can be derived.

6.3.2 Covariance of the system matrices

The sensitivity $\mathcal{J}_{R(s),A_c,C_c}$ of the matrix $R(s)$ with respect to the system matrices A_c and C_c is derived, which is needed for the generalized cosine computation in (6.1)–(6.4). In the following we generalize the sensitivity computation for acceleration data to the simplified and

more general formula of $R(s)$ in (2.28). Define

$$Z(s) = C_c(sI - A_c)^{-1}, \quad H = \begin{bmatrix} C_c A_c \\ C_c \end{bmatrix}, \quad L = \begin{bmatrix} I \\ 0 \end{bmatrix},$$

such that $R(s) = Z(s)H^\dagger L$. Applying the product rule, a first-order perturbation of $R(s)$ yields

$$\text{vec}(\Delta R(s)) = \begin{bmatrix} \mathcal{J}_{R(s),A_c} & \mathcal{J}_{R(s),C_c} \end{bmatrix} \begin{bmatrix} \text{vec}(\Delta A_c) \\ \text{vec}(\Delta C_c) \end{bmatrix},$$

where

$$\begin{aligned} \mathcal{J}_{R(s),A_c} &\overset{\text{def}}{=} \left(M(s)^T \otimes Z(s)\right) + \left(L^T \otimes Z(s)\right) \mathcal{J}_{H^\dagger} S_1^T (I_n \otimes C_c), \\ \mathcal{J}_{R(s),C_c} &\overset{\text{def}}{=} \left(M(s)^T \otimes I_r\right) + \left(L^T \otimes Z(s)\right) \mathcal{J}_{H^\dagger} \left(S_1^T (A_c^T \otimes I_r) + S_2^T\right), \end{aligned}$$

with $M(s) \overset{\text{def}}{=} (sI - A_c)^{-1} H^\dagger L$, the selection matrices $S_1 \overset{\text{def}}{=} I_n \otimes [I_r \;\; 0_{r,r}]$ and $S_2 \overset{\text{def}}{=} I_n \otimes [0_{r,r} \;\; I_r]$, and the sensitivity $\mathcal{J}_{H^\dagger}$ given in Chapter 4. Stacking the real and imaginary parts of $\text{vec}(\Delta R(s))$, it follows from (6.5) and (6.6)

$$(\text{vec}(\Delta R(s)))_{\text{re}} = \mathcal{J}_{R(s)} \begin{bmatrix} \text{vec}(\Delta A_c) \\ \text{vec}(\Delta C_c) \end{bmatrix}, \tag{6.7}$$

where

$$\mathcal{J}_{R(s)} = \begin{bmatrix} \text{Re}(\mathcal{J}_{R(s),A_c}) & \text{Re}(\mathcal{J}_{R(s),C_c}) \\ \text{Im}(\mathcal{J}_{R(s),A_c}) & \text{Im}(\mathcal{J}_{R(s),C_c}) \end{bmatrix}.$$

The covariance of $(\text{vec}(\Delta R(s)))_{\text{re}}$ from (6.7) is

$$\text{cov}\left((\text{vec}(R(s)))_{\text{re}}\right) = \mathcal{J}_{R(s)} \, \Sigma_{A_c,C_c} \, \mathcal{J}_{R(s)}^T.$$

6.3.3 Covariance of the damage quantification

To find the covariance of $\Gamma(s)$, lets first recall (6.3) and split this equation in upper and bottom parts, such that

$$\Gamma_j(s) = \frac{\Gamma_j(s)^{\text{up}}}{\Gamma_j(s)^{\text{bot}}} = \frac{\|(l_j(s))^H \; U_1\|^2}{\|l_j(s)\|^2}. \tag{6.8}$$

Note that $l_j(s)$ and U_1 are composed by complex numbers which lead to the complex result $\Gamma_j(s)$. Since statistical derivations are not allowed for complex matrix, an equivalent equation in real form is necessary. First, lets rewrite the upper part of (6.8) as

$$\Gamma_j(s)^{\text{up}} = (U_1^H \; l_j(s))^H \; (U_1^H \; l_j(s)).$$

Then, developing $\Gamma_j(s)^{\text{up}}$ and considering the real-valued notation in (6.6)

$$\Gamma_j(s)^{\text{up}} = (U_1^H \; l_j(s))_{\text{re}}^T \; (U_1^H \; l_j(s))_{\text{re}}$$

which is the same as

$$\Gamma_j(s)^{\text{up}} = ((U_1^H)_{\text{Re}}\ (l_j(s))_{\text{re}})^T\ ((U_1^H)_{\text{Re}}\ (l_j(s))_{\text{re}})$$

and finally, using the relation $(X^H)_{\text{Re}} = (X_{\text{Re}})^T$ (Chapter 4)

$$\Gamma_j(s)^{\text{up}} = ((U_{1\ (\text{Re})})^T\ (l_j(s))_{\text{re}})^T\ ((U_{1\ (\text{Re})})^T\ (l_j(s))_{\text{re}}).$$

Considering also the bottom part of (6.8) in the real form $((l_j(s))_{\text{re}})^T\ (l_j(s))_{\text{re}}$ the final development of (6.8) is then

$$\Gamma_j(s) = \frac{\Gamma_j(s)^{\text{up}}}{\Gamma_j(s)^{\text{bot}}} = \frac{((U_{1\ (\text{Re})})^T\ (l_j(s))_{\text{re}})^T\ ((U_{1\ (\text{Re})})^T\ (l_j(s))_{\text{re}})}{((l_j(s))_{\text{re}})^T\ (l_j(s))_{\text{re}}}.$$

Now, using the chain rule and the norm derivation such that $\Delta\|X\|^2 = 2X^T\Delta X$, the sensitivity of $\Gamma_j(s)$ is

$$\Delta\Gamma_j(s) = \frac{2\ ((U_{1\ (\text{Re})})^T\ (l_j(s))_{\text{re}})^T}{((l_j(s))_{\text{re}})^T\ (l_j(s))_{\text{re}}}\ \Delta(U_{1\ (\text{Re})})^T\ l_j(s))_{\text{re}})$$

and in the vectorized form defined in Section 6.3.1

$$\Delta\Gamma_j(s) = \frac{2\ ((U_{1\ (\text{Re})})^T\ (l_j(s))_{\text{re}})^T}{((l_j(s))_{\text{re}})^T\ (l_j(s))_{\text{re}}}\ (((l_j(s))_{\text{re}})^T\ \otimes\ I_{2t})\ \text{vec}(\Delta(U_{1\ (\text{Re})})^T) \tag{6.9}$$

where $\Delta\Gamma_j(s)$ is a scalar and, for this reason, the vectorized term $(\text{vec}(\Delta\Gamma_j(s)))_{\text{re}}$ is suppressed.

The covariance associated to the matrices $R(s)$ and $\tilde{R}(s)$ can be obtained in the reference and damaged states of the structure for a chosen Laplace value s. These covariances are propagated to the matrix U_1 in the image of $\delta R(s) = \tilde{R}(s) - R(s)$ and finally to $\Gamma_j(s)$, such as in Section 6.2. Then, let t be the rank of δR and let U_1 be a matrix in the column space of δR. Suppose that the complex singular vectors u_j and v_j, $j = 1, \ldots, t$. Thus, considering property (6.5) the sensitivity $\mathcal{J}_{U_1}$ with $\text{vec}(\Delta(U_{1\ (\text{Re})})^T) = \mathcal{J}_{U_1}\ (\text{vec}(\Delta\delta R(s)))_{\text{re}}$ yields

$$\mathcal{J}_{U_1} = P_1\ \left(I_t \otimes \begin{bmatrix} I_{2r} & 0_{2r,2r} \end{bmatrix}\right) \begin{bmatrix} B_1^\dagger C_1 \\ \vdots \\ B_t^\dagger C_t \end{bmatrix}, \tag{6.10}$$

and

$$B_j \overset{\text{def}}{=} \begin{bmatrix} I_{2r} & -\frac{1}{\sigma_j}(\delta R^T)_{\text{Re}} \\ -\frac{1}{\sigma_j}(\delta R^T)_{\text{Re}}^T & I_{2r} \end{bmatrix} (I_{4r} - E_{3r+1,3r+1}^{4r,4r}),$$

$$C_j \overset{\text{def}}{=} \frac{1}{\sigma_j} \begin{bmatrix} (v_j^T \otimes I_r)_{\text{Re}} - (u_j)_{\text{re}}((\overline{v}_j \otimes u_j)^T)_{\text{re}} \\ [(u_j^T \otimes I_r)_{\text{Re}} - (v_j)_{\text{re}}((\overline{u}_j \otimes v_j)^T)_{\text{re}}]P_2 \end{bmatrix},$$

and

$$P_1 \stackrel{\text{def}}{=} \mathcal{P}_{2r,2t} \begin{bmatrix} & I_{2rt} & \\ I_t \otimes \begin{bmatrix} 0_{r,r} & -I_r \\ I_r & 0_{r,r} \end{bmatrix} \end{bmatrix}, \; P_2 \stackrel{\text{def}}{=} \begin{bmatrix} \mathcal{P}_{r,r} & 0_{r^2,r^2} \\ 0_{r^2,r^2} & -\mathcal{P}_{r,r} \end{bmatrix}.$$

Then, from (6.3) and (6.9) it follows

$$\text{vec}(\Delta\Gamma_j(s)) = \mathcal{J}_{\Gamma_j(s)} \; (\text{vec}(\Delta\delta R(s)))_{\text{re}},$$

where

$$\mathcal{J}_{\Gamma_j(s)} \stackrel{\text{def}}{=} \frac{2 \; ((U_{1\;(\text{Re})})^T \; (l_j(s))_{\text{re}})^T}{((l_j(s))_{\text{re}})^T \; (l_j(s))_{\text{re}}} \; (((l_j(s))_{\text{re}})^T \; \otimes \; I_{2t}) \; \mathcal{J}_{U_1}, \tag{6.11}$$

and together with (6.7) it follows

$$\Delta\Gamma_j(s) = \mathcal{J}_{\Gamma_j(s)} \, \mathcal{J}_{\tilde{R}(s)} \begin{bmatrix} \text{vec}(\Delta\tilde{A}_c) \\ \text{vec}(\Delta\tilde{C}_c) \end{bmatrix} - \mathcal{J}_{\Gamma_j(s)} \, \mathcal{J}_{R(s)} \begin{bmatrix} \text{vec}(\Delta A_c) \\ \text{vec}(\Delta C_c) \end{bmatrix}. \tag{6.12}$$

Since the system matrices from the damaged and reference states are obtained from different statistically independent measurements, the covariance expression

$$\Sigma_{\Gamma_j(s)} \stackrel{\text{def}}{=} \text{cov}(\Gamma_j(s)_{\text{re}}) = \mathcal{J}_{\Gamma_j(s)} \, \mathcal{J}_{\tilde{R}(s)} \, \Sigma_{\tilde{A}_c,\tilde{C}_c} \, \mathcal{J}^T_{\tilde{R}(s)} \, \mathcal{J}^T_{\Gamma_j(s)} + \mathcal{J}_{\Gamma_j(s)} \, \mathcal{J}_{R(s)} \, \Sigma_{A_c,C_c} \, \mathcal{J}^T_{R(s)} \, \mathcal{J}^T_{\Gamma_j(s)} \tag{6.13}$$

follows.

6.3.4 Statistical aggregation and evaluation

Since the computation of $\Gamma(s_i)$ at multiple Laplace variables s_i, $i = 1, \ldots, \kappa$, increases the information content on the damage location (see Section 6.2), a joint evaluation of these generalized cosines increases the robustness of the statistical approach, where only one Laplace variable s was considered. The joint statistical evaluation requires the covariance computation of the stacked (real-valued) generalized cosine results

$$\overline{\Gamma} \stackrel{\text{def}}{=} \begin{bmatrix} \Gamma(s_1)_{\text{re}} \\ \vdots \\ \Gamma(s_\kappa)_{\text{re}} \end{bmatrix}. \tag{6.14}$$

Stacking (6.12) for each s_i accordingly leads to

$$\Delta\overline{\Gamma} = \begin{bmatrix} \mathcal{J}_{\Gamma(s_1)}\mathcal{J}_{\tilde{R}(s_1)} \\ \vdots \\ \mathcal{J}_{\Gamma(s_\kappa)}\mathcal{J}_{\tilde{R}(s_\kappa)} \end{bmatrix} \begin{bmatrix} \text{vec}(\Delta\tilde{A}_c) \\ \text{vec}(\Delta\tilde{C}_c) \end{bmatrix} - \begin{bmatrix} \mathcal{J}_{\Gamma(s_1)}\mathcal{J}_{R(s_1)} \\ \vdots \\ \mathcal{J}_{\Gamma(s_\kappa)}\mathcal{J}_{R(s_\kappa)} \end{bmatrix} \begin{bmatrix} \text{vec}(\Delta A_c) \\ \text{vec}(\Delta C_c) \end{bmatrix},$$

and, analogously to (6.13), to the covariance $\Sigma_{\overline{\Gamma}} \stackrel{\text{def}}{=} \operatorname{cov}(\overline{\Gamma})$ with

$$\Sigma_{\overline{\Gamma}} = \begin{bmatrix} \mathcal{J}_{\Gamma(s_1)}\mathcal{J}_{\tilde{R}(s_1)} \\ \vdots \\ \mathcal{J}_{\Gamma(s_\kappa)}\mathcal{J}_{\tilde{R}(s_\kappa)} \end{bmatrix} \Sigma_{\tilde{A}_c,\tilde{C}_c} \begin{bmatrix} \mathcal{J}_{\Gamma(s_1)}\mathcal{J}_{\tilde{R}(s_1)} \\ \vdots \\ \mathcal{J}_{\Gamma(s_\kappa)}\mathcal{J}_{\tilde{R}(s_\kappa)} \end{bmatrix}^T + \begin{bmatrix} \mathcal{J}_{\Gamma(s_1)}\mathcal{J}_{R(s_1)} \\ \vdots \\ \mathcal{J}_{\Gamma(s_\kappa)}\mathcal{J}_{R(s_\kappa)} \end{bmatrix} \Sigma_{A_c,C_c} \begin{bmatrix} \mathcal{J}_{\Gamma(s_1)}\mathcal{J}_{R(s_1)} \\ \vdots \\ \mathcal{J}_{\Gamma(s_\kappa)}\mathcal{J}_{R(s_\kappa)} \end{bmatrix}^T . \tag{6.15}$$

While in previous works [Ber13] the generalized cosine $\Gamma(s_i)$ at multiple Laplace variables were aggregated empirically as in (6.4), the covariance expression (6.15) allows a new statistical aggregation scheme for damage localization based on a statistical test for each element j of the structure. In this scheme, *all* generalized cosine values at the different Laplace variables in $\overline{\Gamma}$ corresponding to an element j are tested for being the higher (and thus possibly damaged) in a hypothesis test, where the computed generalized cosine values are pondered individually by their covariance. A scalar test variable χ_j^2 is computed for each element j in such a test as follows.

First, the selection matrix for retrieving all entries in vector $\overline{\Gamma}$ corresponding to an element j is described. Let $T_j \in \mathbb{R}^{n_j \times e}$ be the matrix that selects all entries computed for an element j in $\Gamma(s)$. The number n_j of these generalized cosine resultants for an element j depends on the kind of the element and the way of the computation of the generalized cosine resultant(s), which is up to the user. Accounting for the real and imaginary parts of the generalized cosine vector, and the stacking for all Laplace variables in (6.14), the vector $\overline{\Gamma}_j$ containing all generalized cosine values corresponding to an element j is

$$\overline{\Gamma}_j = P_j\,\overline{\Gamma} \in \mathbb{R}^{2\kappa n_j} \quad \text{where} \quad P_j = I_\kappa \otimes \begin{bmatrix} T_j & 0_{n_j,e} \\ 0_{n_j,e} & T_j \end{bmatrix}.$$

Second, the covariance of vector $\overline{\Gamma}_j$ is selected from $\Sigma_{\overline{\Gamma}}$ accordingly as

$$\Sigma_j = P_j\,\Sigma_{\overline{\Gamma}}\,P_j^T.$$

Since an estimate of vector $\overline{\Gamma}_j$ is asymptotically Gaussian distributed, it can finally be tested for being the higher and thus potentially damaged with the χ^2-test variable

$$\chi_j^2 = \overline{\Gamma}_j^T\,\Sigma_j^{-1}\,\overline{\Gamma}_j, \tag{6.16}$$

which has $2\kappa n_j$ degrees of freedom and non-centrality parameter 0 in the damaged case. Thus, the scalar variable χ_j^2 contains a statistically meaningful aggregation of all generalized cosine results computed for an element j, and it can be decided if an element j is potentially damaged if χ_j^2 is above a threshold. Such a threshold can be theoretically obtained from the properties of the χ^2-distribution for a desired type I or type II error, but for practical purposes it is often sufficient to announce potential damage locations in the elements j with the higher values of χ_j^2.

6.4 Applications

Four applications of increasing difficulty are applied to the new damage localization algorithm with robust statistical aggregation of the stochastic version of the ILDL method from Section 6.3.4. The first and the second numerical applications are on a spring-mass system and on a truss system, respectively. The third application is a numerical simulation of a plate and the last is based on measurements of a real beam in a lab experiment.

For each application, the robust statistical aggregation of the computed generalized cosine in Equation (6.16) from Section 6.3.4 is compared to the previously suggested deterministic aggregation in Equation (6.4) from Section 6.2. Moreover, the robust statistical aggregation for the SDDLV method and SDDLV deterministic aggregation [Ber10] are also depicted and compared. Note that while in the SDDLV method the "stresses" close to zero correspond to potentially damaged elements, in the ILDL method potentially damaged elements from the generalized cosine correspond to the higher elements resultants.

The different Laplace variables (s-values) considered in theses applications are empirically chosen within the range of the identified poles as suggested in [Ber10] and no criterion is available for the pertinence of the choice of such values. In all applications, the presented results include the information coming from ILDL and SDDLV at all different s-values mixed with their respective aggregations. The plate and the real bean experiments are normalized to a scale between 0 (possibly damaged, red) and 1 (not damaged, blue) for a visual presentation. Note in the plate and the real beam results that the statistical and the deterministic aggregated result corresponding to the SDDLV method have their results inverted to depict damaged and undamaged zones comparable to the statistical and the deterministic aggregated results corresponding to the ILDL method. The results were obtained in Matlab 2011b, where the overall computation time of the algorithms was less than a minute after the choice of modes.

6.4.1 Spring-mass

The considered structure is a 5 DOFs spring-mass chain (Figure 6.1). Damage was simulated by a 10% stiffness decrease in spring 2. For both the undamaged and the damaged state, a data sample of length $N = 25{,}000$ of acceleration data was generated with 5% added output noise using Gaussian white noise excitation. Five sensors were positioned at the DOFs.

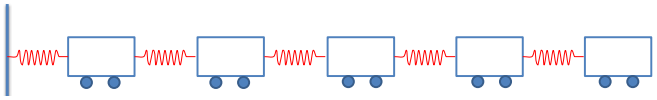

Figure 6.1 – Spring-mass system with 5 DOFs.

From the output-only data, first the system matrices and their covariances were estimated corresponding to the discrete-time state-space system (2.20), using SSI and the uncertainty quantification in [RPDR08] at system order $n = 10$. In order to obtain the matrices $\widehat{A}_c$ and $\widehat{C}_c$ of the continuous-time system and their respective covariances, a discrete to continuous

transformation was made with five well-estimated modes chosen for both the undamaged and the damaged state using the system modes selection. The Laplace variables different from zero ($s_i > 0$) were empirically chosen near to a pole of $\widehat{A}_c$. Results are displayed in two different Laplace variables sets: the first with $s_1 = 0 + 0\mathrm{i}$, and the second with four Laplace variables $s_i = [1 + 10\mathrm{i}, 1 + 15\mathrm{i}, 1 + 21\mathrm{i}, 1 + 30\mathrm{i}]$.

Final results are displayed in Figures 6.2 and 6.3, organized as: only the stress result $S_j(s)$ from the SDDLV method [Ber10] in Figures 6.2(a) and 6.3(a); SDDLV and statistical decision making method using χ^2_j in Figures 6.2(b) and 6.3(b); only the generalized cosine result $\Gamma_j(s)$ from the ILDL method [Ber13] in Figures 6.2(c) and 6.3(c); the new method linking the ILDL and statistical decision making method using χ^2_j (6.16) in Figures 6.2(d) and 6.3(d). Note that while methods related to SDDLV point to potentially damage locations at the lower positions "j", methods related to ILDL point to potentially damage locations as the higher positions "j".

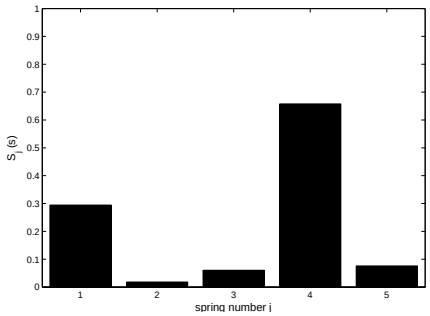

(a) Deterministic result with SDDLV.

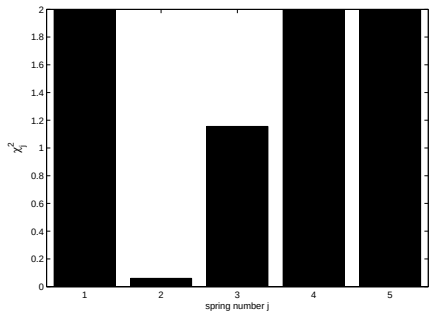

(b) Statistical result with SDDLV.

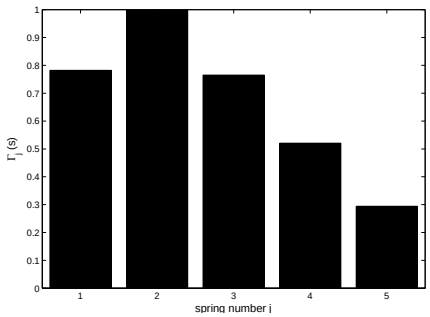

(c) Deterministic result with ILDL.

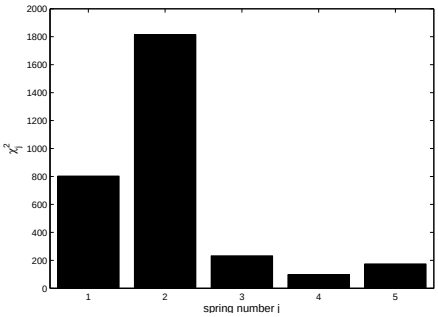

(d) Statistical result with ILDL.

Figure 6.2 – Damage localization in a spring-mass system using $s = 0 + 0\mathrm{i}$ *comparing the statistical (right) and the deterministic (left) results. Damage is on spring* 2.

Damage on spring 2 was correctly found for the case where $s = 0 + 0\mathrm{i}$ shown in Figure 6.2. Statistical results (χ^2_j) show better accuracy on the damage location. Either the SDDLV

method (Figure 6.2(a)) and the ILDL method (Figure 6.2(c)) display also the damage at position 2. While the generalized cosine of the ILDL method show also positions 1 and 3 near to the damaged position 2, the new method connecting the ILDL and the statistical decision making method using χ^2_j (6.16) in Figure 6.2(d) is clearly distinguishable.

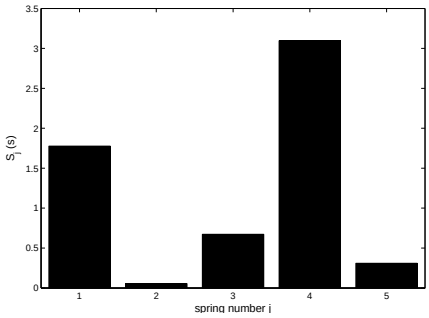

(a) Aggregated deterministic result with SDDLV.

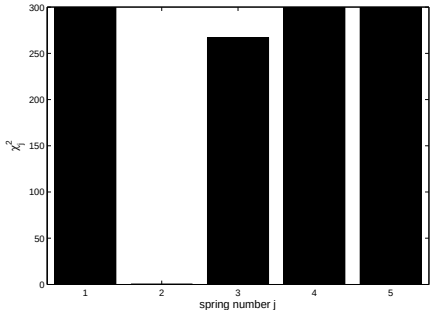

(b) Aggregated statistical result with SDDLV.

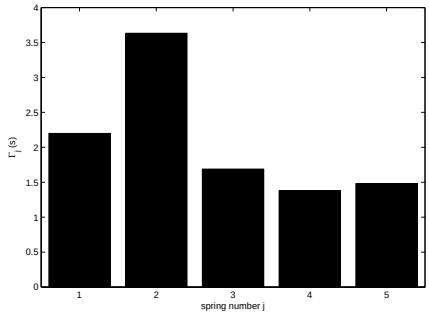

(c) Aggregated deterministic result with ILDL.

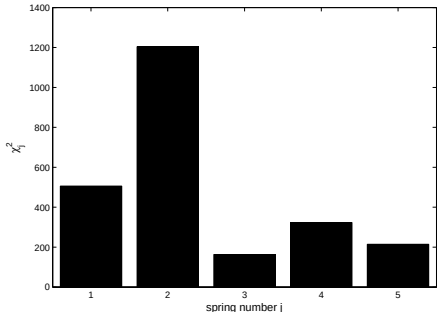

(d) Aggregated statistical result with ILDL.

Figure 6.3 – Damage localization in a spring-mass system using $s_i = [1 + 10\mathrm{i}, 1 + 15\mathrm{i}, 1 + 21\mathrm{i}, 1 + 30\mathrm{i}]$ *comparing the statistical (right) and the deterministic (left) results. Damage is on spring* 2.

For the case with different Laplace variables s_i, the damage on spring 2 was again correctly found as demonstred in Figure 6.3. Now, all results show accuracy on the damage location because more information is provided (aggregated results) in either the deterministic and the statistical cases. Note that the difference between the undamaged and damaged positions are better defined in the statistical aggregation in Figures 6.3(b) and 6.3(d) when compared to the deterministic results in Figures 6.3(a) and 6.3(c).

6.4.2 Truss

A numerical application using a simulated 25 DOF truss structure (Figure 6.4) is also used to validate the new damage localization method with statistical decision making and compared with other methods. Damage was simulated by a stiffness reduction in the elements

16. For both the undamaged and the damaged state, a data sample of length $N = 25{,}000$ of acceleration data was generated with 5% added output noise using Gaussian white noise excitation. From the output-only data the system matrices and their covariances were estimated corresponding to the discrete-time state-space system (2.20), using SSI and the uncertainty quantification in [RPDR08]. In order to obtain the matrices $\widehat{A}_c$ and $\widehat{C}_c$ of the continuous-time system and their respective covariances the system modes selection was performed with four well-estimated modes chosen for both the undamaged and the damaged state. The Laplace variables different of zero ($s_i > 0$) were empirically chosen near to a pole of $\widehat{A}_c$.

The application is performed with three sets of Laplace variables "s": the first with $s = 0 + 0\mathrm{i}$ (Figure 6.5), the second (Figure 6.6) and the third (Figure 6.7) with six s-values. Note that the Laplace variables near to the poles of $\widehat{A}_c$ are empirically chosen for the cases where $s > 0$ [Ber10]. Since there is no guarantee that these Laplace variables are well-chosen for the damage localization procedure, the second and the third set of Laplace variables applied to the methods have their results compared.

Results are organized on the left-top part for the SDDLV method [Ber10] (Figures 6.5(a), 6.6(a) and 6.7(a)), on the right-top part for the SDDLV with the statistical decision making method (Figures 6.5(b), 6.6(b) and 6.7(b)), on the left-bottom part for the ILDL method [Ber13] (Figures 6.5(c), 6.6(c) and 6.7(c)), and on the right-bottom part for the new method connecting the ILDL with the statistical decision making 6.5(d), 6.6(d) and 6.7(d).

The first set of results with $s = 0+0\mathrm{i}$ are shown in Figure 6.5. They show two elements as damaged: the damaged element 16 as well as the undamaged element 23 that is a neighboring of element 16 (see Figure 6.4). In fact, for the considered sensors set, element 23 is inseparable from element 16 at $s = 0 + 0\mathrm{i}$ [Ber02] (i.e. if the stress in 16 is zero, so it must be in 23). The elements 1–15, 17–22 and 24–25 are correctly classified as undamaged and element 16 is correctly classified as damaged in all results. Note that the new method connecting the ILDL with statistical decision making clearly highlights the damage in element 16 (and the inseparable element 23).

The second set of results with $s_i = [1 + 5\mathrm{i}, 1 + 15\mathrm{i}, 1 + 25\mathrm{i}, 1 + 35\mathrm{i}, 1 + 45\mathrm{i}, 1 + 55\mathrm{i}]$ are displayed in Figure 6.6. Element 16 is correctly classified as damaged while elements 1–15, 17–22 and 24–25 are correctly classified as undamaged. Note that element 23 is now separable and not classified as damaged anymore. Although Figures 6.5(a) and 6.5(c) show the damaged element 16 correctly, statistical decision making methods in Figures 6.5(b) and 6.5(d) highlight the damaged position. The new method demonstrates clearly the damaged element.

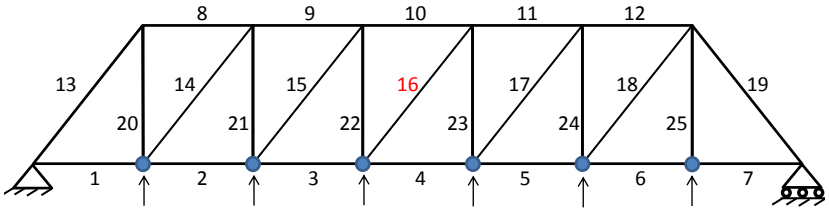

Figure 6.4 – Truss structure with six sensors.

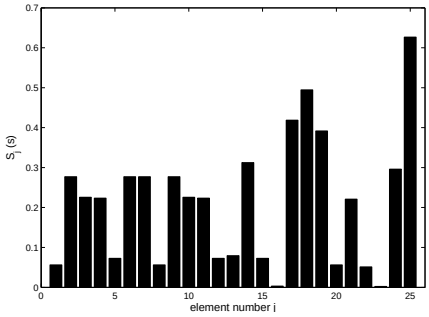

(a) Deterministic result with SDDLV.

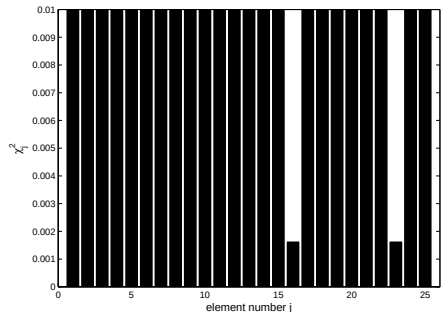

(b) Statistical result with SDDLV.

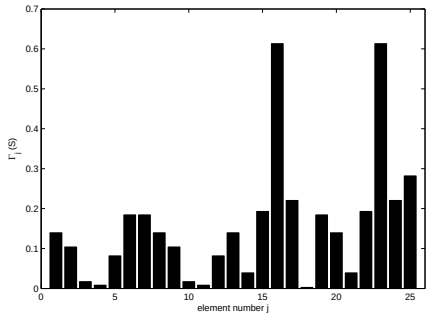

(c) Deterministic result with ILDL.

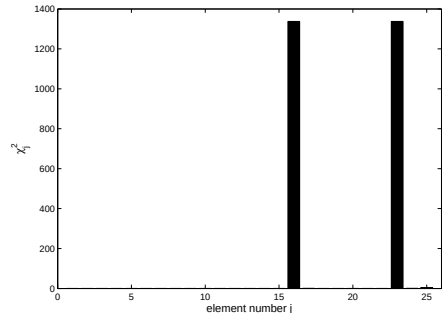

(d) Statistical result with ILDL.

Figure 6.5 – Damage localization in the truss structure using $s = 0 + 0\mathrm{i}$ comparing the statistical (right) and the deterministic (left) results. Damage is on element 16.

The third and last set of results with $s_i = [10{+}5\mathrm{i}, 10{+}15\mathrm{i}, 10{+}25\mathrm{i}, 10{+}35\mathrm{i}, 10{+}45\mathrm{i}, 10{+}55\mathrm{i}]$ are shown in Figure 6.7. The new method was capable to show correctly the damaged on element 16 (Figure 6.7(d)) while others were not (Figures 6.7(a), 6.7(b) and 6.7(c)). In comparison to the previous results with different Laplace variables, Figure 6.6 clearly demonstrates that the choice of the s-values can change significantly the damage location result depending on the chosen method. Both statistical decision making methods provide complementary results and can be used together to localize the damaged element.

6.4.3 Plate

The considered plate structure (see Figure 6.8) is composed by 100 elements and has the dimensions 150 cm width, 100 cm height and 1 cm of thickness. The edges of the plate are fixed. Damage was simulated by stiffness reduction in element "P66", decreased by 50%. For both the undamaged and the damaged states, acceleration data collection of length $N = 24{,}000$ with a sampling frequency of 400 Hz was generated at the ten sensor positions (circles in the nodes in the Figure 6.8). Data was generated from the band limited white noise

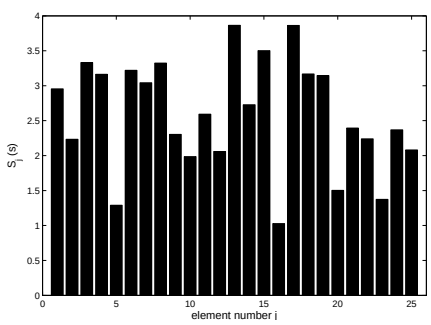

(a) Aggregated deterministic result with SDDLV.

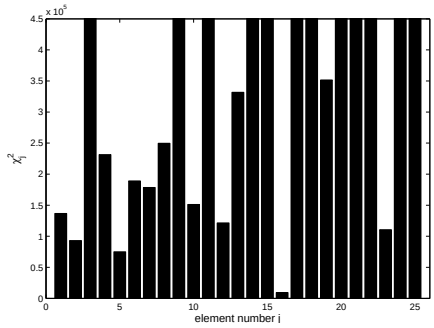

(b) Aggregated statistical result with SDDLV.

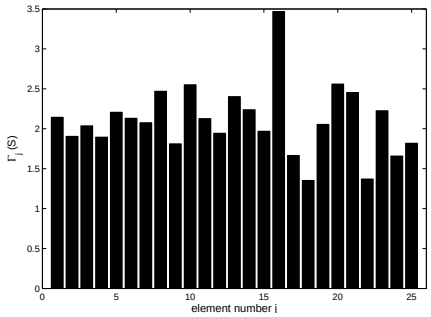

(c) Aggregated deterministic result with ILDL.

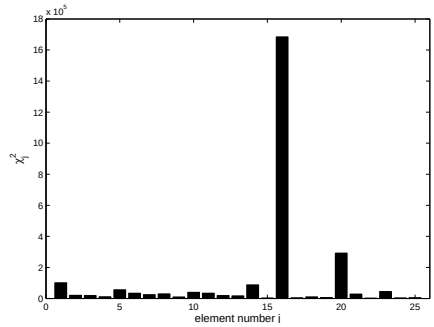

(d) Aggregated statistical result with ILDL.

Figure 6.6 – Damage localization in the truss structure using $s_i = [1 + 5\mathrm{i}, 1 + 15\mathrm{i}, 1 + 25\mathrm{i}, 1 + 35\mathrm{i}, 1 + 45\mathrm{i}, 1 + 55\mathrm{i}]$ comparing the statistical (right) and the deterministic (left) results. Damage is on element 16.

excitation until 150 Hz and 5% of Gaussian white noise excitation is added on the output.

From the SSI identification, five well-estimated modes were chosen based on the frequencies in a stabilization diagram for both the undamaged and the damaged state, which are shown in Table 6.1. Then, matrices $\widehat{A}_c$ and $\widehat{C}_c$ in both states are filled and their uncertainty is obtained from the same dataset. The choice of modes and the procedure to build the system matrices in continuous time is detailed previously in this Chapter. The matrix $\mathcal{L}_{\mathrm{model}}(s)$ from Section 6.2 is obtained from the FEM of the plate model, such that the moments m_{xx} and m_{yy} are computed as the generalized cosine resultants for each of the 100 plate elements from U_1 at the sensor coordinates. Then, the generalized cosine $\Gamma(s_i)$ containing these moments and their covariance are computed for the Laplace variables $s_1 = 1 + 40\mathrm{i}$, $s_2 = 1 + 140\mathrm{i}$, $s_3 = 1 + 200\mathrm{i}$, $s_4 = 1 + 250\mathrm{i}$. Thus, 16 stress related values are computed for each plate element j. These values are aggregated statistically in the variable χ^2_j in (6.16) and shown in Figure 6.9(d) for each element j with the new method as described. The previous deterministic aggregation of these values in (6.4) is performed for comparison and displayed in Figure 6.9(c). These results are also compared with the SDDLV method [Ber10] and the pre-

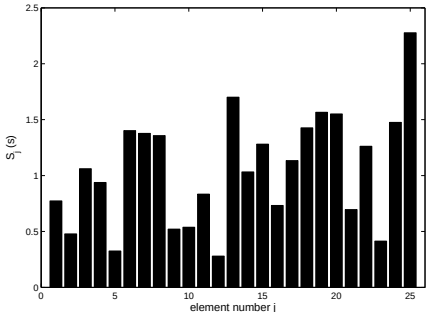

(a) Aggregated deterministic result with SDDLV.

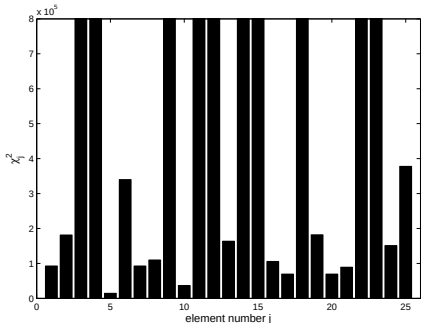

(b) Aggregated statistical result with SDDLV.

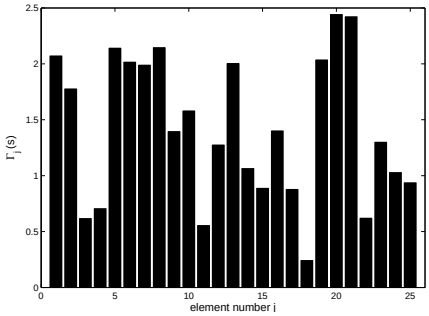

(c) Aggregated deterministic result with ILDL.

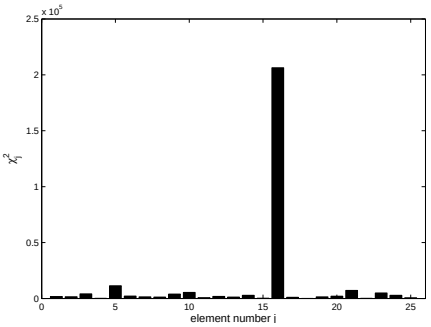

(d) Aggregated statistical result with ILDL.

Figure 6.7 – Damage localization in the truss structure using $s_i = [10{+}5\mathrm{i}, 10{+}15\mathrm{i}, 10{+}25\mathrm{i}, 10{+}35\mathrm{i}, 10{+}45\mathrm{i}, 10{+}55\mathrm{i}]$ *comparing the statistical (right) and the deterministic (left) results. Damage is on element 16.*

vious method that connects the SDDLV to the statistical decision making in Figures 6.9(a) and 6.9(b), respectively. All results are normalized and depicted in Figure 6.9. Statistical and the deterministic aggregated result corresponding to the SDDLV method have their results inverted to depict damaged and undamaged zones comparable to the statistical and the deterministic aggregated results corresponding to the ILDL method.

The damage localization fails with the SDDLV and ILDL deterministic aggregation in Figures 6.9(a) and 6.9(c) but is successfully localized with the SDDLV statistical aggregation in Figure 6.9(b) and the ILDL statistical aggregation in Figure 6.9(d). In the statistical aggregation results the element P66 is well classified as damaged and indeed has the lowest χ^2 indicator value, close in the scale to 0. Note that elements in the vicinity of P66 have relatively low values in Figure 6.9(b), since close elements in the plate are hardly separable. However, the vicinity on the damage location P66 in Figure 6.9(d) is better separable and the possible damage zone is reduced. Then, comparing the results of the statistical aggregations in Figures 6.9(b) and 6.9(d) and deterministic aggregations in Figures 6.9(a) and 6.9(c), the importance of the statistical evaluation in the computed damage location results is evident.

Table 6.1 – Identified frequencies of the simulated plate in reference and damaged states

Mode	1	2	3	4	5
Description	Bending	Bending	Torsion	Bending	Bending
Reference Frequencies	34.44	65.77	105.78	117.82	134.91
Damage Frequencies	34.25	65.68	105.38	117.41	134.73

Comparing the statistical decision making methods, the new method leads to a significant improvement in the damage localization procedure.

6.4.4 Real beam experiment

The real beam experiment was conducted by Brüel & Kjær as a benchmark for damage localization in a lab experiment. There, vibration test was conducted on a beam (Figure 6.10) that was artificially damaged. The considered beam is made of PVC with $50\,\text{cm} \times 8\,\text{cm} \times 1\,\text{cm}$, which is fixed on one side. For both the undamaged and the damaged states, acceleration data of length $N = 295{,}936$ with a sampling frequency of 8192 Hz was recorded under white noise excitation by a shaker. The available data was downsampled and decimated by factor 6. The beam has 27 sensors on the top and on the bottom (see Figure 6.10) as follows:

- Sensors 1, 4, 7, ..., 25 are installed on the top of the beam and are vertical accelerometers.
- Sensors 2, 5, 8, ..., 26 are installed on the top of the beam and are horizontal accelerometers.
- Sensors 3, 6, 9, ..., 27 are installed on the bottom of the beam and are horizontal accelerometers.

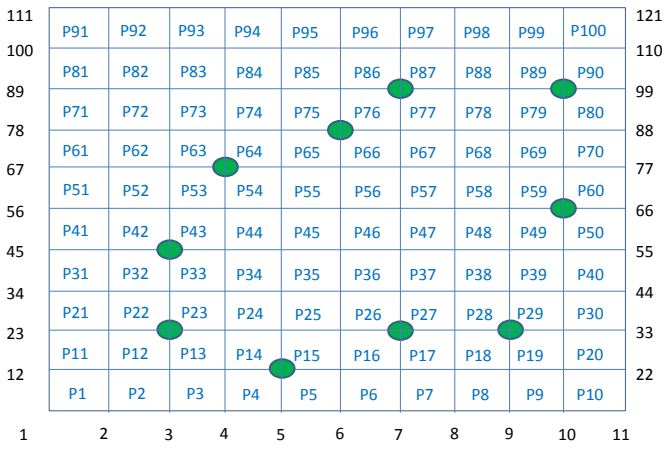

Figure 6.8 – Geometry description of the plate with ten sensors.

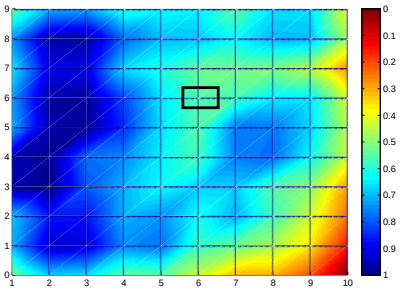

(a) Aggregated deterministic result with SDDLV.

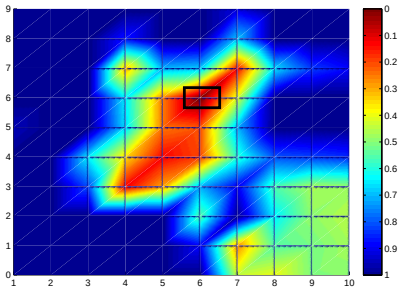

(b) Aggregated statistical result with SDDLV.

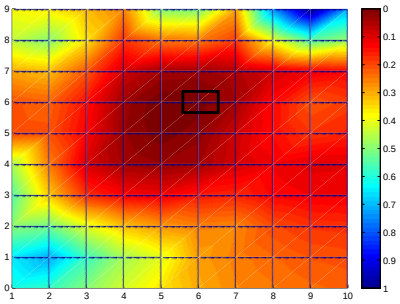

(c) Aggregated deterministic result with ILDL.

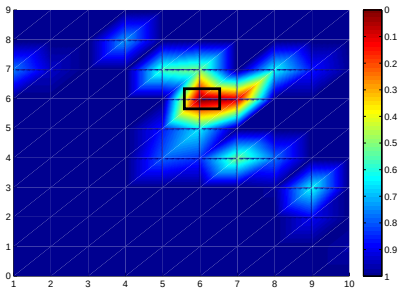

(d) Aggregated statistical result with ILDL.

Figure 6.9 – Damage localization in the plate structure using $s_i = [1 + 40\mathrm{i}, 1 + 140\mathrm{i}, 1 + 200\mathrm{i}, 1 + 250\mathrm{i}]$ *comparing the statistical (right) and the deterministic (left) results. Damage is on element P66.*

Since the shaker acts in the horizontal direction, the vertical accelerometers are dismissed and only the 18 accelerometers in horizontal direction are used for the following damage localization.

A FEM of the beam in the reference state was made consisting of 72 plate elements as depicted in Figure 6.11, from which matrix $\mathcal{L}_{\mathrm{model}}(s)$ is obtained. The computation of the generalized angles using the model is performed analogously to the previous section. Note that the beam from Figure 6.10 is rotated for convenience in the model in Figure 6.11, where the sensors on the top are now on the bottom and vice versa.

The beam was damaged by drilling 5 holes located around positions P02 and P20 in the model (see Figure 6.11). Note that in the experiment the shaker influences the properties of the beam since it may change the mass at the shaker position, which is slightly different between the undamaged and the damaged states. Therefore, damage may also be localized in the vicinity of the shaker position and should be discarded. This effect would not appear in real operational cases.

From the measurement data, eight well-estimated modes were chosen in the undamaged and the damaged states. The corresponding frequencies for each chosen mode are demonstred in Table 6.2. Then, the matrices $\widehat{A}_c$ and $\widehat{C}_c$ and their covariances are obtained in the different states. The generalized angle resultants and their covariances are computed for two different sets of Laplace variables s_i of different size: the first with four values $s_i \in \{1+3\mathrm{i}, 1+110\mathrm{i}, 1+520\mathrm{i}, 1+1600\mathrm{i}\}$ and the second with ten values $s_i \in \{1+3\mathrm{i}; 1+50\mathrm{i}; 1+110\mathrm{i}; 1+530\mathrm{i}; 1+560\mathrm{i}; 1+700\mathrm{i}; 1+855\mathrm{i}; 1+900\mathrm{i}; 1+940\mathrm{i}; 1+1600\mathrm{i}\}$. Then, the deterministic aggregations with

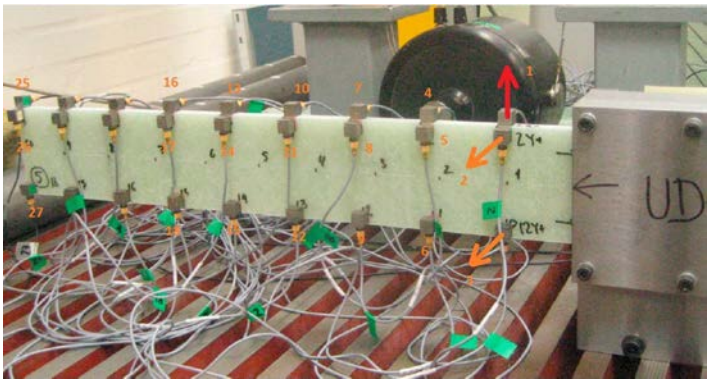

Figure 6.10 – Experimental set of the beam.

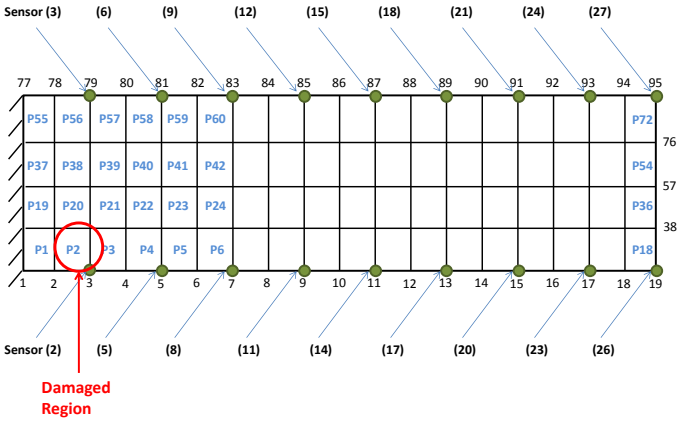

Figure 6.11 – Geometry description of the beam with 18 sensors.

Table 6.2 – Modes description and eigenfrequencies in the reference and damage states – beam

Mode	1	2	3	4	5	6	7	8
Description	Bending	Bending	Torsion	Torsion	Bending	Bending	Bending	Bending
Reference Frequencies	16.52	84.17	173.27	206.52	286.32	326.62	529.69	561.83
Damage Frequencies for five holes	15.79	83.80	168.45	203.47	264.96	322.45	523.74	550.79

the ILDL [Ber13] and SDDLV [Ber10] methods for the damage localization are compared with the SDDLV statistical method and the new ILDL statistical method in (6.16). The results are visualized in Figures 6.12 and 6.13 for both sets of Laplace variables. The statistical and the deterministic aggregated result corresponding to the SDDLV method have their results inverted to depict damaged and undamaged zones comparable to the statistical and the deterministic aggregated results corresponding to the ILDL method.

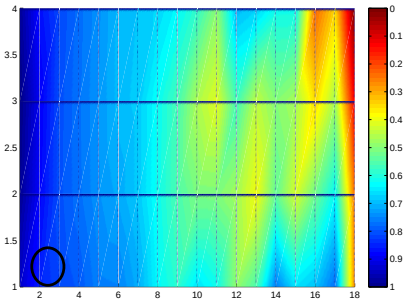

(a) Aggregated deterministic result with SDDLV.

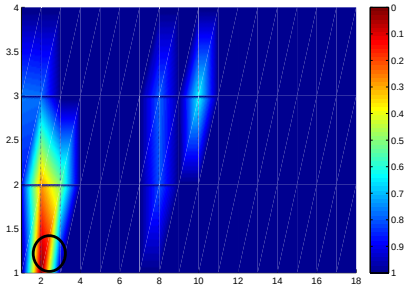

(b) Aggregated statistical result with SDDLV.

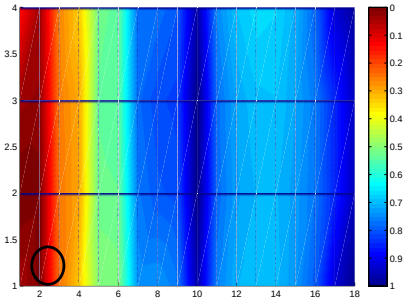

(c) Aggregated deterministic result with ILDL.

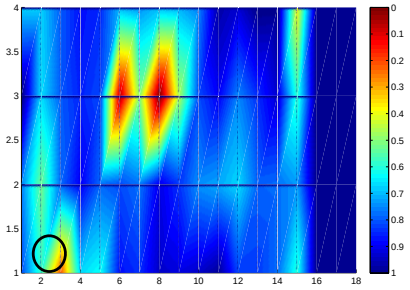

(d) Aggregated statistical result with ILDL.

Figure 6.12 – Damage localization in the beam structure using $s_i = [1+3\mathrm{i}; 1+110\mathrm{i}; 1+520\mathrm{i}; 1+1600\mathrm{i}]$ *comparing the statistical (right) and the deterministic (left) results.*

Figures 6.12 and 6.13 indicate the damage in element P02 for the SDDLV statistical aggregation method in 6.12(b) and 6.13(b) and for the ILDL statistical aggregation method in 6.12(d) and 6.13(d). The deterministic aggregation of the stress results (Figures 6.12(a) and

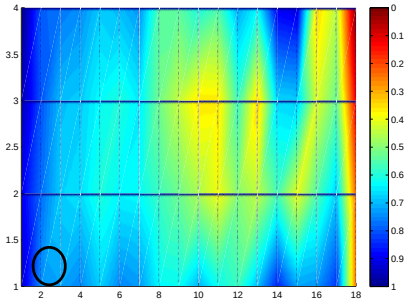

(a) Aggregated deterministic result with SDDLV.

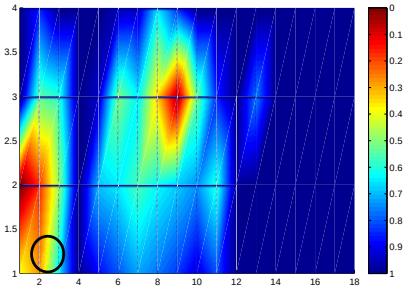

(b) Aggregated statistical result with SDDLV.

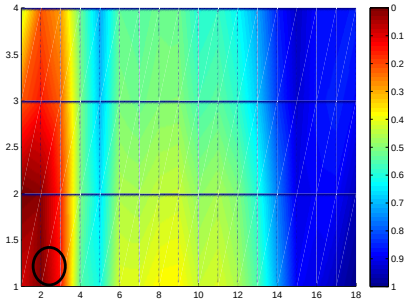

(c) Aggregated deterministic result with ILDL.

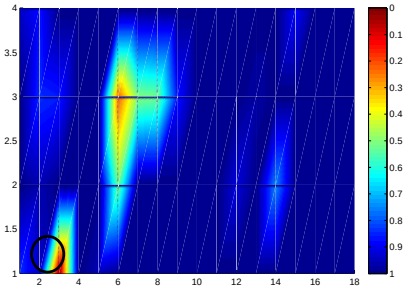

(d) Aggregated statistical result with ILDL.

Figure 6.13 – Damage localization in the beam structure using $s_i = [1+3\mathrm{i}; 1+50\mathrm{i}; 1+110\mathrm{i}; 1+530\mathrm{i}; 1+560\mathrm{i}; 1+700\mathrm{i}; 1+855\mathrm{i}; 1+900\mathrm{i}; 1+940\mathrm{i}; 1+1600\mathrm{i}]$ *comparing the statistical (right) and the deterministic (left) results.*

6.13(a)) and of the generalized cosine results (Figures 6.12(c) and 6.13(c)) are not successful. Note that change in the position of the shaker between the reference and damaged states is clearly visible as a damage in the middle of the beam (corresponding to elements in the vicinity of P23 and P41), which should be discarded. Minimal test values found in the lower part of the beam for the statistical methods correctly indicating the damage location with the new procedure. The previous SDDLV statistical method indicate the damage spreaded in the vertical axis. The proximity to the fixed part of the beam and the lack of sensors on the vertical axis impose difficulties for the localization approach.

The use of more Laplace variables for the statistical aggregation results leads also to clearer localization results. The deterministic aggregation of the stress vectors from the SDDLV and of the generalized cosine from the ILDL approach could not provide sufficient resolution for damage localization in this experiment. However, the SDDLV statistical aggregation of the same stress vectors made a correct damage localization and the new ILDL statistical method is even more exact to point the damage location.

Shaker effect: In the considered experiment conducted by Brüel & Kjær in a lab, the bean was attached to a shaker to produce the desired excitation (see Figure 6.10) and then the output is collected by sensors. Figures 6.12 and 6.13 shown the shaker effect clearly identified around positions P23 and P41, mainly in the statistical aggregation results. Since the shaker effect points to a spurious damaged element, alternatives to reduce its effect is desirable. Note that in real situations the excitation is produced by some environmental effect (i.e. earthquake) and the artificial excitation from the shaker would not appear in real operational cases.

An option to reduce the shaker effect is by increasing the mass around the positions where the shaker is located. Then, in theory, the shaker effect starts to lose its influence as spurious damaged element. Two examples were performed by reducing the shaker effect from the ILDL statistical aggregation results shown in Figure 6.13(d). In the first example, depicted in Figure 6.14(a), the elements around the shaker has the original mass of the FEM slightly increased in two times. In the second example, depicted in Figure 6.14(b), the same original mass of the FEM is highly increased in fifty times in the positions around the shaker. While in the first example the shaker effect is lessened, the second example almost discards the shaker effect and only the damaged zone is available.

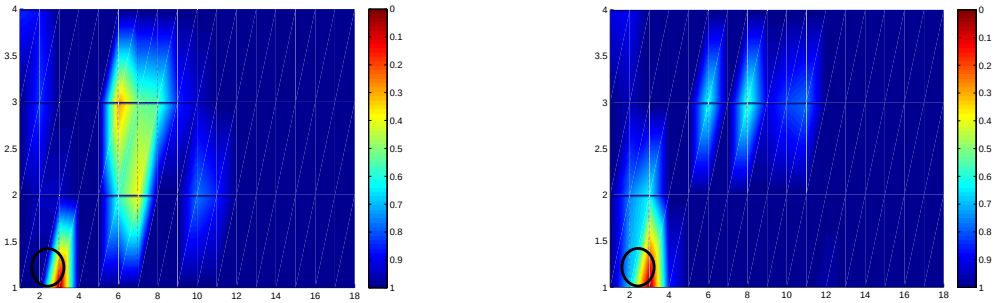

(a) FEM mass slightly increased by two times (Figure 6.13(d)).

(b) FEM mass highly increased by fifty times (Figure 6.13(d)).

Figure 6.14 – The beam structure with modified mass around the shaker position.

6.5 Conclusion

In this chapter, an extension of the damage localization approach based on the ILDL method into the stochastic case was developed as well as the combination of the structural model information and data driven uncertainties computation. Then, a statistical decision making framework of the stochastic ILDL method taking into account the inherent uncertainties from the SSI was considered. Now, the decision on whether a location is damaged or not is no more based on empirical thresholds. The selection of these Laplace variables itself was not addressed. Numerical and real applications were depicted and compared between the new

presented method in this chapter and other damage localization methods. The new method has proved to be efficient to find the damage location in all applications. Future work will focus on the optimal Laplace variable choice and on the use of larger real experiments.

6.6 Dissemination

Parts of this chapter have been submitted to:

[MDBM13c] L. Marin, M. Döhler, D. Bernal, and L. Mevel. Statistical based decision making for damage localization with influence lines. In *The 9th International Workshop on Structural Health Monitoring*, 2013.

Conclusions and future works

The last decades have seen the growth of techniques for structural health monitoring proposes. In this context, Operational Modal Analysis (OMA) techniques have therefore been developed where the modal parameters are extracted from the dynamic response to operational forces. There, ambient forces are usually modeled as stochastic quantities with unknown parameters but with known behavior, for instance, as white noise time series with zero mean and unknown covariance. In the offline analysis situation, where data is collected at two different times with information about changes in the structural condition in the interval between the measurements, the damage characterization can be ameliorated by decoupling as detection, localization, and quantification.

Damage localization methods based in the flexibility changes of structures were described in this thesis. In theory, system matrices are plugged in models of structures (i.e. finite element model) and results should present the exact information about the damage location. However, these system matrices are afflicted by intrinsic uncertainties that exists in the system identification. In this thesis, decision making methods based in the sensitivity based theory to overcome these uncertainties were developed.

The first contribution is described in Chapter 4. There, the Stochastic Dynamic Damage Location Vector (SDDLV) was introduced as an output-only damage localization method. Damage is related to a residual derived from the null space of the difference between the transfer matrices in both reference and damage states and a model of the reference state. Deciding that this residual corresponds to a damage position is done using an empirically defined threshold. Since the SDDLV does not take into account the intrinsic uncertainties (i.e. noise and limited data length), the first contribution replaces empirical rules by sensitivity-based rules as the damage localization criterion. The development of this contribution considered the case were only one Laplace variable is available (the static case) for the transfer matrix computation. Numerical examples were provided for the contribution evaluation.

In second contribution, Chapter 5, the SDDLV method is again considered but with its original features in a robust alternative. Different Laplace variables were considered (the dynamic case) increasing the robustness and helping the decision making. The necessary system identification steps with the construction of parametric system matrices from identified modes was explained in details and the robust statistical approach for the aggregation of damage localization results for different Laplace variables were derived. Numerical and real applications were used for the contribution validation.

The last contribution in Chapter 6 refers to a robust statistical decision making method applied to the Influence Lines Damage Localization (ILDL) approach. Based on the image (column space) from the difference between the transfer matrices in both reference and damage states as the Influence Line (IL), the damage is thus located at points where the subspace angle between the image and the IL computed from a model (i.e. finite element model) is zero (in practice small). Similarly to the SDDLV, currently empirical thresholds are used in the ILDL . Then, by first adapting the computation of the subspace angles into the stochastic case, finally sensitivity based methods are applied for the derivation and the intrinsic uncertainties are overcome. Numerical and real applications were used for the contribution validation.

Note that both damage localization approaches, the SDDLV and the ILDL, are complementary methods based in the changes of the flexibility matrix from some pre-defined structural model. On one hand, the SDDLV uses the null space obtained from the output-only data as the loads to a FEM and lead to stress resultants for the damage location. On the other hand, the ILDL uses the image obtained from the output-only data and damage is located at points from the subspace angle between the image and the IL computed from the FEM. From the derivation of the intrinsic uncertainties in both SDDLV and ILDL methods this thesis also provided a complete statistical decision making framework, where the application results depicted in each contribution reinforce their complementary importance.

In all contributions, the covariance-driven subspace identification method was used and the system matrices were constructed from the identified parameters (eigenvalues and mode shapes). All output-only damage localization methods used in this thesis are model dependent, which is crucial for the success of the damage localization. Thus, well-designed structural models lead to better location results while the opposite is not recommended. In summary, all contributions successfully improved the related output-only damage localization approaches by overcoming their uncertainties into new statistical decision making methods.

Future works would consider to substitute the covariance-driven subspace identification method for other system identification methods in order to approve or reprove their efficacy in the contributions of this thesis, include input data in applications when this is available (i.e. real beam application in the contribution chapters), and apply the contributions of this thesis in bigger structures, such as real bridges and buildings.

Bibliography

[Å70] K.J. Åström. *Introduction to stochastic control theory*. Academic Press, New York, NY, USA, 1970.

[AB65] K.J. Åström and T. Bohlin. Numerical identification of linear dynamic systems from normal operating records. In *IFAC conference on self-adaptive systems*, 1965.

[Add02] P.S. Addison. *The illustrated wavelet transform handbook: Introductory theory and applications in science, engineering, medicine and finance*. Taylor and Francis, 1st edition edition, 2002.

[AE71] K.J. Åström and P. Eykhoff. System identification: a survey. *Automatica*, 7(2):123–162, 1971.

[Aka74] H. Akaike. Stochastic theory of minimal realization. *IEEE Transactions on Automatic Control*, 19(6):667–674, 1974.

[BAMT96] R. Brincker, P. Andresen, Martinez M.E., and F. Tallav. Modal analysis of an offshore platform using two different arma approaches. In *Proceedings of the 14th international modal analysis conference*, 1996.

[Bas98] M. Basseville. On-board component fault detection and isolation using the statistical local approach. *Automatica*, 34(11):1391–1415, 1998.

[Bat96] K.J. Bathe. *Finite element procedures*. Prentice-Hall, 2nd edition edition, 1996.

[Bau05] D. Bauer. Asymptotic properties of subspace estimators. *Automatica*, 41(3):359–376, 2005.

[BBM00] A. Benveniste, M. Basseville, and L. Mevel. Convergence rates for eigenstructure identification using subspace methods. In *Proc. 39th IEEE Conference on Decision and Control*, pages 1550–1554, 2000.

[BBM+08] É. Balmès, M. Basseville, L. Mevel, H. Nasser, and W. Zhou. Statistical model-based damage localization: a combined subspace-based and substructuring approach. *Structural Control and Health Monitoring*, 15(6):857–875, 2008.

[BDS99] D. Bauer, M. Deistler, and W. Scherrer. Consistency and asymptotic normality of some subspace algorithms for systems without observed inputs. *Automatica*, 35(7):1243–1254, 1999.

[BEGG10] J.M.W. Brownjohn, Carden E.P., C.R. Goddard, and Oudin G. Real-time performance monitoring of tuned mass damper system for a 183 m reinforced concrete chimney. *Journal of Wind Engineering and Industrial Aerodynamics*, 98(3):169–179, 2010.

[Ber02] D. Bernal. Load vectors for damage localization. *Journal of Engineering Mechanics*, 128(1):7–14, 2002.

[Ber06] D. Bernal. Flexibility-based damage localization from stochastic realization results. *Journal of Engineering Mechanics*, 132(6):651–658, 2006.

[Ber07] D. Bernal. Damage localization from the null space of changes in the transfer matrix. *AIAA Journal*, 45(2):374–381, 2007.

[Ber10] D. Bernal. Load vectors for damage location in systems identified from operational loads. *Journal of Engineering Mechanics*, 136(1):31–39, 2010.

[Ber13] D. Bernal. Damage quantification from the column space of flexibility changes. In *The 31th International Modal Analysis Conference*, Garden Grove, CA, USA, 2013.

[BF85] A. Benveniste and J.-J. Fuchs. Sinlgle sample modal identification of nonstationary stochastic process. *IEEE Transactions on Automatic Control*, AC-30(1):66–74, 1985.

[BG63] R.E.D. Bishop and G.M.L. Gladwell. An investigation into the theory of resonance testing. *Philosophical Transactions of the Royal Society of London*, 255A(1055):241–280, 1963.

[BH95] W.L. Briggs and V.E. Henson. *The DFT*. SIAM, Philadelphia, PA, USA, 1995.

[BJ90] R. Beale and T. Jackson. *Neural computing: an introduction*. Institute of Physics Publishing, 1st edition edition, 1990.

[BL02] D. Bauer and L. Ljung. Some facts about the choice of the weighting matrices in larimore type of subspace algorithms. *Automatica*, 38(5):763–773, 2002.

[BM07] A. Benveniste and L. Mevel. Nonstationary consistency of subspace methods. *IEEE Transactions on Automatic Control*, AC-52(6):974–984, 2007.

[BMG04] M. Basseville, L. Mevel, and M. Goursat. Statistical model-based damage detection and localization: subspace-based residuals and damage-to-noise sensitivity ratios. *Journal of Sound and Vibration*, 275(3):769–794, 2004.

[BN93] M. Basseville and I. Nikiforov. *Detection of Abrupt Changes – Theory and Applications*. Prentice Hall, 1993.

[BNKF97] W. Banzhaf, P. Nordin, R.E. Keller, and F.D. Francone. *Genetic Programming: An Introduction*. Morgan Kaufmann, 1st edition edition, 1997.

[BNSR98] T. Bastogne, H. Noura, P. Sibille, and A. Richard. Multivariable identification of a winding process by subspace methods for tension control. *Control Engineering Practice*, 6(9):1077–1088, 1998.

[Bow09] A.F. Bower. *Applied Mechanics of Solids*. CRC Press, 2009.

[Bre78] John W. Brewer. Kronecker products and matrix calculus in system theory. *IEEE Transactions on Circuits and Systems*, 25(9):772–781, 1978.

[Bro05] J. Brownjohn. Long-term monitoring of dynamic response of a tall building for performance evaluation and loading characterisation. In *Proceedings of the 1st international operational modal analysis conference*, 2005.

[CA79] P. Cawley and R.D. Adams. The location of defects in structures from measurements of natural frequencies. *Journal of Strain Analysis for Engineering Design*, 14:49–57, 1979.

[CB02] G. Casella and R.L. Berger. *Statistical inference*. Duxbury Press, 2002.

[CF04] E.P. Carden and P. Fanning. Vibration based condition monitoring: a review. *Structural Health Monitoring*, 3(4)(4):355–377, 2004.

[CI10] T.G. Carne and James G.H. III. The inception of oma in the development of modal testing technology for wind turbines. *Mechanical Systems and Signal Processing*, 24(5):1213–1226, 2010.

[CM11] E. Carden and A. Mita. Challenges in developing confidence intervals on modal parameters estimated for large civil infrastructure with stochastic subspace identificaiton. *Structural Control and Health Monitoring*, 18(1):53–78, 2011.

[CP04a] A. Chiuso and G. Picci. The asymptotic variance of subspace estimates. *Journal of Econometrics*, 118(1-2):257–291, 2004.

[CP04b] A. Chiuso and G. Picci. Asymptotic variance of subspace methods by data orthogonalization and model decoupling: a comparative analysis. *Automatica*, 40(10):1705–1717, 2004.

[CP04c] A. Chiuso and G. Picci. Subspace identification by data orthogonalization and model decoupling. *Automatica*, 40(10):1689–1703, 2004.

[CPH03] C.V. Camp, S. Pezeshk, and H. Hansson. Flexural design of reinforced concrete frames using a genetic algorithm. *Journal of Structural Engineering*, 129(1):105–115, 2003.

[CSC11] H. Clarke, J. Stainsby, and E.P. Carden. Operational modal analysis of resiliently mounted marine diesel generator/alternator. In *Proceedings of the 29th international modal analysis conference series*, 2011.

[CT65] J.W. Cooley and J.W. Tukey. An algorithm for the machine calculation of complex fourier series. *Mathematics of Computation*, 19(90):297–301, 1965.

[DÏ1] Michael Döhler. *Subspace-based system identification and fault detection: Algorithms for large systems and application to structural vibration analysis*. PhD thesis, Université de Rennes 1, France, 2011.

[Dau92] I. Daubechies. *Ten lectures on wavelets*. SIAM: Society for Industrial and Applied Mathematics, 1st edition edition, 1992.

[Daw76] Brian Dawson. Vibration condition monitoring techniques for rotating machinery. *The Shock and Vibration Digest*, 8(12), 1976.

[DDDRR06] D. Dooms, G. Degrande, G. De Roeck, and E. Reynders. Finite element modelling of a silo based on experimental modal analysis. *Engineering Structures*, 28(4):532–542, 2006.

[DdSCK00] G.R. Darbre, de Smet C.A.M., and C. Kraemer. Natural frequencies measured from ambient vibration response of the arch dam of mauvoisin. *Earthquake Engineering and Structural Dynamics*, 29(5):577–586, 2000.

[DFP+96] S. C. Doebling, C. R. Farrar, M. B. Prime, , and D. W. Schevitz. Damage identification and health monitoring of structural and mechanical systems from changes in their vibration characteristics: A literature review, 1996. Los Alamos National Laboratory.

[DFP98] S.W. Doebling, C.R. Farrar, and M.B. Prime. A summary review of vibration-based damage identification methods. *Shock and Vibration Digest*, 30(2):91–105, 1998.

[DHL+11] M. Döhler, F. Hille, X.-B. Lam, L. Mevel, and W. Rücker. Confidence intervals of modal parameters during progressive damage test. In *Proc. 29th International Modal Analysis Conference*, Jacksonville, FL, USA, 2011.

[DLM11] M. Döhler, X.-B. Lam, and L. Mevel. Uncertainty quantification for stochastic subspace identification on multi-setup measurements. In *Proc. 50th IEEE Conference on Decision and Control*, Orlando, FL, USA, 2011.

[DLM13] M. Döhler, X.-B. Lam, and L. Mevel. Uncertainty quantification for modal parameters from stochastic subspace identificaiton on multi-setup measurements. *Mechanical Systems and Signal Processing*, 36:562–581, 2013.

[DLT03] E. Douka, S. Loutridis, and A. Trochidis. Crack identification in beams using wavelet analysis. *International Journal of Solid and Structures*, 40:3557–3569, 2003.

[DM11] M. Döhler and L. Mevel. Robust subspace based fault detection. In *Proc. 18th IFAC World Congress*, Milan, Italy, 2011.

[DM12] M. Döhler and L. Mevel. Fast multi-order computation of system matrices in subspace-based system identication. *Control Engineering Practice*, 20(9):882–894, 2012.

[DM13] M. Döhler and L. Mevel. Efficient multi-order uncertainty computation for stochastic subspace identification. *Mechanical Systems and Signal Processing*, 38(2):346–366, 2013. - to be published (2013).

[DMBM13a] M. Döhler, L. Marin, D. Bernal, and L. Mevel. Comparison of two statistical damage localization approaches. In *Proccedings of the 5th International Operational Modal Analysis Conference*, 2013.

[DMBM13b] M. Döhler, L. Marin, D. Bernal, and L. Mevel. Statistical decision making for damage localization with stochastic load vectors. *Mechanical Systems and Signal Processing*, 37, 2013.

[Doe96] S.W. Doebling. Minimum-rank optimal update of elemental stiffness parameters for structural damage identification. *American Institute of Aeronautics and Astronautics*, 34(12):2615–2621, 1996.

[Dou99] E.R. Dougherty. *Random processes for image and signal processing*. SPIE Press, Bellingham, WA, USA, 1999.

[DPS95] M. Deistler, K. Peternell, and W. Scherrer. Consistency and relative effciency of subspace methods. *Automatica*, 31(12):1865–1875, 1995.

[Ewi00] D.J. Ewins. *Modal testing*. Research Studies Press, 2000.

[Fac05] P.L. Fackler. Notes on matrix calculus. Technical report, North Carolina State University, 2005.

[Fou22] J.B.J. Fourier. *Thorie analytique de la chaleur*. Firmin Didot, 1822.

[FP97] M. I. Friswell and J. E. T. Penny. Is damage location using vibration measurements practical? In *DAMAS 97, Structural Damage Assessment using Advanced Signal Processing Procedures*, 1997.

[FPW98] G.F. Franklin, J.D. Powell, and M. Workman. *Digital control of dynamic systems*. Addison-Wesley, Menlo Park, CA, USA, 1998.

[Fra90] P Frank. Fault diagnosis in dynamic systems using analytical and knowledge-based redundancy: A survey and some new results. *Automatica*, 26(3):459–474, 1990.

[Fri05] C-P. Fritzen. Vibration based structural health monitoringconcepts and applications. *Key Engineering Materials*, 293–294:3–18, 2005.

[Fri07] M. Friswell. Damage identification using inverse methods. *Philosophical Transactions of the Royal Society of London*, 365(1951):393–410, 2007.

[FW07] C. R. Farrar and K. Worden. An introduction to structural health monitoring. *Philosophical Transactions of the Royal Society A: Mathematical, Physical and Engineering Sciences*, 365(1851):306, 2007.

[GDTDDS06] P. Guillaume, T. De Troyer, C. Devriendt, and G. De Sitter. Omaxa combined experimental-operational modal analysis approach. In *Proceedings of ISMA international conference on noise and vibration engineering*, 2006.

[Gev06] M. Gevers. A personal view of the development of system identification. *IEEE Control Systems Magazine*, 26(6):93–105, 2006.

[GM03] A. Gentile and A. Messina. On the continuous wavelet transforms applied to discrete vibrational data for detecting open cracks in damaged beams. *International Journal of Solid and Structures*, 40:295–315, 2003.

[Gol89] D.E. Goldberg. *Genetic algorithms in search, optimization and machine learning*. Addison-Wesley Professional, 1st edition edition, 1989.

[GPSDM05] I. Goethals, J. Pelckmans, J.A.K. Suykens, and B. De Moor. Subspace identification of hammerstein systems using least squares support vector machines. *IEEE Transactions on Automatic Control*, 50(10):1509–1519, 2005.

[GS07] C. Gentile and A. Saisi. Ambient vibration testing of historic masonry towers for structural identification and damage assessment. *Construction and Building Materials*, 21(6):1311–1321, 2007.

[GS08] H.M. Gomes and N.R.S. Silva. Some comparisons for damage detection on structures using genetic algorithms and modal sensitivity method. *Applied Mathematical Modelling*, 32:2216–2232, 2008.

[GSJB07] Y. Gao, B.F. Spencer Jr, and D. Bernal. Experimental verification of the flexibility-based damage locating vector method. *Journal of Engineering Mechanics*, 133(10):1043–1049, 2007.

[GVL96] G. Golub and C. Van Loan. *Matrix computations*. John Hopkins University Press, 3rd edition edition, 1996.

[GZ08] M.P. González and J.L. Zapico. Seismic damage identification in buildings using neural networks and modal data. *Computers and Structures*, 86:416–426, 2008.

[Hay98] S. Haykin. *Neural networks: a comprehensive foundation*. Prentice Hall, 2nd edition edition, 1998.

[HdAH99] L. Hernans and Van der Auweraer H. Modal testing and analysis of structures under operational conditions: industrial applications. *Mechanical Systems and Signal Processing*, 13(2):193–216, 1999.

[HF95] F.M. Hemez and C. Farhat. Structural damage detection via a finite element model updating methodology. *Modal Analysis: The International Journal of Analytical and Experimental Modal Analysis*, 10(3):152–166, 1995.

[Hib09] R. C. Hibbeler. *Structural analysis*. Pearson Prentice Hall, New Jersey, 7th edition edition, 2009.

[HK66] B. Ho and R. Kalman. Effective reconstruction of linear statevariable models from input/output functions. *Regelungstechnik*, 14(12):545–548, 1966.

[HKLL02] J.C. Hong, Y.Y. Kim, H.C. Lee, and Y.W. Lee. Damage detection using lipschitz exponent estimated by the wavelet transform: applications to vibration modes of beam. *International Journal of Solid and Structures*, 39:1803–1846, 2002.

[HLS97] W. Heylen, S. Lammens, and P. Sas. *Modal analysis theory and testing.* PhD thesis, Katholieke Universiteit euven, 1997.

[Hol92] J.H. Holland. *Adaptation in natural and artificial systems: an introductory analysis with applications to biology, control, and artificial intelligence.* A Bradford Book, 1992.

[Jam03] G.H. III James. Modal parameter estimation from space shuttle flight data. In *Proceedings of the 21st international modal analysis conference*, 2003.

[JP85] J-N. Juang and R.S. Pappa. An eigensystem realization algorithm for modal parameter identification and model reduction. *Journal of Guidance, Control, and Dynamics*, 8(5):620–627, 1985.

[JSL01] B.C. Juricek, D.E. Seborg, and W.E. Larimore. Identification of the tennessee eastman challenge process with subspace methods. *Control Engineering Practice*, 9(12):1337–1351, 2001.

[Jua94] J-N. Juang. *Applied system identification.* Prentice- Hall, 1994.

[Jur64] E.I. Jury. *Theory and application of the z-transform method.* Wiley, New York, NY, USA, 1964.

[Kai80] T. Kailath. *Linear systems.* Prentice-Hall, 1980.

[Kai10] G. Kaiser. *A Friendly Guide to Wavelets.* Birkhäuser, 2010.

[KCL03] C.G. Koh, Y.F. Chen, and C.Y. Liaw. A hybrid computational strategy for identification of structural parameters. *Computers and Structures*, 81(2):107–117, 2003.

[Kir44] P. G. Kirshmer. The effect of discontinuities on the natural frequency of beams. *ASTM Journal*, 44:897–904, 1944.

[KP47] C. Kennedy and C. Pancu. Use of vectors in vibration measurement and analysis. *Journal of the Aeronautic Science*, 14(11):603–625, 1947.

[KSH99] T. Kailath, A.H. Sayed, and B. Hassibi. *Linear estimation*. Prentice Hall, 1999.

[Lar83] W.E. Larimore. System identication, reduced order filters and modelling via canonical variate analysis. In *Proceedings of American Control Conference*, pages 445–451, San Francisco, CA, USA, 1983.

[Lin90] C.S. Lin. Location of modeling errors using modal test data. *American Institute of Aeronautics and Astronautics*, 28:1650–1654, 1990.

[Lju99] L. Ljung. *System identification: theory for the user*. Prentice Hall, Englewood Cliffs, NJ, USA, 1999.

[LK94] T.W. Lim and A.L. Kashangaki. Structural damage detection of space truss structures using best achievable eigenvectors. *American Institute of Aeronautics and Astronautics*, 32:1049–1057, 1994.

[LRZ02] Q. Lu, G. Ren, and Y. Zhao. Multiple damage location with flexibility curvature and relative frequency change for beam structures. *Journal of Sound and Vibration*, 253(5):1101–1114, 2002.

[MAL96] T. McKelvey, H. Akay, and L. Ljung. Subspace-based multivariable system identification from frequency response data. *IEEE Transactions on Automatic Control*, 41(7):960–979, 1996.

[MBB+06] L. Mevel, A. Benveniste, M. Basseville, M. Goursat, B. Peeters, and H. Van der Auweraer. Input/output versus output-only data processing for structural identification - application to in-flight data analysis. *Journal of Sound and Vibration*, 295(3):531–552, 2006.

[MBG03] L. Mevel, M. Basseville, and M. Goursat. Stochastic subspace-based structural identification and damage detection - application to the steel-quake benchmark. *Mechanical Systems and Signal Processing*, 17(1):91–101, 2003.

[MCC08] F Magalhes, E. Caetano, and Cunha. Operational modal analysis and finite element model correlation of the braga stadium suspended roof. *Engineering Structures*, 30(6):1688–1698, 2008.

[MDBM12] L. Marin, M. Döhler, D. Bernal, and L. Mevel. Uncertainty quantification for stochastic damage localization for mechanical system. In *Proccedings of the 8th IFAC Safeprocess*, Mexico City, Mexico, 2012.

[MDBM13a] L. Marin, M. Döhler, D. Bernal, and L. Mevel. Damage localization using a statistical test on residuals from the sddlv approach. *Society for Experimental Mechanics Series*, 41:143–152, 2013.

[MDBM13b] L. Marin, M. Döhler, D. Bernal, and L. Mevel. Robust statistical damage localization with stochastic load vectors. *Structural Control and Health Monitoring*, 00:1–29, 2013. Under revision.

[MDBM13c] L. Marin, M. Döhler, D. Bernal, and L. Mevel. Statistical based decision making for damage localization with influence lines. In *The 9th International Workshop on Structural Health Monitoring*, 2013.

[Meh97] K. Mehrotra. *Elements of artificial neural networks*. The M.I.T. Press, 1997.

[Mei75] L. Meirovitch. *Elements of vibration analysis*. McGraw-Hill, 1975.

[MF93] J. E. Mottershead and M. I. Friswell. Model updating in structural dynamics: A survey. *Journal of Sound and Vibration*, 167(2):347–375, 1993.

[MP43] W. McCulloch and W. Pitts. A logical calculus of the ideas immanent in nervous activity. *Bulletin of Mathematical Biophysics*, 5(4):115–133, 1943.

[MS97] N.M.M. Maia and J.M.M. Silva. *Theoretical and experimental modal analysis*. Research Studies Press, 1997.

[OS04] A.V. Ovanesova and L.E. Suarez. Application of wavelet transform to damage detection in frame structures. *Engineering Structures*, 26:39–49, 2004.

[Pan08] J.H. Pan, Y. adn Lee. Modified subspace identification for long-range prediction model for inferential control. *Control Engineering Practice*, 16(12):1487–1500, 2008.

[PB94] A.K. Pandy and M. Biswas. Damage detection in structures using changes in flexibility. *Journal of Sound and Vibration*, 169(1):3–17, 1994.

[PBS91] A.K. Pandy, M. Biswas, and M.M. Samman. Damage detection from changes in curvature mode shapes. *Journal of Sound and Vibration*, 145(2):321–332, 1991.

[PCB+05] E. Parloo, B. Cauberghe, F. Benedettini, R. Alaggio, and P. Guillaume. Sensitivity-based operational mode shape normalization: application to a bridge. *Mechanical Systems and Signal Processing*, 19(1):43–55, 2005.

[PDR99] B. Peeters and G. De Roeck. Reference-based stochastic subspace identification for output-only modal analysis. *Mechanical Systems and Signal Processing*, 13(6):855–878, 1999.

[PDR01] B. Peeters and G. De Roeck. Stochastic system identification for operational modal analysis: a review. *ASME Journal of Dynamic Systems, Measurement, and Control*, 123(4):659–667, 2001.

[PFC89] R.J Patton, P.M. Frank, and R.N. Clarke. *Fault diagnosis in dynamic systems: theory and application.* Prentice Hall, 1989.

[PGS07] R. Pintelon, P. Guillaume, and J. Schoukens. Uncertainty calculation in (operational) modal analysis. *Mechanical Systems and Signal Processing*, 21(6):2359–2373, 2007.

[Pin02] R. Pintelon. Frequency-domain subspace system identification using nonparametric noise models. *Automatica*, 38(8):1295–1311, 2002.

[PRM07] R. Perera, A. Ruiz, and Manzano. An evolutionary multiobjective framework for structural damage localization and quantification. *Engineering Structures*, 29:2540–2550, 2007.

[PS01] R. Pintelon and J. Schoukens. *System identification.* IEEE Press, New York, NY, USA, 2001.

[PSG08] R. Pintelon, J. Schoukens, and P. Guillaume. Continuous-time noise modeling from sampled data. *IEEE Transactions on Instrumentation and Measurement*, 55(6):2253–2258, 2008.

[PVdAVG07] B. Peeters, H. Van der Auweraer, F. Vanhollebeke, and P. Guillaume. Operational modal analysis for estimating the dynamic properties of a stadium structure during a football game. *Shock and Vibration*, 14(4):283–303, 2007.

[PVGVO02] E. Parloo, P. Verboven, P. Guillaume, and M. Van Overmeire. Sensitivity-based operational mode shape normalization. *Mechanical Systems and Sygnal Processing*, 16(5):757–767, 2002.

[QWZA01] S.T. Quek, Q. Wang, L. Zhang, and K.K. Ang. Sensitivity analysis of crack detection in beams by wavelet technique. *International Journal of Mechanical Science*, 43:2899–2910, 2001.

[Rat00] C.P. Ratcliffe. A frequency and curvature based experimental method for locating damage in structures. *Journal of Vibration and Acoustics*, 122:324–329, 2000.

[RDDRM10] E. Reynders, Degrauwe D., G. De Roeck, and F Magalhes. Combined experimental-operational modal testing of footbridges. *ASCE Journal of Engineering Mechanics*, 136(6):687–696, 2010.

[RDR08] E. Reynders and G. De Roeck. Reference-based combined deterministic-stochastic subspace identification for experimental and operational modal analysis. *Mechanical Systems and Signal Processing*, 22(3):617–637, 2008.

[RDR10] E. Reynders and G. De Roeck. A local flexibility method for vibration-based damage localization and quantification. *Journal of Sound and Vibration*, 329(12):2367–2383, 2010.

[RDRBS07] E. Reynders, G. De Roeck, P.G. Bakir, and C. Sauvage. Damage identification on the tilff bridge by vibration monitoring using optical fibre strain sensors. *ASCE Journal of Engineering Mechanics*, 133(2):185–193, 2007.

[Rey12] E. Reynders. System identification methods for (operational) modal analysis: reviwe and comparison. *Archives of Computational Methods in Engineering*, 19:51–124, 2012.

[RHDR12] E. Reynders, J. Houbrechts, and G. De Roeck. Fully automated (operational) modal analysis. *Mechanical Systems and Sygnal Processing*, 29:228–250, 2012.

[RN09] S. Russel and P. Norvig. *Artificial Intelligence: A Modern Approach*. Prentice Hall, 3rd edition edition, 2009.

[RPDR08] E. Reynders, R. Pintelon, and G. De Roeck. Uncertainty bounds on modal parameters obtained from stochastic subspace identification. *Mechanical Systems and Signal Processing*, 22(4):948–969, 2008.

[RW06] M. Rucka and K. Wilde. Application of continuous wavelet transform in vibration based damage detection method for beams and plates. *Journal of Sound and Vibration*, 297:536–550, 2006.

[Ryt93] A. Rytter. *Vibrational based inspection of civil engineering structures*. PhD thesis, Aalborg University, 1993.

[SFH+04] H. Sohn, C. R. Farrar, F. M. Hemez, , and J. J. Czarnecki. A review of structural health monitoring literature: 1996-2001, 2004. Los Alamos National Laboratory.

[SL98] Z.Y. Shi and S.S. Law. Structural damage localization from modal strain energy change. *Journal of Sound and Vibration*, 218(5):825–844, 1998.

[SM11] S. Sankararaman and S. Mahadevan. Uncertainty quantification in structural damage diagnosis. *Structural Control and Health Monitoring*, 18(8):807–824, 2011.

[SM13] S. Sankararaman and S. Mahadevan. Bayesian methodology for diagnosis uncertainty quantification and health monitoring. *Structural Control and Health Monitoring*, 20(1):88–106, 2013.

[SP91] J. Schoukens and R. Pintelon. *Identification of linear systems: a practical guide to accurate modeling*. Pergamon Press, Oxford, UK, 1991.

[SPDR05] J. Schoukens, R. Pintelon, T. Dobrowiecki, and Y. Rolain. Identification of linear systems with nonlinear distortions. *Automatica*, 41(3):491–504, 2005.

[SPE08] J. Schoukens, R. Pintelon, and M. Enqvist. Study of the lti relations between the outputs of two coupled wiener systems and its application to the generation of initial estimates for wiener-hammerstein systems. *Automatica*, 44(7):1654–1665, 2008.

[SPG03] O.A.Z. Sotomayor, S.W. Park, and C. Garcia. Multivariable identification of an activated sludge process with subspace-based algorithms. *Control Engineering Practice*, 11(8):961–969, 2003.

[SS83] T. Söderström and P. Stoica. *Instrumental variable methods for system identification*. Springer, New York, NY, USA, 1983.

[SS03] M. Sahin and R.A. Shenoi. Quantification and localisation of damage in beam-like structures by using artificial neural networks with experimental validation. *Engineering Structures*, 25:1785–1802, 2003.

[TN04] C. Truesdell and W. Noll. *The non-linear field theories of mechanics*. Springer, 2004.

[Ver94] M. Verhaegen. Identification of the deterministic part of mimo state space models given in innovations form from input-output data. *Automatica*, 30(1):61–74, 1994.

[Vib95] M. Viberg. Subspace-based methods for the identification of linear time-invariant systems. *Automatica*, 31(12):1835–1851, 1995.

[VODM94] P. Van Overschee and B. De Moor. N4sid: Subspace algorithms for the identification of combined deterministic-stochastic systems. *Automatica*, 30(1):75–93, 1994.

[VODM96] P. Van Overschee and B. De Moor. *Subspace Identification for Linear Systems: Theory, Implementation, Applications*. Kluwer, 1996.

[Wil76] A.S. Willsky. A survey of design methods for failure detection in dynamic systems. *Automatica*, 12(6):601–611, 1976.

[WL04] D. Wu and S.S. Law. Damage localization in plate structures from uniform load surface curvature. *Journal of Sound and Vibration*, 276:227–244, 2004.

[Wu04] H.-C. Wu. *Continuum Mechanics and Plasticity (Modern Mechanics and Mathematics)*. Chapman and Hall/CRC, 2004.

[YG05] A.-M Yan and J.-C Golinval. Structural damage localization by combining flexibility and stiffness methods. *Engineering Structures*, 27(12):1752–1761, 2005.

[ZA98] Z. Zhang and A.E. Aktan. Application of modal flexibility and its derivatives in structural identification. *Research in Nondestructive Evaluation*, 10(1):43–61, 1998.

[ZD99] J. Zhao and J.T. Dewolf. Sensitivity study for vibrational parameters used in damage detection. *Journal of Structural Engineering, American Society of Civil Engineering*, 125(4):410–416, 1999.

[ZK94] D.C. Zimmerman and M. Kaouk. Structural damage detection using a minimum rank update theory. *Journal of Vibration and Acoustic*, 116:222–230, 1994.

[ZTZ05] O.C. Zienkiewicz, R.L. Taylor, and J.Z. Zhu. *The finite element method: its basis and fundamentals*. Elsevier, 6th edition edition, 2005.

Abstract

Mechanical systems under vibration excitation are prime candidate for being modeled by linear time invariant systems. Damage localization using both finite element information and modal parameters estimated from ambient vibration data collected from sensors is possible by the Stochastic Dynamic Damage Location Vector (SDDLV) approach, where the damage location is empirically related to positions where the stress is close to zero. The first contribution in this thesis shows how the uncertainty in the estimates of the state space system can be used to derive uncertainty bounds on the damage localization residuals to decide about the damage location with a hypothesis test using one chosen Laplace value. In the second contribution, the damage localization method is extended with a statistical framework and robustness of the localization information is achieved by aggregating results at different values in the Laplace domain. The Influence Line Damage Location (ILDL) is a complementary approach of the SDDLV where the subspace angle is computed and damage is empirically located at points near zero. The last contribution describes how robustness of the localization information is achieved by aggregating results at different values in the Laplace domain based on the previous two contributions. The proposed methods are validated and successfully applied to damage localization of several applications in civil structures.

Résumé

Les systèmes mécaniques soumis et excités par vibrations sont les candidats naturels à être modélisé par des systèmes linéaires invariables dans le temps. La localisation de dommages utilisant les paramètres modaux évalués à partir de données de vibration ambiantes mesurées grâce à de capteurs est possible notamment par l'approche nommée Stochastic Dynamic Damage Location Vector (SDDLV), où l'emplacement des dommages est empiriquement relié aux positions où le stress est proche de zéro. La premiere contribution dans cette thèse montre comment l'incertitude sur les paramètres du système d'état peut être utilisée pour déduire des bornes d'incertitude sur les résidus de localisation de dommages, ceci afin de décider de l'emplacement de dommage utilisant un test d'hypothèse. Dans la deuxième contribution, la méthode de localisation de dommages est étendue pour être robuste au choix des variables de Laplace utilisées dans cette méthode. Ceci est obtenue en agrégeant statistiquement les résultats à valeurs différentes dans le domaine de Laplace. L'Influence Line Damage Location (ILDL) est une approche complémentaire du SDDLV où l'angle entre les sous-espaces principaux est calculé et les dommages sont empiriquement localisés aux points près du zéro. L'approche développée pour la SDDLV est étendue à cette nouvelle approche, l'ILDL. Les méthodes proposées sont validées et appliquées avec succès pour la localisation de dommages dans des structures civiles.